REPORT NO.
UCB/EERC-88/07
APRIL 1988

EARTHQUAKE ENGINEERING RESEARCH CENTER

PB91-217976

THEORETICAL AND EXPERIMENTAL STUDIES OF CYLINDRICAL WATER TANKS IN BASE ISOLATED STRUCTURES

by

MICHEL S. CHALHOUB
JAMES M. KELLY

Report to the National Science Foundation

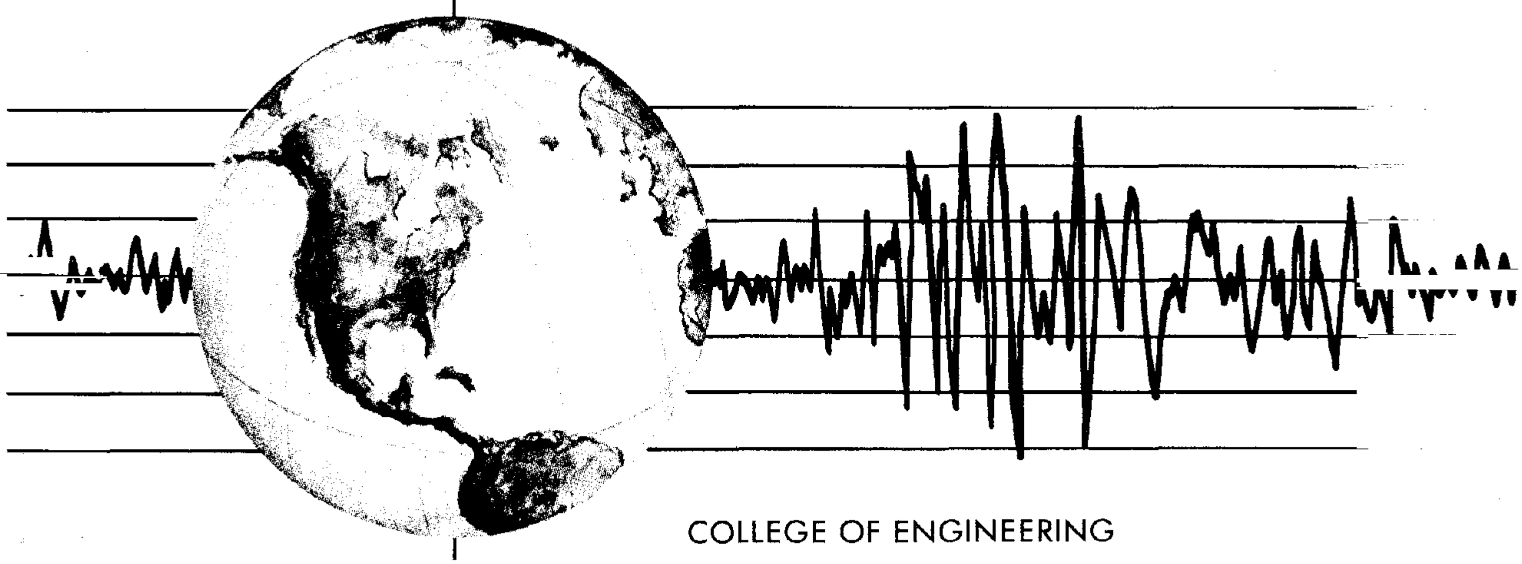

COLLEGE OF ENGINEERING

VERSITY OF CALIFORNIA AT BERKELEY

For sale by the National Technical Information Service, U.S. Department of Commerce, Springfield, Virginia 22161

See *back of report for up to date listing of* EERC reports.

THEORETICAL AND EXPERIMENTAL STUDIES OF CYLINDRICAL WATER TANKS IN BASE ISOLATED STRUCTURES

by

Michel S. Chalhoub

and

James M. Kelly

Report to the National Science Foundation

Report No. UCB/EERC-88/07
Earthquake Engineering Research Center
College of Engineering
University of California at Berkeley

April 1988

ABSTRACT

This report presents the results obtained from an experimental study of two similar cylindrical water tanks, and a corresponding theoretical solution. One of the tanks was directly fixed to the earthquake simulator, the other was mounted on the base of a scaled nine-story steel structure. The structure was isolated on eight multilayered elastomeric bearings. Because the base accelerations were lower for the tank in the isolated structure, the dynamic pressure was reduced for this tank. Free surface water elevation was slightly higher because of the lower frequency that characterizes the motion of base isolated structures. This problem can be overcome by appropriate selection of the isolation system or by the addition of dampers at the locations of maximum water particle velocities. For the tank in the isolated structure, the accelerations and displacements at the tank rim were lower than for the tank directly fixed to the shake table. A theoretical solution developed from linear wave theory correlates very well with the experimental results. The advantages of using base isolation for large storage tanks are investigated.

ACKNOWLEDGEMENTS

The research reported herein was supported by the National Science Foundation under Grant No. ECE-8414036 and was conducted at the Earthquake Simulator Laboratory of the University of California at Berkeley.

The authors would like to thank the National Science Foundation for its support.

The staff of the Earthquake Engineering Research Center provided assistance and advice over the course of the experimental work.

TABLE OF CONTENTS

LIST OF TABLES

LIST OF FIGURES

Chapter four: Test Results and Correlation (pp. 50-72)

CHAPTER ONE
INTRODUCTION

Extensive work has been done on the response of internal equipment in structures subjected to ground motion [1]. An important advantage of base isolation is the protection of internal equipment in buildings located in seismic regions, against high accelerations transmitted from the ground and amplified in the structure. Studies have been made on oscillators simulating the contents of a building, where each oscillator was tuned to a chosen frequency [2].

Fluid containers are an important category of internal equipment for certain buildings and power plants. In the present research, the response of a cylindrical water tank fixed to the shake table is compared with that of a similar one installed at the bottom of a base isolated nine-story steel structure.

Quantities of interest in the response are the dynamic pressure at the tank walls, displacements and accelerations in the shell, and the water free surface deformation. These quantities were measured at certain locations. A detailed description of the experimental set-up is presented in the next chapter. From a structural viewpoint, it is of primary concern to study the stresses and deformations in the shell; however, in the present treatment we are mainly concerned with the loading exerted by the fluid on the container in terms of the dynamic pressure at the interface, and the effect of base isolation on the sloshing.

A theoretical solution is worked out and expressions for the dynamic pressure and the free surface elevation are proposed and compared with some experimental results. It is commonly accepted that the pressure at the interface consists of two components: an impulsive pressure and a convective pressure. The first component is due to the container wall accelerating against the fluid, the second component is due to the change in the fluid free surface elevation. The convective pressure is mainly attributed to the sloshing resulting from the formation of forced waves in the tank. Sloshing in tanks is a phenomenon of relatively low frequency (the first mode is predominant): for this reason base isolation might increase it, causing a slightly higher convective pressure component. However, base isolation has more effect on the impulsive component and thus leads to a much lower resultant dynamic pressure.

This study provides some insight into the advantages of mounting large tanks in seismic regions directly on base isolators, in order to reduce the hydrodynamic loading on the shell. The approach should be studied further using the earthquake simulator. Meanwhile, since the expressions presented in Chapter Three show good agreement with the experimental results, they can be used to predict the response of the fluid in a base isolated rigid tank.

Finally, the validity of the theoretical results and the ease of the numerical determination of the convolution integrals involved in the final expressions, suggest the direct use of the hydrodynamic solution instead of converting the problem into an equivalent mechanical analog that provides a modeling of only the overall behavior of the contained fluid.

Future research based on this work should include the effects of the tank flexibility on the response of the fluid. It should also include studies of the response of tanks independently isolated and of tanks isolated as groups on a simple isolation pad.

CHAPTER TWO
EXPERIMENTAL SET-UP AND TEST PROGRAM

1. Structural Model

The structural model used is the nine-story K-braced steel frame described in [3]. The structure was mounted on an isolation system consisting of eight elastomeric bearings provided by the Malaysian Rubber Producers' Research Association (MRPRA SET #1). Each bearing had a horizontal stiffness of about 1.1 kips/in. at 60% shear strain and a vertical stiffness of about 420 kips/in. The extremely high vertical stiffness provides a conventional support condition in the vertical direction and the high horizontal flexibility causes the entire structure to move like a rigid body at a very low frequency. This arrangement reduces drastically the ground accelerations transmitted to the structure. Since the total weight of the model was 91 kips, the natural frequency of the base isolated structure was 0.97 Hz.

2. Tanks

Two similar tanks were used for the purpose of comparison. One of them was directly fixed on the shake table, the other was fixed on the base of the isolated structure (Figures 2.1 and 2.2). They were cylindrical steel tanks, 1/25 in. thick, 2 feet in height and 4 feet in diameter. Each tank was fixed at its bottom by six 2×2×1/4 in. angles; two of the angles were along the diameter of excitation and the four others were installed by pairs at 45° from that diameter. The tank on the structure was mounted on a 1 in. thick steel plate welded to the bottom flanges of the two base beam girders.

For each tank, eight Piezo-electric pressure transducers were used to measure the dynamic water pressure. Six of them were installed along two vertical lines in the plane of excitation at the bottom, at mid-height and near the water free surface, while two others were installed at mid-height in a plane perpendicular to the plane of excitation. Two accelerometers were installed at the shell rim, at the north and west sides respectively, to measure horizontal accelerations. Two DCDTs were installed at the north and south sides of the shell rim, respectively, to measure rim displacements relative to the tank base. The locations of these instruments and their channel numbers are shown in Figures 2.3 to 2.6. A list of the channels with the symbols used and a brief description is given Table 2.1.

The free surface water elevation was measured at the shell wall at the north and south sides, using water level gages. The gages consisted of two parallel conductor wires connected to an electric bridge. The resistance in the circuit varied with the water elevation and thus was converted from mΩ to inches.

3. Input Signals.

The shake table and the signals used were derived from previously recorded ground motions, these are described in [3]. When the tanks were filled with water, these signals were applied at spans ranging from 50 to a maximum of 100 due to water spilling for spans larger than 100. The spilling problem can be solved by addition of a cover, however this problem is not pursued in the present work. The data processed for comparison with theoretical prediction corresponded to spans of 50 and 75. Table displacement and acceleration time histories are shown with the experimental results in Chapter 4.

4. Test Sequence

Initially the model was loaded with a different mass distribution, and weighed about 120 kips. The bearings on which it was mounted were of the MRPRA SET #3 type, and had a horizontal stiffness of 0.8 kip/in. each at 60% shear strain. For this arrangement, the natural frequency of the isolated structure was of 0.7 Hz, which is very close to the frequency of the first sloshing mode in the tanks. A first test sequence was performed, starting with sine input signals at 1.5 Hz. The input frequency was then lowered to 0.7 Hz and 0.8 Hz. For this set of runs, overtopping of the water gages and sometimes spilling occurred because of resonance. The files corresponding to this set-up were used only for observation and were not compared with theoretical prediction.

The structural model was then lightened to 91 kips and the bearings replaced by eight MRPRA SET #1 bearings which had a horizontal stiffness of 1.1 kips/in. each at 60%. This resulted in a slightly higher base isolated natural frequency. Ground motions were used at various spans but spilling still occurred for some spans higher than 100. The files used for comparison with the theoretical solution were chosen from the ones of spans lower than 75 and are listed in Table 2.2 under "last test sequence".

It is to be noted, however, that the time scaling was dictated by the model and was fixed to 2, and that if the tanks were to be tested without the structural model, the time scaling could be much higher.

Table 2.1 Channel numbering

CHANNEL NUMBERING FOR WATER TANK INSTRUMENTATION

Channel	Name	Units	Remarks
84	ac1 tb	g's	north accelerometer for tank on table
85	ac2 tb	g's	west accelerometer for tank on table
86	ac1 md	g's	north accelerometer for tank on model
87	ac2 md	g's	west accelerometer for tank on model
88	ds1 tb	inches	north DCDT for tank on table
89	ds2 tb	inches	south DCDT for tank on table
90	ds1 md	inches	north DCDT for tank on model
91	ds2 md	inches	south DCDT for tank on model
92	wg1 tb	inches	north water gage for tank on table
93	wg2 tb	inches	south water gage for tank on table
94	wg1 md	inches	north water gage for tank on model
95	wg2 md	inches	south water gage for tank on model
96	pz1 tb	psi	north bottom pressure for tank on table
97	pz2 tb	psi	north mid-hi pressure for tank on table
98	pz3 tb	psi	north top pressure for tank on table
99	pz4 tb	psi	south bottom pressure for tank on table
100	pz5 tb	psi	south mid-hi pressure for tank on table
101	pz6 tb	psi	south top pressure for tank on table
102	pz7 tb	psi	west mid-hi pressure for tank on table
103	pz8 tb	psi	east mid-hi pressure for tank on table
104	pz1 md	psi	north bottom pressure for tank on model
105	pz2 md	psi	north mid-hi pressure for tank on model
106	pz3 md	psi	north top pressure for tank on model
107	pz4 md	psi	south bottom pressure for tank on model
108	pz5 md	psi	south mid-hi pressure for tank on model
109	pz6 md	psi	south top pressure for tank on model
110	pz7 md	psi	west mid-hi pressure for tank on model
111	pz8 md	psi	east mid-hi pressure for tank on model

Table 2.2 Test sequence.

TESTING OF WATER TANKS.
TANK DIAMETER: 48"
TANK HEIGHT : 24"
WATER DEPTH : 17.5"
ONE TANK MOUNTED ON THE ISOLATED BASE
ONE TANK MOUNTED ON THE SHAKE TABLE

1st TEST SEQUENCE

BEARINGS USED : MRPRA #3, Kh=0.8 k/in
TOTAL WEIGHT OF MODEL : 120 KIPS

FILENAME	SIGNAL	TIME	RATE	REMARKS
861009.01	sine	20 secs	.005	1.54 hz
861009.02	sine	10 secs	.005	0.9 hz
861009.03	sine	20 secs	.005	0.9 hz and stop
861009.04	sine	10 secs	.005	0.7 hz sph=80
861009.05	sine	10 secs	.005	0.75 hz sph=60
861009.06	sine	10 secs	.005	0.8hz sph=8
861009.07	sine	10 secs	.005	0.8 hz sph=10
861009.08	sine	10 secs	.005	0.8 hz sph=12
861009.09	random30.d	32 secs	.005	sph=300
861009.10	sine	10 secs	.005	3.0 hz sph=70
861010.01	sine	10 secs	.005	2.0 hz sph=90
861010.02	ec2	18 secs	.005	sph=150

Excessive spilling occurred for both tanks since the sine inputs had frequencies close to the first sloshing mode frequency.

LAST TEST SEQUENCE

BEARINGS USED : MRPRA #1, Kh=1.1 k/in
TOTAL WEIGHT OF MODEL : 91 KIPS

The files listed below were used for comparison with theoretical solution.

861023.01	ec2	19 secs	.005	sph=50	ts=1/4
861023.02	ec2	19 secs	.005	sph=75	ts=1/4
861023.03	ec2	19 secs	.005	sph=70	ts=1/4
861023.04	sf2	12 secs	.005	sph=50	ts=1/4
861023.05	sf2	12 secs	.005	sph=150	ts=1/4
861023.06	sf2	12 secs	.005	sph=75	ts=1/4
861023.07	pac2	12 secs	.005	sph=50	ts=1/4
861023.08	pac2	12 secs	.005	sph=75	ts=1/4
861023.09	park2	14 secs	.005	sph=50	ts=1/4
861023.10	park2	14 secs	.005	sph=75	ts=1/4
861023.11	taft2	19 secs	.005	sph=50	ts=1/4
861023.12	taft2	19 secs	.005	sph=75	ts=1/4
861023.13	buc1	12 secs	.005	sph=50	ts=1/4
861023.14	buc1	12 secs	.005	sph=25	ts=1/4
861023.15	sct	35 secs	.005	sph=25	ts=1/4
861023.16	sct	35 secs	.005	sph=50	ts=1/4

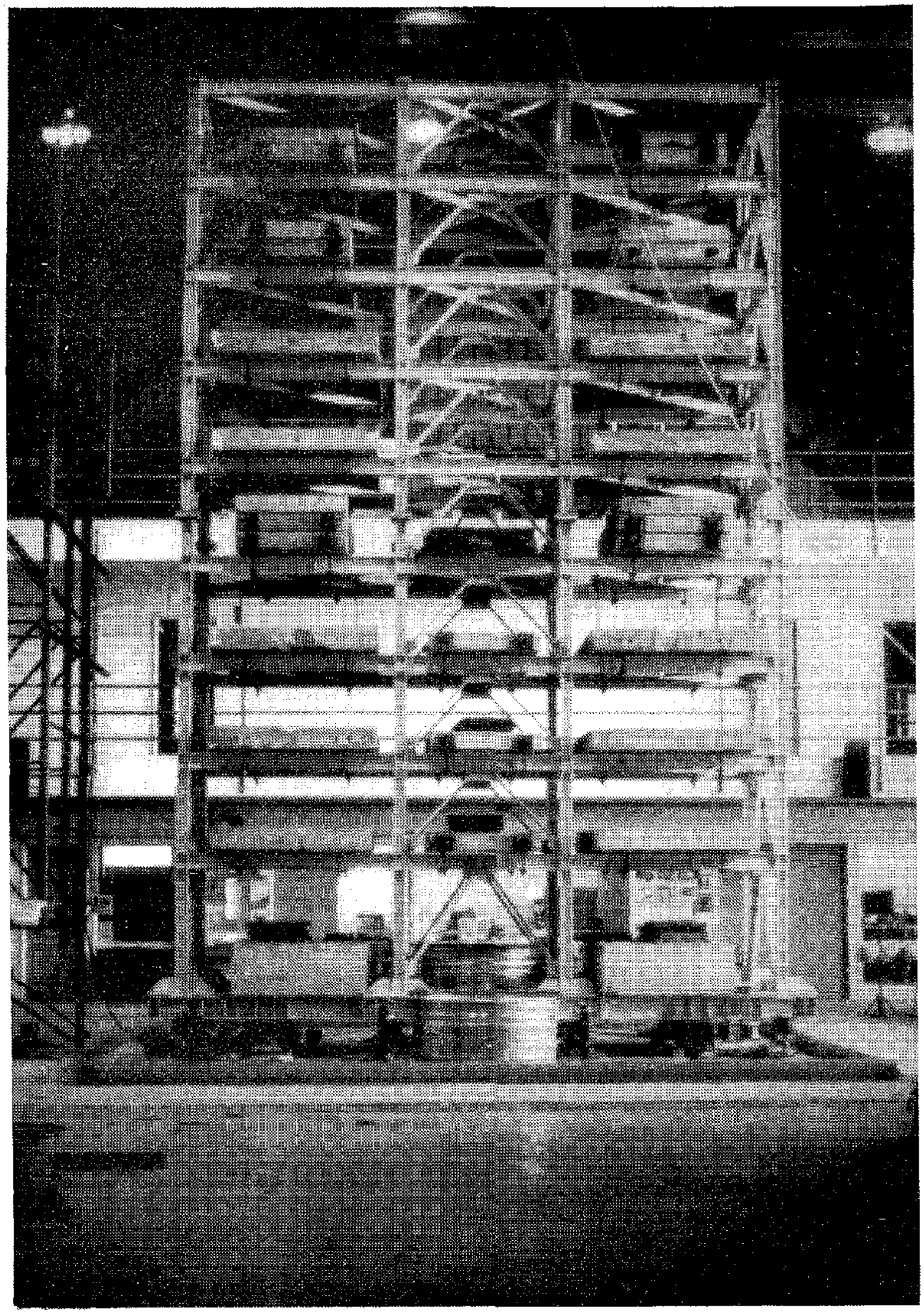

Figure 2.1 **1/4 scale nine-story structural model and the tanks. Tank #1 fixed to the shake table, tank #2 fixed to the isolated base.**

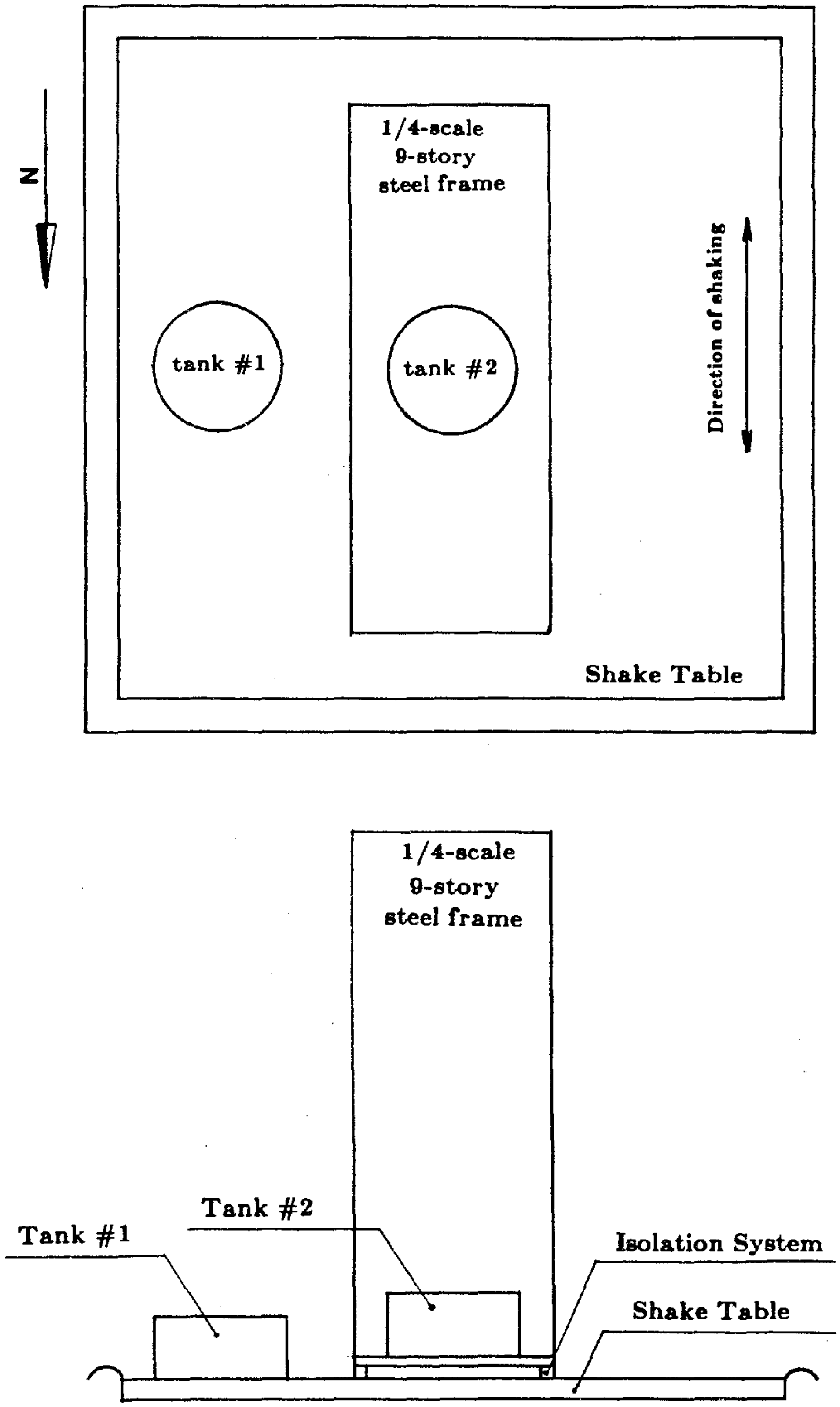

Figure 2.2 Plan view and section view of the experimental set-up.

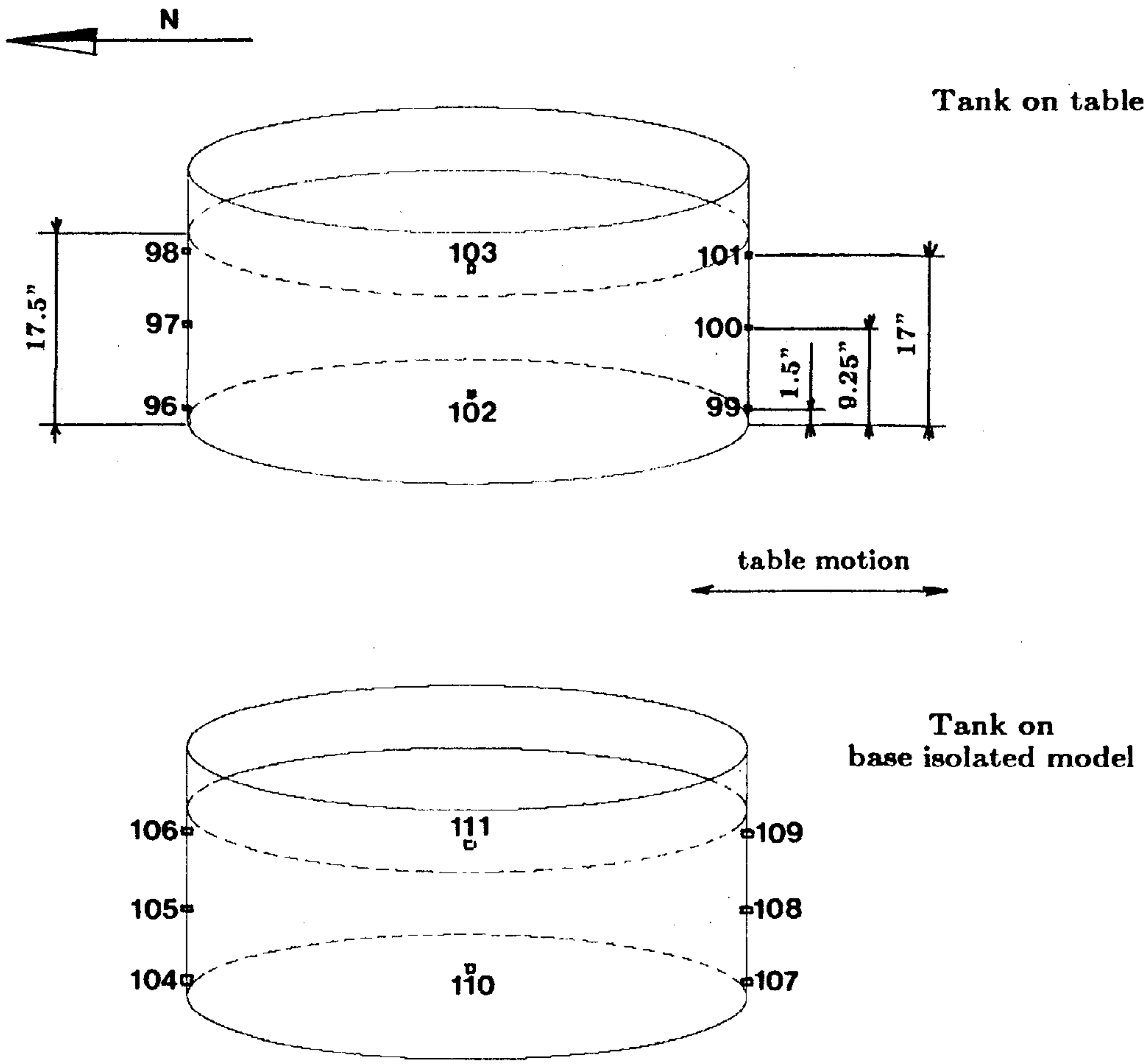

Figure 2.3 Location and channel numbering of pressure transducers.

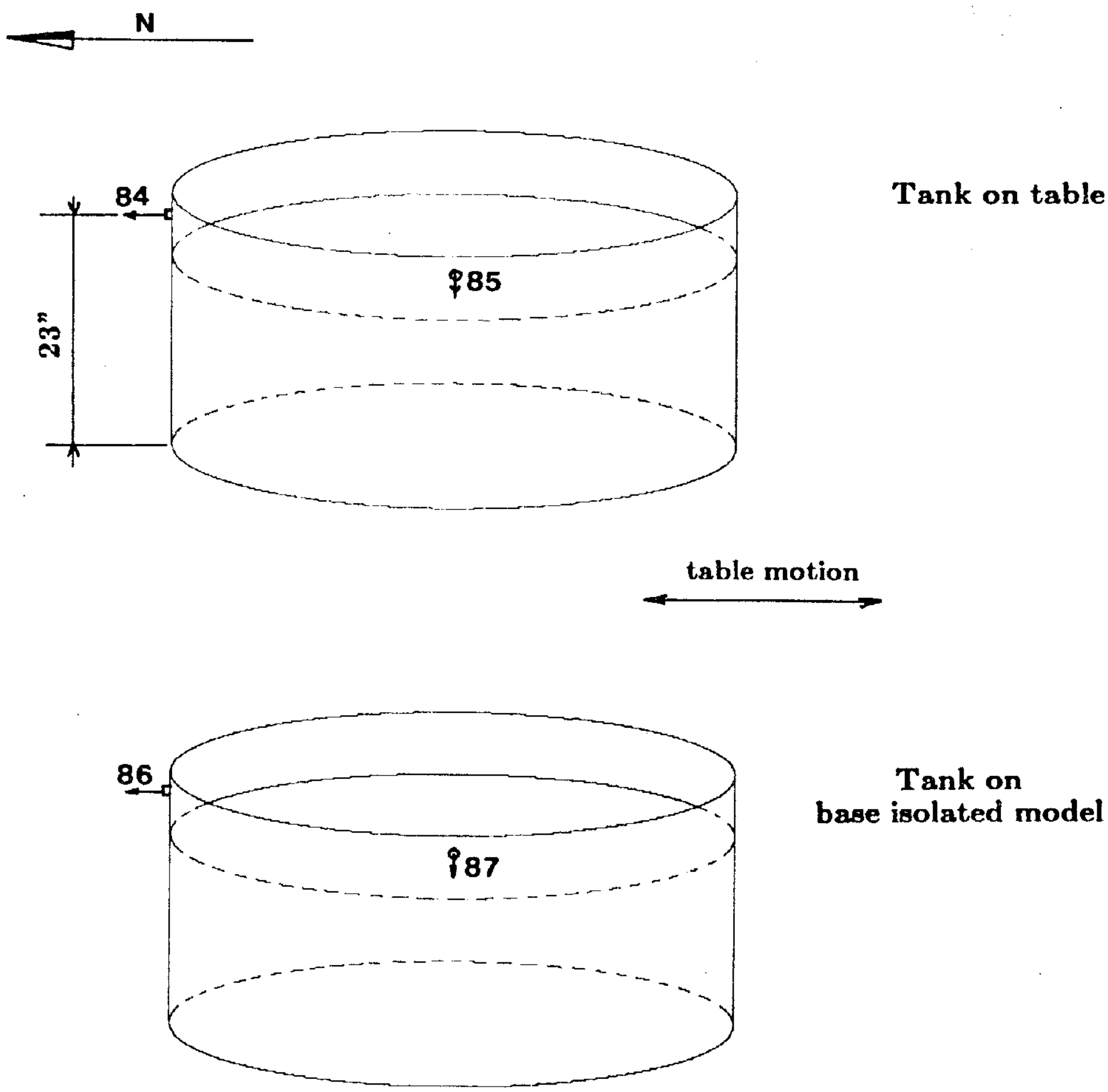

Figure 2.4 Location and channel numbering of accelerometers.

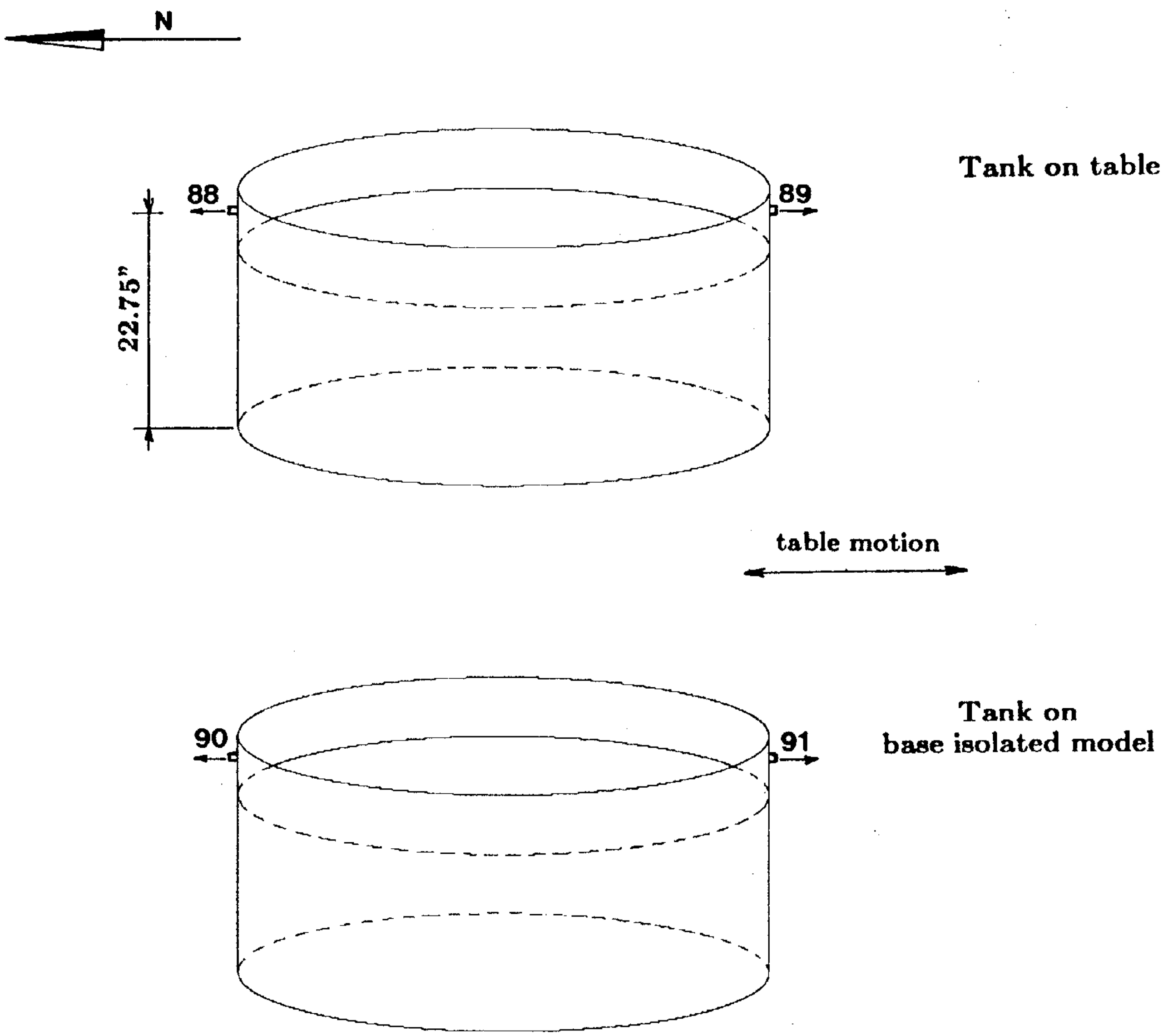

Figure 2.5 Location and channel numbering of DCDTs.

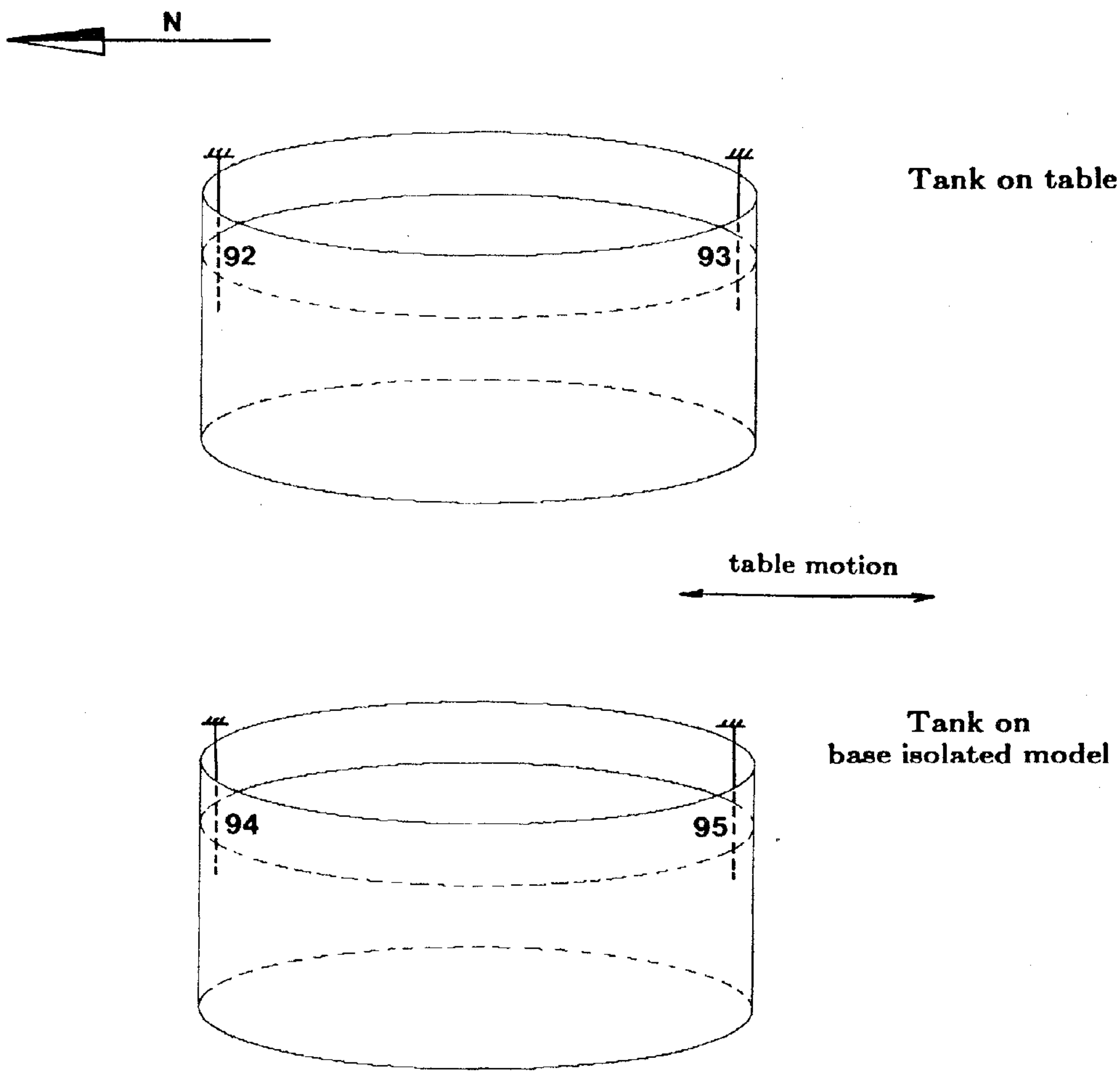

Figure 2.6 Location and channel numbering of water level gages.

CHAPTER THREE
THEORETICAL SOLUTION

1. General.

The equations of fluid motion for many applications have been solved with various boundary conditions [4, 5]. Of particular interest were fluid containers of cylindrical shape because of their numerous applications ranging from ground supported containers to aircraft fuel tanks. The problem of forced oscillations of a fluid induced by the vibrations of its container is old and equivalent mechanical models have been proposed [6].

In the following treatment, the equations of motion relevant to our problem will be stated for completeness, then solved using commonly accepted boundary conditions for cylindrical fluid containers. It is found, however, that the solution can be carried out differently in order to yield an expression for the quantities of interest, such as dynamic pressure at the tank wall and water surface deformation, in terms of convolution integrals that represent the responses of single degree of freedom oscillators of frequencies equal to the ones of the fluid sloshing modes, and subjected to the ground motion. These integrals can be easily determined, and the exact solution involving the first few modes can be directly used. This approach is much closer to the real behavior than the mechanical analogs currently used in tank design. Furthermore, the expressions for the pressure and water elevation time histories proposed here are simple to evaluate at any location in the tank, and render the conversion of the hydrodynamics problem into a mechanical analogy unnecessary.

It is shown that the dynamic pressure at the tank wall is highly influenced by the ground acceleration, and hence can be drastically reduced by base isolation.

2. Governing Equations - Boundary Conditions.

Consider a cylindrical tank of radius R_0 and height H filled to a depth h with a fluid of density ρ, and subjected to a horizontal translation described by a function of time $v_g(t)$. A cylindrical coordinate system (r,ϕ,z) is used and is shown in Figure 3.1. u, v and w are the water particle velocities in the r, ϕ and z directions, respectively. Assuming that the fluid is nonviscous, denoting by P the total fluid pressure and by F an external force potential, the equations of motion for the water particles satisfy Euler's equations:

$$\frac{\partial u}{\partial t} + u\frac{\partial u}{\partial r} + \frac{v}{r}\frac{\partial u}{\partial \phi} + w\frac{\partial u}{\partial z} - \frac{v^2}{r} = -\frac{1}{\rho}\frac{\partial P}{\partial r} - \frac{\partial F}{\partial r} \tag{3.1a}$$

$$\frac{\partial v}{\partial t} + u\frac{\partial v}{\partial r} + \frac{v}{r}\frac{\partial v}{\partial \phi} + w\frac{\partial v}{\partial z} + \frac{vu}{r} = -\frac{1}{\rho r}\frac{\partial P}{\partial \phi} - \frac{\partial F}{\partial \phi} \tag{3.1b}$$

$$\frac{\partial w}{\partial t} + u\frac{\partial w}{\partial r} + \frac{v}{r}\frac{\partial w}{\partial \phi} + w\frac{\partial w}{\partial z} = -\frac{1}{\rho}\frac{\partial P}{\partial z} - \frac{\partial F}{\partial z} \tag{3.1c}$$

For an irrotational fluid flow, the equations expressing the irrotationality condition in polar coordinates are

$$\frac{1}{r}\frac{\partial w}{\partial \phi} - \frac{\partial v}{\partial z} = 0 \tag{3.2a}$$

$$\frac{\partial u}{\partial z} - \frac{\partial w}{\partial r} = 0 \tag{3.2b}$$

$$\frac{\partial v}{\partial r} + \frac{v}{r} - \frac{1}{r}\frac{\partial u}{\partial \phi} = 0 \tag{3.2c}$$

If $\vec{V}$ denotes the water particle velocity vector, then $\vec{\text{curl}}\,\vec{V} = \vec{0}$ and there exists a scalar function $\Omega(r,\phi,z,t)$ that would define a velocity potential, or such that $\vec{\nabla}\,\Omega = \vec{V}$. This equation is equivalent to three scalar equations, namely:

$$-\frac{\partial \Omega}{\partial r} = u \tag{3.3a}$$

$$-\frac{1}{r}\frac{\partial \Omega}{\partial \phi} = v \tag{3.3b}$$

$$-\frac{\partial \Omega}{\partial z} = w \tag{3.3c}$$

Substituting equations (3.2a,b,c) and (3.3a,b,c) into equations (3.1a,b,c), and integrating the three resulting equations with respect to r, ϕ and z, respectively, we have

$$-\frac{\partial \Omega}{\partial t} + \frac{P}{\rho} + F + \frac{1}{2}(u^2 + v^2 + w^2) = G(\phi,z,t)$$

$$-\frac{\partial \Omega}{\partial t} + \frac{P}{\rho} + F + \frac{1}{2}(u^2 + v^2 + w^2) = H(r,z,t)$$

$$-\frac{\partial \Omega}{\partial t} + \frac{P}{\rho} + F + \frac{1}{2}(u^2 + v^2 + w^2) = L(r,\phi,t)$$

where G, H and L are arbitrary functions. Noting that the left hand sides are the same expression and that r, ϕ and z are independent variables, the arbitrary functions on the right hand side are all the same function of time only, G(t). Thus, the preceding treatment reduces to the Bernouilli equation

$$-\frac{\partial\Omega}{\partial t} + \frac{P}{\rho} + F + \frac{1}{2}(u^2 + v^2 + w^2) = G(t) \tag{3.4}$$

A function f(t) is defined such that $G(t) = \frac{df(t)}{dt}$, and when substituted in equation (3.4), a new velocity potential $\Theta = \Omega + f(t)$ can be defined. The total pressure $P(r,\phi,z,t)$ is then expressed as

$$P(r,\phi,z,t) = \rho\,(\frac{\partial\Theta}{\partial t} - \frac{1}{2}\{u^2 + v^2 + w^2\} - F)$$

Linear wave theory is developed for small velocity magnitude and neglects the term V^2; thus,

$$P(r,\phi,z,t) = \rho\,(\frac{\partial\Theta}{\partial t} - F)$$

Furthermore the only body force acting on the fluid is gravity and F can be replaced by -gz where g is the gravitational constant:

$$P(r,\phi,z,t) = \rho\,(\frac{\partial\Theta}{\partial t} + gz) \tag{3.5}$$

Note that the total pressure is here expressed as the sum of the static component ρgz and the dynamic component $\rho\frac{\partial\Theta}{\partial t}$.

From the definition of Θ, equations (3.3a,b,c) can be rewritten as

$$-\frac{\partial\Theta}{\partial r} = u \tag{3.6a}$$

$$-\frac{1}{r}\frac{\partial\Theta}{\partial\phi} = v \tag{3.6b}$$

$$-\frac{\partial\Theta}{\partial z} = w \tag{3.6c}$$

For constant fluid density, the condition of continuity in cylindrical coordinates is written

$$\frac{\partial u}{\partial r} + \frac{u}{r} + \frac{1}{r}\frac{\partial v}{\partial\phi} + \frac{\partial w}{\partial z} = 0 \tag{3.7}$$

When equations (3.6a,b,c) are substituted in equation (3.7), the Laplace equation to be solved for the velocity potential is obtained:

$$\frac{\partial^2\Theta}{\partial r^2} + \frac{1}{r}\frac{\partial\Theta}{\partial r} + \frac{1}{r^2}\frac{\partial^2\Theta}{\partial\phi^2} + \frac{\partial^2\Theta}{\partial z^2} = 0 \tag{3.8}$$

At the free surface, the pressure P is constant at all points. This is expressed by setting to zero the total derivative of P with respect to time:

$$\frac{DP}{Dt} = \frac{\partial P}{\partial t} + u\frac{\partial P}{\partial r} + \frac{v}{r}\frac{\partial P}{\partial\phi} + w\frac{\partial P}{\partial z} = 0 \tag{3.9}$$

at the level z=0. Note that if the free surface deflection is expressed by a function $\eta(r,\phi,z,t)$ the above condition should be satisfied at $z = \eta$. Setting the condition at z=0 is, however, a commonly accepted approximation. Substituting equation (3.9) into equation (3.8) yields the free surface boundary condition

$$\frac{\partial^2\Theta}{\partial t^2} + g\frac{\partial\Theta}{\partial z} = 0 \qquad \text{at } z = 0 \tag{3.10}$$

At the bottom of the tank, the fluid particles have zero vertical velocity. This results in the bottom boundary condition

$$\frac{\partial\Theta}{\partial z} = 0 \qquad \text{at } z = -h \tag{3.11}$$

At the tank lateral surface the water particles and the tank wall must have the same velocity. Since the tank is considered rigid, its displacement in the x direction is described by the ground motion $v_g(t)$. Along r the tank wall velocity is then $v_{g,t}(t)\cos\phi$ and we can write

$$u = \frac{\partial\Theta}{\partial r} = v_{g,t}(t)\cos\phi \qquad \text{at } r = R_o \tag{3.12}$$

3. Solution.

Equation (3.8) can be solved by separation of variables. If the velocity potential Θ is considered as the product of three functions at any given time t, we have

$$\Theta(r,\phi,z) = R(r)\ \Phi(\phi)\ Z(z)$$

Substituting in equation (3.8) and dividing by $R\ \Phi\ Z$ we have

$$\frac{\Phi_{,\phi\phi}}{\Phi} = -r^2\frac{Z_{,zz}}{Z} - r^2\frac{R_{,rr}}{R} - r\frac{R_{,r}}{R}$$

Since Φ is a function of ϕ only while Z and R do not depend on ϕ, $\frac{\Phi_{,\phi\phi}}{\Phi}$ is equal to a constant. Note that, in order to determine the sign of this constant, we must have $\Phi(2\pi) = \Phi(0)$. Thus Φ has to be a combination of trigonometric functions and the constant is then negative; and the above equation yields

$$\frac{\Phi_{,\phi\phi}}{\Phi} = -k^2$$

which has the solution

$$\Phi(\phi) = K_1 \cos k\phi + K_2 \sin k\phi$$

where K_1 and K_2 are arbitrary constants and $k \neq 0$ since $\Phi(\phi)$ must not be constant. Also we have

$$\frac{Z_{,zz}}{Z} = \frac{k^2}{r^2} - \frac{1}{r}\frac{R_{,r}}{R} - \frac{R_{,rr}}{R} = n^2 \tag{3.13}$$

where n is a constant by the same reasoning followed earlier. If $n = 0$, then

$$Z_0 = K_3\, z + K_4$$

where K_3 and K_4 are arbitrary constants. The equation in R, for this case ($n = 0$) is rewritten as

$$r R_{,r} + r^2 R_{,rr} - k^2 R = 0$$

for which $R(r) = r^m$ is a general solution. When $R(r) = r^m$ is substituted into the above expression and the indicial equation solved for m, we find $m = \pm k$ and

$$R = K_5 r^k + K_6 r^{-k}$$

For the case where $n \neq 0$, equation (3.13) in $Z(z)$ has the solution

$$Z(z) = K_7 \cosh nz + K_8 \sinh nz$$

and the equation in $R(r)$ is a Bessel equation of order k and parameter n

$$r^2 R_{,rr} + r R_{,r} + (n^2 r^2 - k^2) R = 0$$

Its general solution has the form

$$R(r) = K_9 J_k(nr) + K_{10} Y_k(nr)$$

and since for $r = 0$ the velocity potential is finite, $K_{10} = 0$.

Finally, the general solution for the velocity potential can be written as

$$\Theta = \Theta_0 + \Theta_n$$

where Θ_0 and Θ_n are the two solutions corresponding to the cases $n = 0$ and $n \neq 0$, respectively:

$$\Theta_0(r,\phi,z) = (K_1 \cos k\phi + K_2 \sin k\phi)(K_3 z + K_4)(K_5 r^k + K_6 r^{-k})$$

$$\Theta_n(r,\phi,z) = (K_1 \cos k\phi + K_2 \sin k\phi)(K_7 \cosh nz + K_8 \sinh nz)(K_9 J_k(nr))$$

The Boundary Condition in equation (3.12) is satisfied if

$$(K_1 \cos k\phi + K_2 \sin k\phi)(K_3 z + K_4)(K_5 k R_o^{k-1} + K_6 k R_o^{-k-1}) = v_{g,t}(t) \cos\phi \tag{3.14a}$$

and

$$(K_1 \cos k\phi + K_2 \sin k\phi)(K_3 \cosh nz + K_4 \sinh nz)\, K_9 J_k'(nR_o) = 0 \tag{3.14b}$$

Equation (3.14a) yields

$k = 1$, $K_2 = K_3 = K_6 = 0$,

$K_1 K_4 K_5 = v_{g,t}(t)$, and $\Theta_0 = v_{g,t}(t)\, r \cos\phi$;

while equation (3.14b) yields after substitution of the determined coefficients

$$(K_1 \cos\phi)(K_3 \cosh nz + K_4 \sinh nz) K_9 J_1'(n R_o) = 0$$

Therefore,

$$J_1'(nR_o) = 0$$

The above equation has an infinite number of real roots for which the derivative of the Bessel function of the first kind and first order is zero. If we denote by $n_i R_o = \alpha_i$ the i^{th} root α_i of $J_1'(\alpha) = 0$, we have (see Table 3.1)

$$\alpha_i = n_i R_o = 1.84118, \quad 5.33144, \quad 8.53632, \quad 11.70600, \quad 14.86359,$$
$$18.01553, \quad 21.16437, \quad 24.31133, \quad 27.45705, \quad 30.60192, \quad \text{etc} \cdots$$

and the general expression for the velocity potential becomes

$$\Theta = \sum_{i=1}^{i=\infty} K_i \, J_1(n_i r)(K_{7_i} \cosh n_i z + K_{8_i} \sinh n_i z) \cos\phi \; + \; v_{g,t}(t)\, r \cos\phi \tag{3.14c}$$

The Boundary Condition for the bottom of the tank, in equation (3.11), applied to the above expression yields

$$K_{7_i} \sinh n_i h = K_{8_i} \cosh n_i h$$

Substituting for K_{8_i} in equation (3.14c) and rearranging the hyperbolic functions, we have

$$\Theta = \sum_{i=1}^{i=\infty} K_i \, J_1(n_i r) \, \frac{\cosh n_i (z+h)}{\cosh n_i h} \cos\phi \; + \; v_{g,t}(t)\, r \cos\phi \tag{3.15}$$

Note that up to this point in the preceding treatment, the equations were developed for a given time t and hence the constants can be functions of time. In order to determine $K_i(t)$, we apply the free surface boundary condition given by equation (3.10) to equation (3.15):

$$\frac{\partial^2 \Theta}{\partial t^2} = \sum_{i=1}^{i=\infty} K_{i,tt}(t) \, J_1(n_i r) \, \frac{\cosh n_i (z+h)}{\cosh n_i h} \cos\phi \; + \; v_{g,ttt}(t)\, r \cos\phi$$

and

$$g \, \frac{\partial \Theta}{\partial z} = g \sum_{i=1}^{i=\infty} K_i(t) \, n_i \, J_1(n_i r) \, \frac{\sinh n_i (z+h)}{\cosh n_i h} \cos\phi$$

The sum of the two above expressions for z=0 yields, after we simplify by $\cos\phi$,

$$\sum_{i=1}^{i=\infty} \left[K_{i,tt}(t) + (g\, n_i \tanh n_i h)\, K_i(t) \right] J_1(n_i r) \; + \; v_{g,ttt}\, r = 0 \qquad (3.16)$$

Equation (3.16) can now be easily solved for the free vibrations if the term $v_{g,ttt}(t)$ representing the forcing function is discarded. $K_i(t)$ will then be a trigonometric function and the frequencies of free oscillations are $(g\, n_i \tanh n_i h)^{1/2}$. In the following, however, the forced oscillations solution will be pursued. By denoting the first expression in the brackets by T(t),

$$T(t) = \sum_{i=1}^{i=\infty} \left[K_{i,tt}(t) + (g\, n_i \tanh n_i h)\, K_i(t) \right]$$

equation (3.16) can be solved for T(t) by noticing that the Bessel solutions satisfy certain Boundary Conditions that make them orthogonal on the interval $\{0, R_o\}$:

$$A_1 J_1(n_i 0) - B_1 J_1'(n_i 0) = 0 \qquad\qquad \text{with } B_1 = 0$$

and

$$A_2 J_1(n_i R_o) - B_2 J_1'(n_i R_o) = 0 \qquad\qquad \text{with } A_2 = 0$$

To use the orthogonality of the Bessel functions, expression (3.16) is multiplied by $r J_1(n_j r)$, so that

$$\sum_{i=1}^{i=\infty} T(t) J_1(n_i r) J_1(n_j r)\, r \; + \; v_{g,ttt}\, r^2 J_1(n_j r) = 0$$

and integrated over the interval { 0 and R_o}. When the only non zero term in the summation is retained, we find

$$T(t) \int_0^{R_o} J_1^2(n_j r)\, r\, dr \; + \; v_{g,ttt} \int_0^{R_o} r^2 J_1(n_j r)\, dr = 0$$

After the two integrals are evaluated, and the above expression solved for $T(t)$, we have

$$T(t) = v_{g,ttt}(t)\, \chi_j$$

or

$$K_{j,tt}(t) + \lambda_j^2 K_j(t) = v_{g,ttt}(t)\chi_j \tag{3.17}$$

where

$$\lambda_j = (g\, n_j \tanh n_j h)^{1/2} \qquad \text{and} \qquad \chi_j = \frac{2 R_o^2 J_2(n_j R_o)\, n_j}{J_1^2(n_j R_o)(1 - (n_j R_o)^2)}$$

The expression for χ_j is further simplified by the use of the Bessel function identity

$$J_{v+1}(x) = \frac{v}{x} J_v(x) - J_v'(x)$$

and by noting that $J_1'(n_j R_o) = 0$. The expression for χ_j becomes

$$\chi_j = \frac{2 R_o}{J_1(n_j R_o)(1 - (n_j R_o)^2)}$$

Equation (3.17) for $K_j(t)$ is transformed to the Laplace domain and the initial conditions on $v_g(t)$ are used. The expression is then solved algebraically for $\overline{K}_i(s)$ where s is the Laplace transform variable. The following two properties of the Laplace transform,

$$L\{f''(t)\} = s^2 L\{f(t)\} - s f(0) - f'(0)$$

and

$$L\{f'''(t)\} = s^3 L\{f(t)\} - s^2 f(0) - s f'(0) - f''(0)$$

are used, together with the assumption that the shake table, and hence the structural model motions, start from rest; so that $v_g(0) = v_{g,t}(0) = v_{g,tt}(0) = 0$. Since the water particle velocities are initially zero, $\Theta(t = 0) = 0$, and since the dynamic pressure in the fluid is initially null, $\frac{\partial \Theta}{\partial t}(t = 0) = 0$, and this yields $K_j(0) = K_{j,t}(0) = 0$. When the transform of equation (3.17) is solved for $\overline{K}_j$, it yields

$$\overline{K}_j(s) = \frac{s^3 \overline{v}_g(s)}{s^2 + \lambda_j^2} \chi_j \tag{3.18}$$

Equation (3.18) describes the response of a physical system to a given excitation, and the relation between the input and the output for zero initial conditions of the excitation $v_g(t)$ has the form

$$\overline{K}_j(s) = \frac{\overline{v}_g(s)}{TR_j(s)}$$

where $TR_j(s)$ is a transfer function. Furthermore since the present system is linear, $TR_j(s)$ is simply the quotient of two polynomials in s :

$$TR_j(s) = \frac{s^2 + \lambda_j^2}{\chi_j\, s^3}$$

The Laplace transformation of the product of two functions of the same variable is expressed as

$$L\{f(t)\}\, L\{g(t)\} = L\{\int_0^t f(t-\tau)\, g(\tau)\, d\tau\} = L\{f(t) * g(t)\} \qquad \text{(notation)}$$

To apply the above theorem, the convolution or Faltung integral theorem, to equation (3.18), we rewrite it in the form

$$\overline{K}_i(s) = \left(\frac{s}{s^2 + \lambda_i^2}\right)(s^2\,\overline{v}_g(s))\chi_i = L\{\cos\lambda_i t\}\, L\{v_{g,tt}(t)\}\,\chi_i$$

Then

$$K_i(t) = \int_0^t \chi_i \cos\lambda_i (t-\tau)\, v_{g,tt}(\tau)\, d\tau \tag{3.19}$$

Finally the velocity potential takes the form

$$\Theta(r,\phi,z,t) = \sum_{i=1}^{i=\infty} \chi_i \left[\int_0^t \cos\lambda_i(t-\tau)\, v_{g,tt}(\tau)\, d\tau \right] J_1(n_i r) \frac{\cosh n_i(z+h)}{\cosh n_i h} \cos\phi$$

$$+ \; v_{g,t}(t)\, r \cos\phi \tag{3.20}$$

The dynamic pressure and the water surface deformation can now be expressed from the velocity potential. The dynamic pressure in the fluid is given by

$$P_d(r,\phi,z,t) = \rho \frac{\partial\Theta}{\partial t}$$

$$= \rho \cos\phi \sum_{i=1}^{i=\infty} \chi_i \left[v_{g,tt}(t) - \lambda_i \int_0^t \sin\lambda_i(t-\tau)\, v_{g,tt}(\tau)\, d\tau \right] J_1(n_i r) \frac{\cosh n_i(z+h)}{\cosh n_i h}$$

$$+ \; \rho\, v_{g,tt}(t)\, r \cos\phi \tag{3.21}$$

The pressure at the tank wall in the plane of excitation is obtained for $r = R_o$ and $\phi = 0$. Rearranging the terms in $v_{g,tt}(t)$, we have

$$\frac{P_d}{\rho R_o} = v_{g,tt}(t) \left(1 + \sum_{i=1}^{i=\infty} C_i \right) - \sum_{i=1}^{i=\infty} C_i \lambda_i I_i(t) \tag{3.22}$$

where

$$C_i = \frac{2}{1 - (n_i R_o)^2} \, \frac{\cosh n_i(z+h)}{\cosh n_i h} \tag{3.23}$$

and

$$I_i(t) = \int_0^t \sin\lambda_i(t-\tau)\, v_{g,tt}(\tau) d\tau \tag{3.24}$$

The convolution integrals $I_i(t)$ can be directly used without transforming the oscillating fluid into a mechanical equivalent system, since they each represent the undamped response of a single degree of freedom oscillator of frequency λ_i, subjected to ground acceleration $v_{g,tt}(t)$. Two points of interest are to be noted:

(1) The coefficients C_i and $\lambda_i C_i$ which control the rate of convergence of the solution decay very rapidly especially at larger depths z; and the convolution integrals are bounded with the maximum value of an $I_i(t)$ being the spectral pseudo-velocity response for a single degree of freedom oscillator of frequency λ_i. Table 3.2 lists those coefficients for the radius $R_o = 24$ in. and for z varying from 0 in. at the water free surface to -17.5 in. at the tank bottom. These numerical values correspond to the tanks used in the experiment. The coefficients are highest at the water surface and decrease with depth; this decrease depends on the mode number. For the first mode, C_1 at the bottom is 48% of C_1 at the water surface, while for the second mode, C_2 at the bottom is about 4% of C_2 at the surface. On the other hand, for a given depth z the coefficients decay rapidly and the two or three first coefficients are enough to yield accurate results. The values of $\lambda_i C_i$ were evaluated and presented in Table 3.3. At the water surface (z=0) where the sloshing contributes most, the fourth mode coefficient $\lambda_4 C_4$ is 4.7% of $\lambda_1 C_1$ and is 3.8% of the sum of the first three constants. The C_i's and the $\lambda_i C_i$'s are plotted in Figures 3.2 to 3.5.

Similar results are obtained when these coefficients are multiplied by their respective convolution integrals. These integrals were evaluated for the first four modes (i=1,..4) for the El Centro and San Francisco table motions at horizontal spans of 50. The forcing functions used were the shake table recorded acceleration and the isolated base recorded acceleration, respectively. Their time history plots are shown in Figures 3.6 and 3.7 for El Centro and in Figures 3.12 and 3.13 for San Francisco. In sum, the first two modes yield accurate results at higher depths and the first three modes at the water free surface.

(2) Equation (3.22) shows explicitly the different factors influencing the dynamic pressure. The first term

$$P_{d_1} = \rho \, R_o \, v_{g,tt} \left(1 + \sum_{i=1}^{i=\infty} C_i \right) \qquad (3.25)$$

represents the direct effect of ground acceleration, and the term

$$P_{d_2} = \rho\ R_o \sum_{i=1}^{i=\infty} \lambda_i C_i I_i(t) \tag{3.26}$$

represents the effect of the sloshing modes.

To illustrate this effect, P_{d_1} and P_{d_2} were evaluated using two modes only and were plotted in Figures 3.8a to 3.9b for the El Centro record and in Figures 3.14a to 3.15b for the San Francisco record, at the location z=-16 in. The resultant pressure time histories for the tank on the table and the tank in the structure were then obtained by summing these components. For the El Centro record, Figures 3.10 and 3.11 show the calculated dynamic pressure time histories using the recorded table acceleration and the recorded isolated base acceleration as forcing functions, respectively. Figures 3.16 and 3.17 show the same for the San Francisco record. Note the drastic reduction in the calculated dynamic pressure for the tank in the structure under the San Francisco record.

The free surface displacement is given by

$$\eta(r,\phi,z,t) = \frac{1}{g}\ \frac{\partial\Theta}{\partial t} \qquad \text{at } z = 0$$

$$= \frac{\cos\phi}{g} \sum_{i=1}^{i=\infty} \left[v_{g,tt} - \lambda_i \int_0^{R_o} \sin\lambda_i(t-\tau)\, v_{g,tt}(\tau)d\tau \right] J_1(n_i\, r) + \frac{\cos\phi}{g} r v_{g,tt} \tag{3.27}$$

At the tank wall and along the diameter of excitation, we have

$$\frac{\eta}{R_o/g} = v_{g,tt}(t)\,(1 + \sum_{i=1}^{i=\infty} C_i') - \sum_{i=1}^{i=\infty} C_i'\lambda_i I_i(t) \tag{3.28}$$

where the constants C_i' are the C_i's at z=0. As mentioned above, the contribution of the sloshing at z=0 is much more important than it is at other locations along the water depth. Nevertheless, only the first three modes are needed to yield accurate results.

In many design situations, only the Peak Ground Acceleration and the response spectrum of the selected design earthquake are given. By noting that the maximum value of $\lambda_i I_i(t)$ is the spectral acceleration S_{a_i}, expressions (3.22) and (3.28) can be used to provide an upper bound of the fluid response. Equation (3.22), for instance yields

$$\frac{P_d}{\rho R_o} \leq \ddot{v}_{max}(1 + \sum_{i=1}^{i=\infty} C_i) + \sum_{i=1}^{i=\infty} C_i S_{a_i}$$

Furthermore, since it was found that a few modes yield good results, the sum can be limited to the first three terms (i=1,2,3) and the root mean square values used similarly to a response spectra analysis for multi-degrees of freedom systems. The predictions of peak values can now be written as

$$\frac{P_d}{\rho R_o} \leq \ddot{v}_{max}(1 + \sum_{i=1}^{i=3} C_i) + (\sum_{i=1}^{i=3} C_i^2 S_{a_i}^2)^{1/2} \tag{3.29}$$

for the dynamic pressure, and as

$$\frac{\eta}{R_o/g} \leq \ddot{v}_{max}(1 + \sum_{i=1}^{i=3} C_i') + (\sum_{i=1}^{i=3} C_i'^2 S_{a_i}^2)^{1/2} \tag{3.30}$$

for the water free surface deformation.

In the next section, the experimental results are presented and compared with the time histories obtained from expressions (3.22) and (3.28).

Table 3.1 **The first ten roots α_i of $J_1'(\alpha)$ and the sloshing frequencies λ_i in rd/sec and f_i in Hertz.**

α_i	λ_i (rd/sec)	f_i (Hz)
1.84118	5.08	0.81
5.33144	9.26	1.47
8.53632	11.72	1.87
11.70600	13.73	2.18
14.86359	15.47	2.46
18.01553	17.03	2.71
21.16437	18.46	2.94
24.31133	19.78	3.15
27.45705	21.03	3.35
30.60192	22.20	3.53

Table 3.2 Coefficients C_i for R_0=24 in. and h=17.5 in.

z	C_1	C_2	C_3	C_4	C_5	C_6
0.0	-0.836840	-0.072928	-2.782851e-2	-1.470259e-2	-9.093955e-3	-6.181247e-3
-0.5	-0.809449	-0.065268	-2.329463e-2	-1.152073e-2	-6.672215e-3	-4.246936e-3
-1.0	-0.783249	-0.058415	-1.949943e-2	-9.027484e-3	-4.895390e-3	-2.917927e-3
-1.5	-0.758202	-0.052282	-1.632257e-2	-7.073807e-3	-3.591737e-3	-2.004812e-3
-2.0	-0.734271	-0.046796	-1.366330e-2	-5.542933e-3	-2.635249e-3	-1.377440e-3
-2.5	-0.711420	-0.041887	-1.143731e-2	-4.343363e-3	-1.933476e-3	-9.463930e-4
-3.0	-0.689616	-0.037495	-9.573992e-3	-3.403396e-3	-1.418588e-3	-6.502361e-4
-3.5	-0.668827	-0.033567	-8.014278e-3	-2.666855e-3	-1.040814e-3	-4.467554e-4
-4.0	-0.649021	-0.030053	-6.708699e-3	-2.089710e-3	-7.636426e-4	-3.069509e-4
-4.5	-0.630171	-0.026910	-5.615854e-3	-1.637469e-3	-5.602829e-4	-2.108959e-4
-5.0	-0.612249	-0.024100	-4.701090e-3	-1.283099e-3	-4.110784e-4	-1.448995e-4
-5.5	-0.595227	-0.021587	-3.935404e-3	-1.005421e-3	-3.016074e-4	-9.955569e-5
-6.0	-0.579081	-0.019341	-3.294511e-3	-7.878376e-4	-2.212887e-4	-6.840144e-5
-6.5	-0.563787	-0.017333	-2.758086e-3	-6.173434e-4	-1.623592e-4	-4.699634e-5
-7.0	-0.549323	-0.015540	-2.309122e-3	-4.837481e-4	-1.191227e-4	-3.228964e-5
-7.5	-0.535667	-0.013939	-1.933382e-3	-3.790664e-4	-8.740021e-5	-2.218517e-5
-8.0	-0.522799	-0.012510	-1.618951e-3	-2.970418e-4	-6.412554e-5	-1.524270e-5
-8.5	-0.510701	-0.011235	-1.355857e-3	-2.327715e-4	-4.704908e-5	-1.047276e-5
-9.0	-0.499354	-0.010099	-1.135758e-3	-1.824141e-4	-3.452023e-5	-7.195498e-6
-9.5	-0.488742	-0.009087	-9.516751e-4	-1.429596e-4	-2.532800e-5	-4.943804e-6
-10.0	-0.478849	-0.008188	-7.977697e-4	-1.120498e-4	-1.858389e-5	-3.396746e-6
-10.5	-0.469661	-0.007390	-6.691622e-4	-8.783725e-5	-1.363604e-5	-2.333826e-6
-11.0	-0.461164	-0.006684	-5.617741e-4	-6.887478e-5	-1.000620e-5	-1.603544e-6
-11.5	-0.453346	-0.006060	-4.722002e-4	-5.402899e-5	-7.343533e-6	-1.101813e-6
-12.0	-0.446194	-0.005510	-3.976000e-4	-4.241253e-5	-5.390669e-6	-7.571229e-7
-12.5	-0.439700	-0.005029	-3.356078e-4	-3.333109e-5	-3.958849e-6	-5.203453e-7
-13.0	-0.433852	-0.004610	-2.842580e-4	-2.624187e-5	-2.909678e-6	-3.577315e-7
-13.5	-0.428642	-0.004248	-2.419221e-4	-2.072113e-5	-2.141748e-6	-2.461051e-7
-14.0	-0.424064	-0.003938	-2.072577e-4	-1.643889e-5	-1.580833e-6	-1.695559e-7
-14.5	-0.420109	-0.003677	-1.791655e-4	-1.313922e-5	-1.172715e-6	-1.171733e-7
-15.0	-0.416773	-0.003461	-1.567548e-4	-1.062488e-5	-8.779487e-7	-8.149133e-8
-15.5	-0.414050	-0.003288	-1.393149e-4	-8.745596e-6	-6.680420e-7	-5.742424e-8
-16.0	-0.411936	-0.003156	-1.262927e-4	-7.389038e-6	-5.227061e-7	-4.154179e-8
-16.5	-0.410428	-0.003062	-1.172752e-4	-6.474126e-6	-4.278933e-7	-3.158025e-8
-17.0	-0.409525	-0.003007	-1.119767e-4	-5.946174e-6	-3.744394e-7	-2.611983e-8
-17.5	-0.409223	-0.002988	-1.102290e-4	-5.773628e-6	-3.571775e-7	-2.438224e-8

Table 3.3 Coefficients $\lambda_i C_i$ for R_0=24 in. and h=17.5 in.

z	$\lambda_1 C_1$	$\lambda_2 C_2$	$\lambda_3 C_3$	$\lambda_4 C_4$	$\lambda_5 C_5$	$\lambda_6 C_6$
0.0	-4.255306	-0.675378	-0.326239	-2.018417e-1	-1.406785e-1	-1.052720e-1
-0.5	-4.116024	-0.604440	-0.273088	-1.581602e-1	-1.032155e-1	-7.232897e-2
-1.0	-3.982798	-0.540975	-0.228596	-1.239321e-1	-7.572898e-2	-4.969481e-2
-1.5	-3.855435	-0.484178	-0.191353	-9.711142e-2	-5.556219e-2	-3.414367e-2
-2.0	-3.733746	-0.433373	-0.160178	-7.609510e-2	-4.076586e-2	-2.345899e-2
-2.5	-3.617550	-0.387911	-0.134082	-5.962703e-2	-2.990982e-2	-1.611789e-2
-3.0	-3.506677	-0.347237	-0.112238	-4.672287e-2	-2.194477e-2	-1.107408e-2
-3.5	-3.400965	-0.310860	-0.093953	-3.661140e-2	-1.610083e-2	-7.608629e-3
-4.0	-3.300253	-0.278318	-0.078647	-2.868819e-2	-1.181313e-2	-5.227639e-3
-4.5	-3.204401	-0.249211	-0.065836	-2.247968e-2	-8.667269e-3	-3.591739e-3
-5.0	-3.113268	-0.223187	-0.055112	-1.761478e-2	-6.359157e-3	-2.467763e-3
-5.5	-3.026712	-0.199915	-0.046136	-1.380273e-2	-4.665700e-3	-1.695519e-3
-6.0	-2.944610	-0.179115	-0.038622	-1.081568e-2	-3.423215e-3	-1.164935e-3
-6.5	-2.866840	-0.160519	-0.032334	-8.475082e-3	-2.511607e-3	-8.003882e-4
-7.0	-2.793291	-0.143914	-0.027070	-6.641043e-3	-1.842762e-3	-5.499204e-4
-7.5	-2.723851	-0.129088	-0.022665	-5.203941e-3	-1.352033e-3	-3.778325e-4
-8.0	-2.658417	-0.115854	-0.018979	-4.077882e-3	-9.919869e-4	-2.595962e-4
-8.5	-2.596899	-0.104046	-0.015895	-3.195559e-3	-7.278234e-4	-1.783601e-4
-9.0	-2.539200	-0.093526	-0.013315	-2.504236e-3	-5.340091e-4	-1.225455e-4
-9.5	-2.485238	-0.084154	-0.011157	-1.962593e-3	-3.918102e-4	-8.419723e-5
-10.0	-2.434933	-0.075828	-0.009352	-1.538254e-3	-2.874826e-4	-5.784951e-5
-10.5	-2.388212	-0.068438	-0.007845	-1.205857e-3	-2.109420e-4	-3.974707e-5
-11.0	-2.345005	-0.061900	-0.006586	-9.455344e-4	-1.547904e-4	-2.730973e-5
-11.5	-2.305251	-0.056121	-0.005536	-7.417267e-4	-1.136004e-4	-1.876483e-5
-12.0	-2.268883	-0.051028	-0.004661	-5.822524e-4	-8.339069e-5	-1.289446e-5
-12.5	-2.235861	-0.046573	-0.003934	-4.575796e-4	-6.124122e-5	-8.861928e-6
-13.0	-2.206124	-0.042693	-0.003332	-3.602565e-4	-4.501112e-5	-6.092476e-6
-13.5	-2.179632	-0.039340	-0.002836	-2.844660e-4	-3.313167e-5	-4.191382e-6
-14.0	-2.156353	-0.036469	-0.002430	-2.256782e-4	-2.445461e-5	-2.887683e-6
-14.5	-2.136242	-0.034052	-0.002100	-1.803792e-4	-1.814126e-5	-1.995562e-6
-15.0	-2.119278	-0.032052	-0.001838	-1.458616e-4	-1.358138e-5	-1.387868e-6
-15.5	-2.105432	-0.030450	-0.001633	-1.200622e-4	-1.033424e-5	-9.779844e-7
-16.0	-2.094682	-0.029227	-0.001481	-1.014390e-4	-8.085977e-6	-7.074924e-7
-16.5	-2.087014	-0.028357	-0.001375	-8.887881e-5	-6.619274e-6	-5.378388e-7
-17.0	-2.082422	-0.027847	-0.001313	-8.163092e-5	-5.792372e-6	-4.448431e-7
-17.5	-2.080887	-0.027672	-0.001292	-7.926216e-5	-5.525341e-6	-4.152504e-7

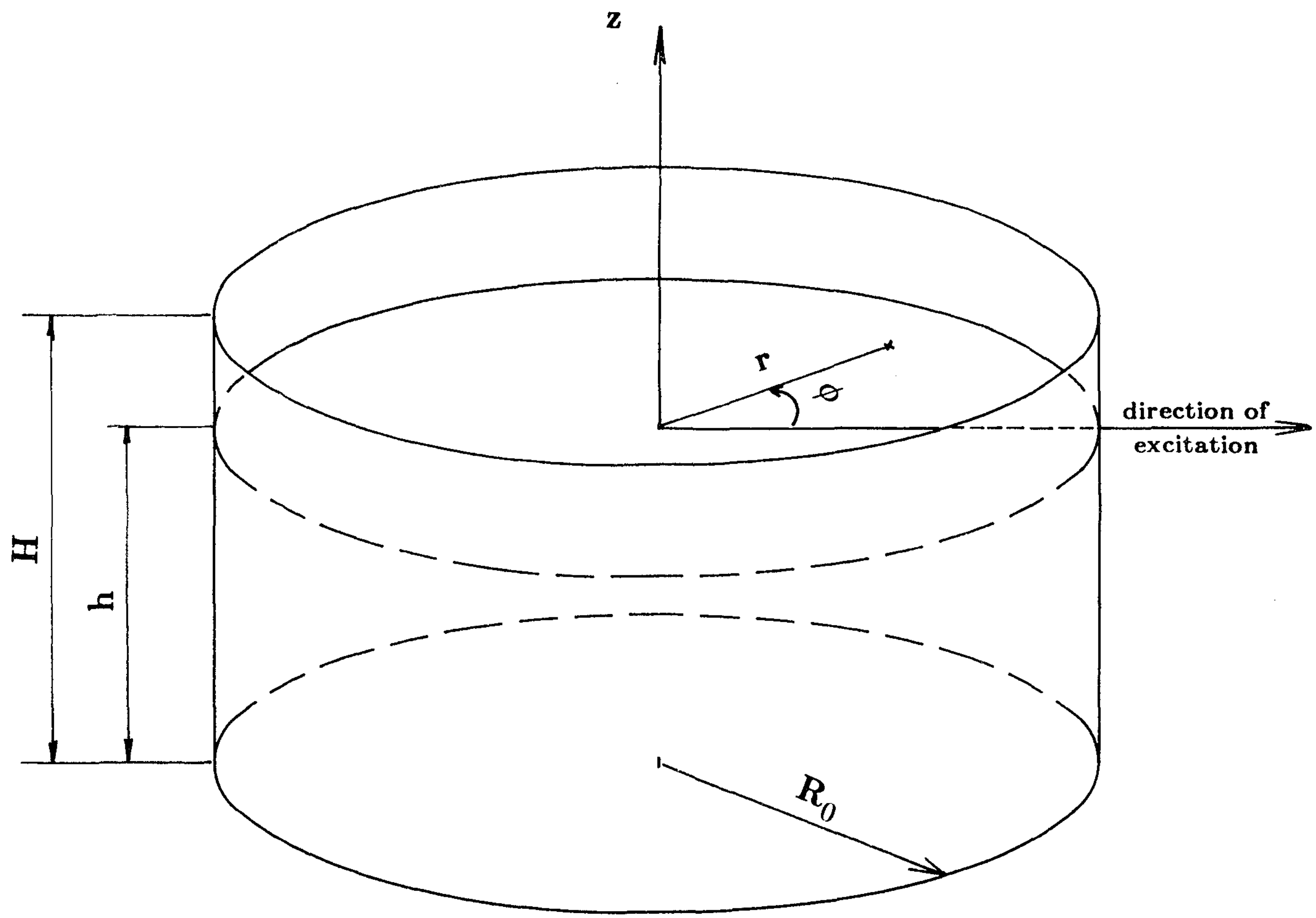

Figure 3.1 Cylindrical tank showing coordinates and dimensions.

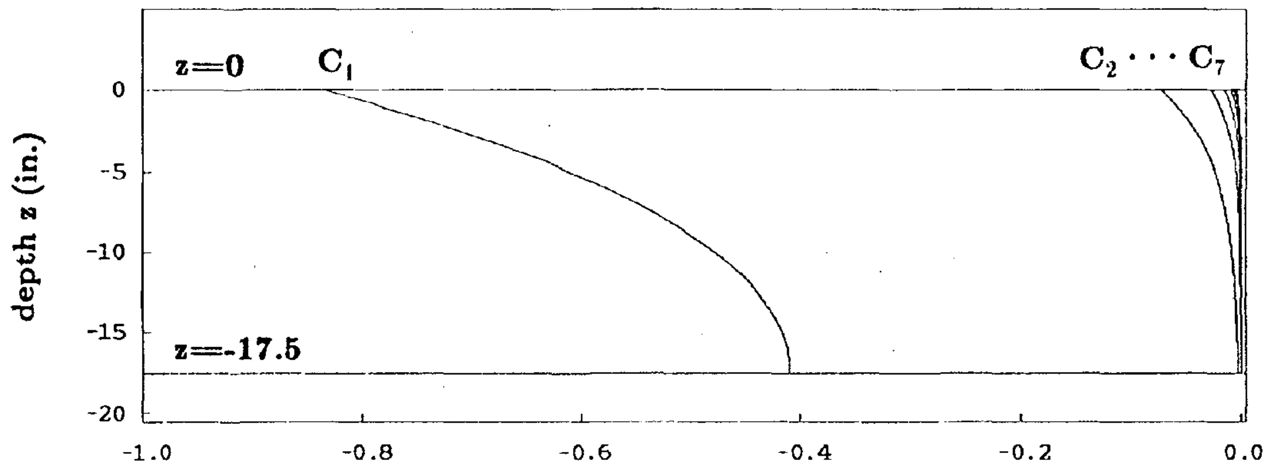

Figure 3.2 **Coefficients C_i (i=1,...,7) showing decrease with increasing depth and mode number.**

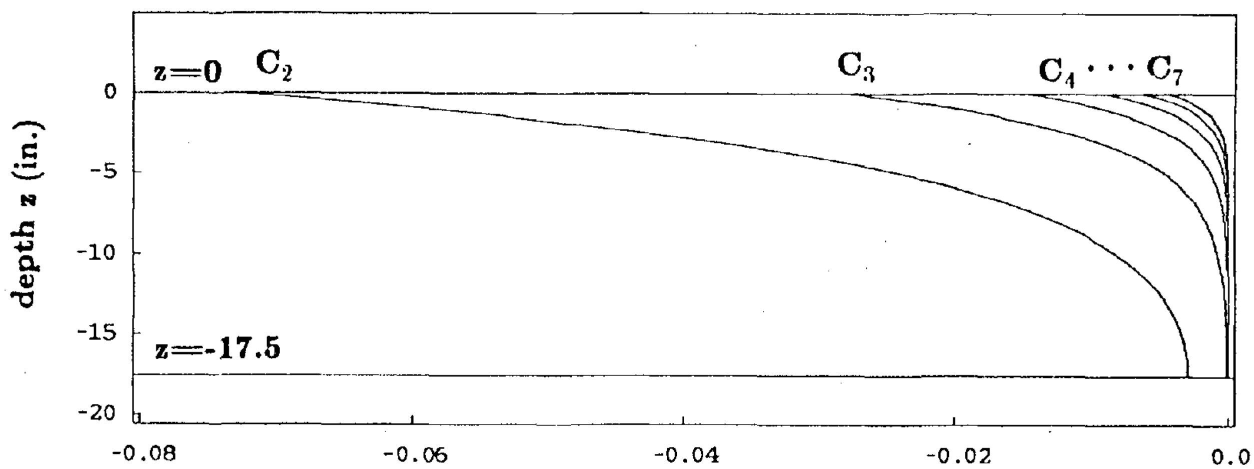

Figure 3.3 **Coefficients C_i (i=2,...,7) showing decrease with increasing depth and mode number.**

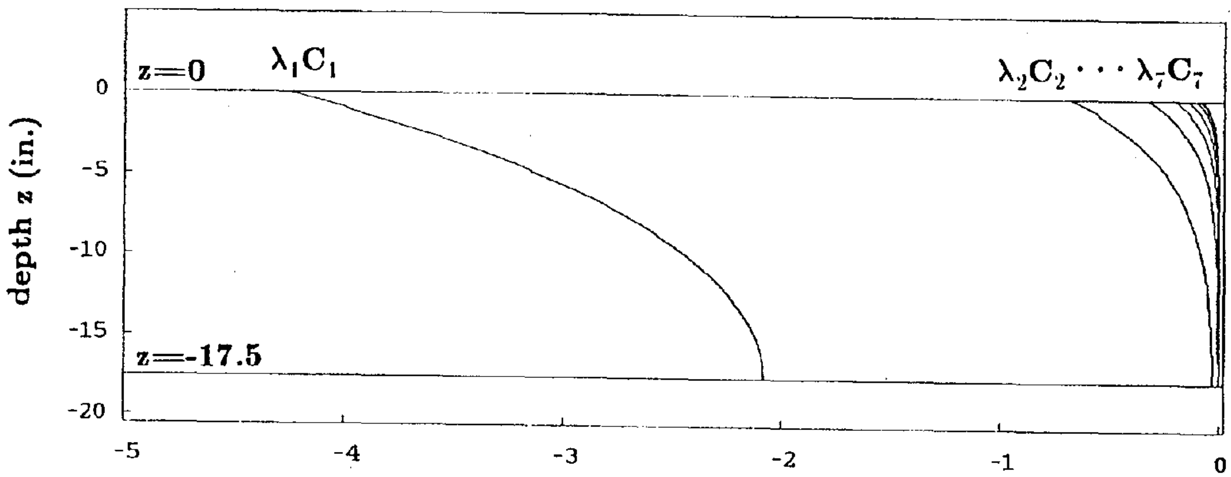

Figure 3.4 **Coefficients $\lambda_i C_i$ (i=1,...,7) showing decrease with increasing depth and mode number.**

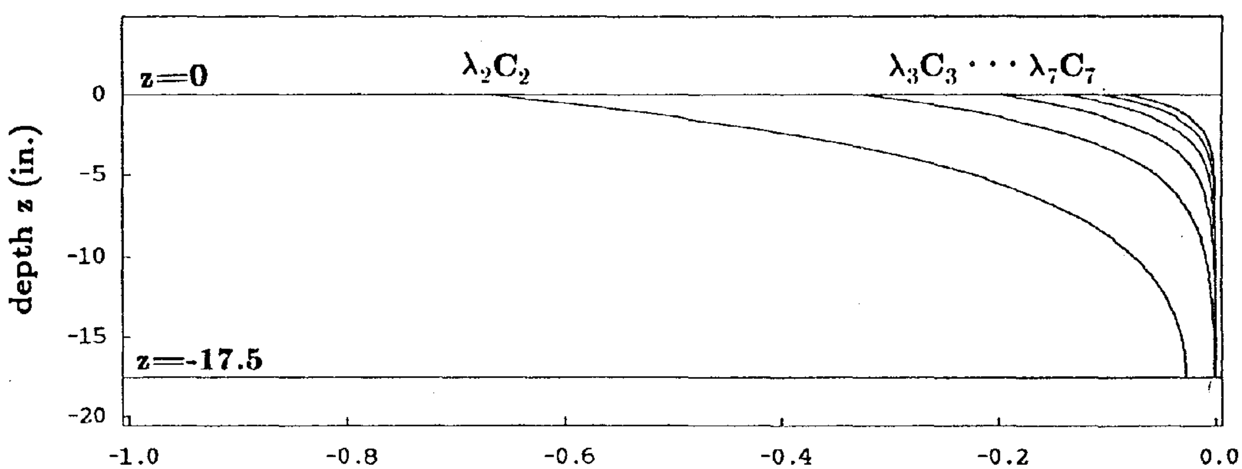

Figure 3.5 **Coefficients $\lambda_i C_i$ (i=2,...,7) showing decrease with increasing depth and mode number.**

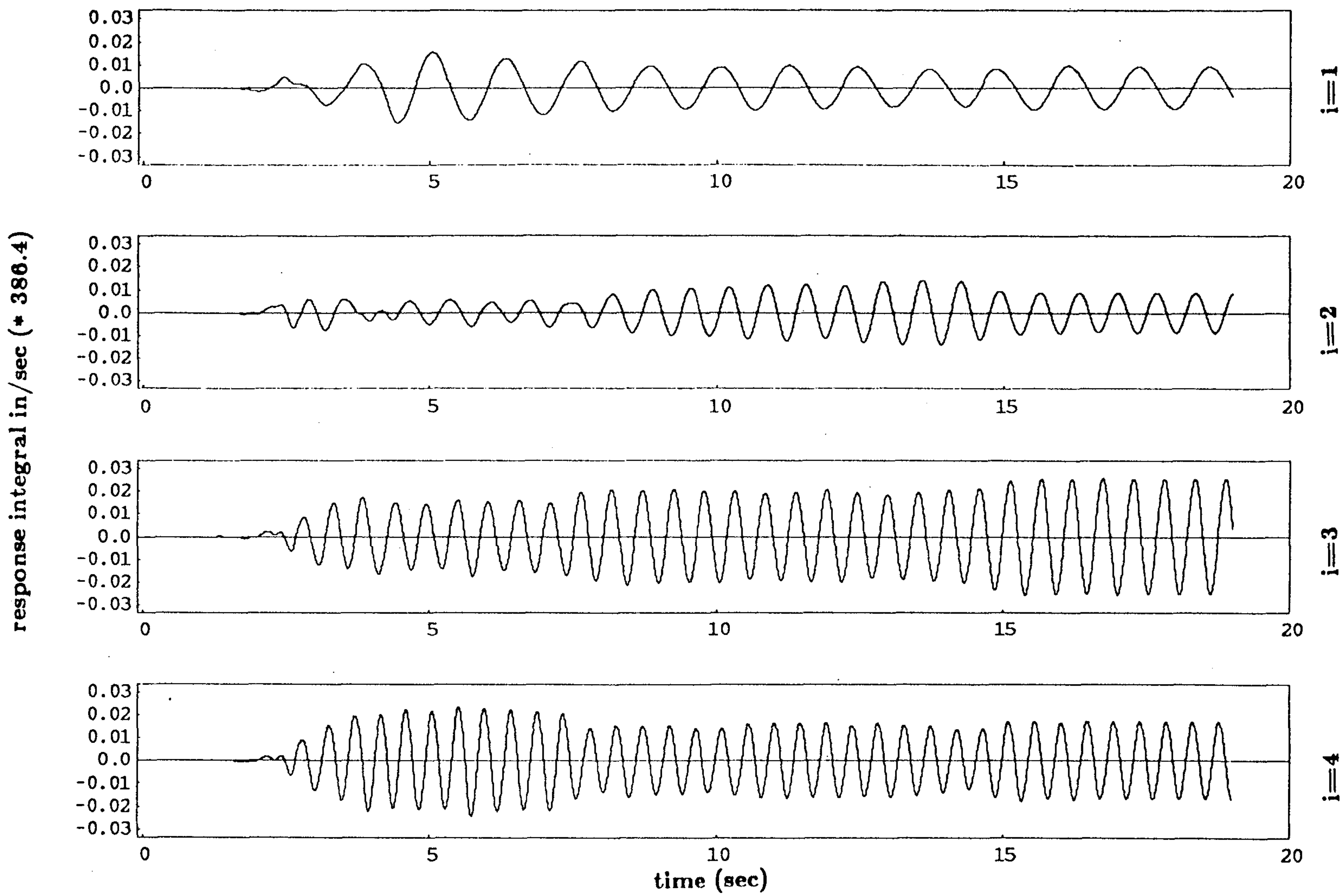

Figure 3.6 Calculated convolution integrals $I_i(t)$ ($i=1,2,3,4$) from equation (3.24). Forcing function: recorded table acceleration. Table input: $\sqrt{4}$ time scaled El Centro horizontal span 50, PTA=0.114 g.

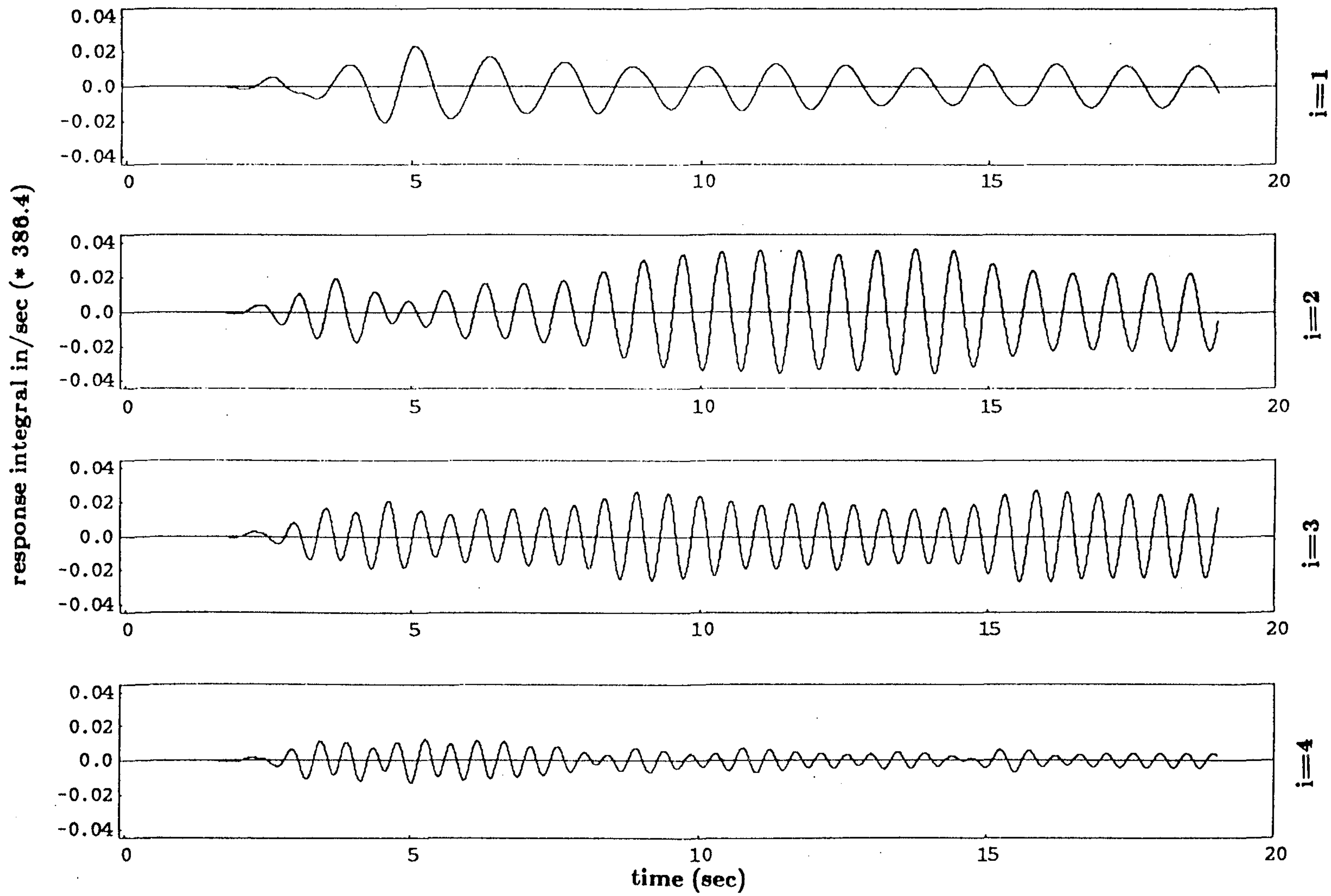

Figure 3.7 Calculated convolution integrals $I_i(t)$ (i=1,2,3,4) from equation (3.24). Forcing function: recorded structure's isolated base acceleration. Table input: $\sqrt{4}$ time scaled El Centro horizontal span 50, PTA=0.114 g.

Theoretical solution using 2 modes

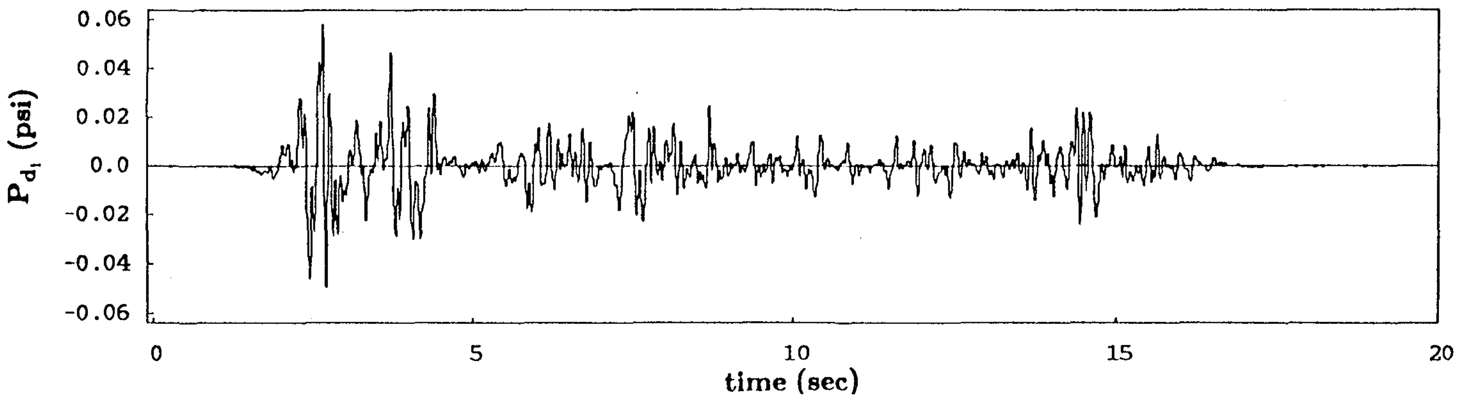

Figure 3.8a Calculated P_{d_1} component from equation (3.25) using two modes. Location: z=-16 in. Forcing function: recorded table acceleration. Table input: $\sqrt{4}$ time scaled El Centro horizontal span 50, PTA=0.114 g.

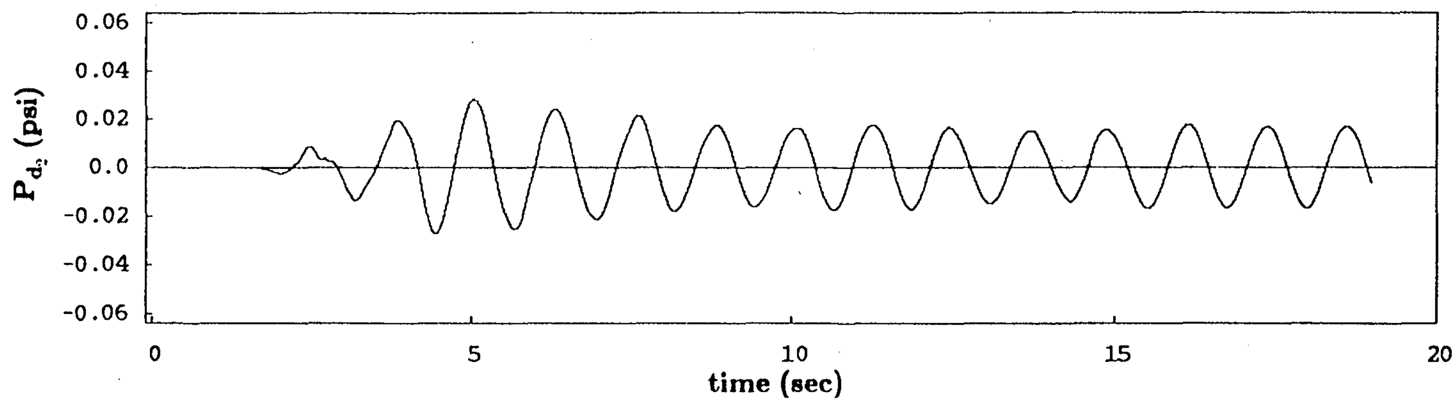

Figure 3.8b Calculated P_{d_2} component from equation (3.26) using two modes. Location: z=-16 in. Forcing function: recorded table acceleration. Table input: $\sqrt{4}$ time scaled El Centro horizontal span 50, PTA=0.114 g.

Theoretical solution using 2 modes

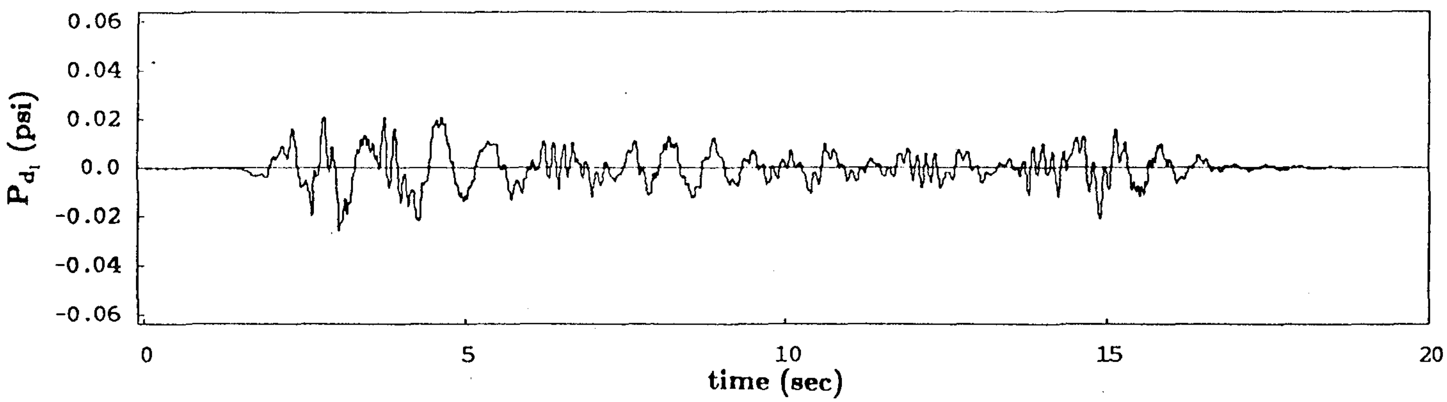

Figure 3.9a Calculated P_{d_1} component from equation (3.25) using two modes. Location: z=-16 in. Forcing function: recorded structure's isolated base acceleration. Table input: $\sqrt{4}$ time scaled El Centro horizontal span 50, PTA=0.114 g.

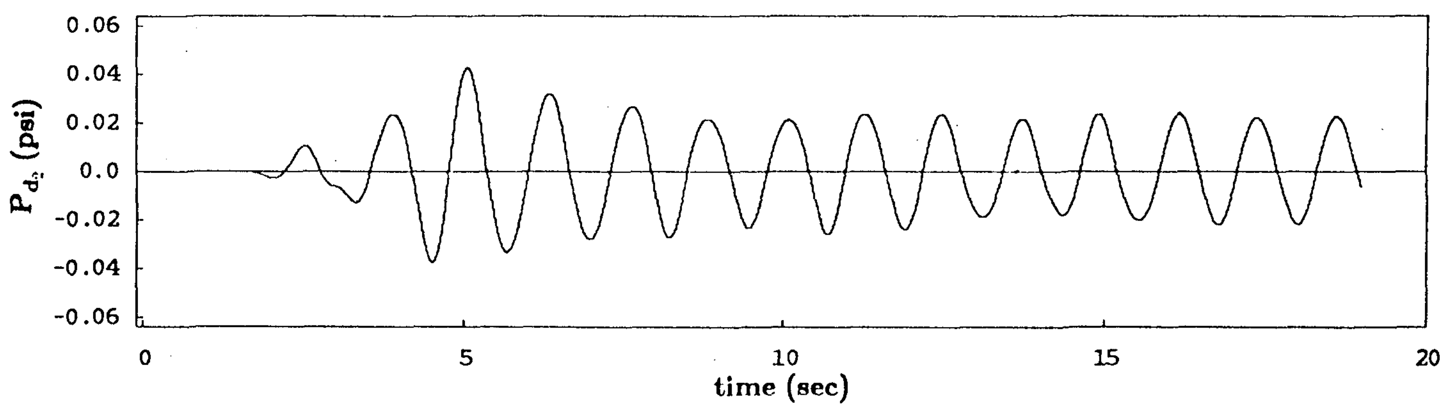

Figure 3.9b Calculated P_{d_2} component from equation (3.26) using two modes. Location: z=-16 in. Forcing function: recorded structure's isolated base acceleration. Table input: $\sqrt{4}$ time scaled El Centro horizontal span 50, PTA=0.114 g.

Theoretical solution using 2 modes

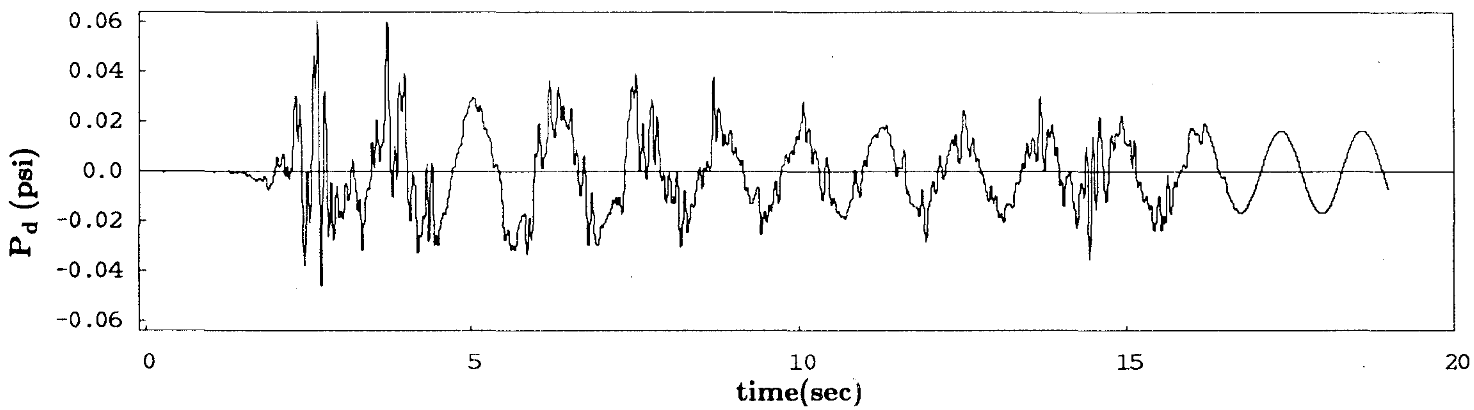

Figure 3.10 **Calculated dynamic pressure $P_d = P_{d_1} + P_{d_2}$ component using two modes. Location: z=-16 in. Forcing function: recorded table acceleration. Table input: $\sqrt{4}$ time scaled El Centro horizontal span 50, PTA=0.114 g.**

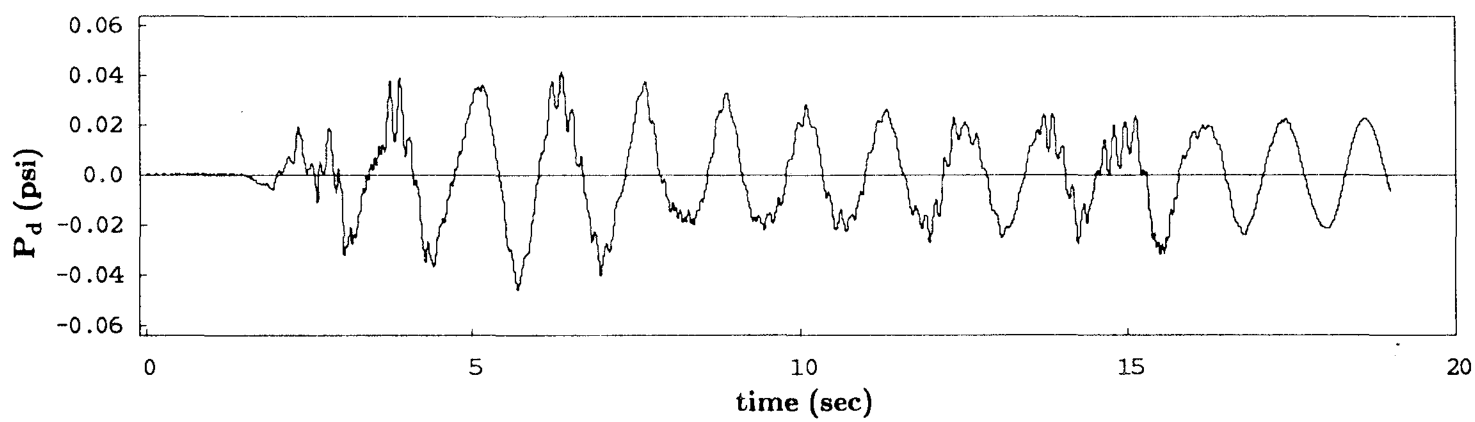

Figure 3.11 **Calculated dynamic pressure $P_d = P_{d_1} + P_{d_2}$ using two modes. Location: z=-16 in. Forcing function: recorded structure's isolated base acceleration. Table input: $\sqrt{4}$ time scaled El Centro horizontal span 50, PTA=0.114 g.**

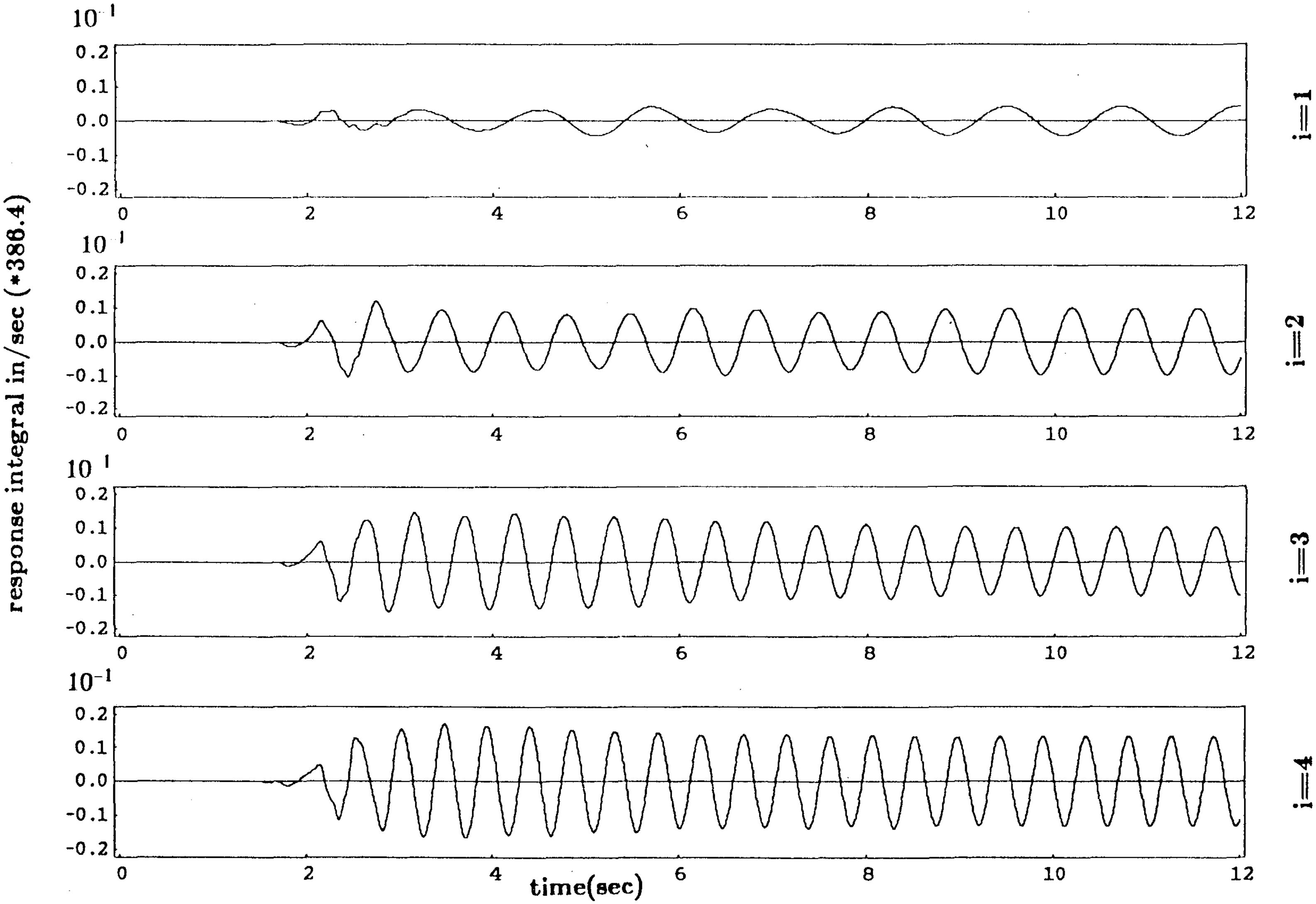

Figure 3.12 Calculated convolution integrals $I_i(t)$ (i=1,2,3,4) from equation (3.24). Forcing function: recorded table acceleration. Table input: $\sqrt{4}$ time scaled San Francisco horizontal span 50, PTA=0.331 g.

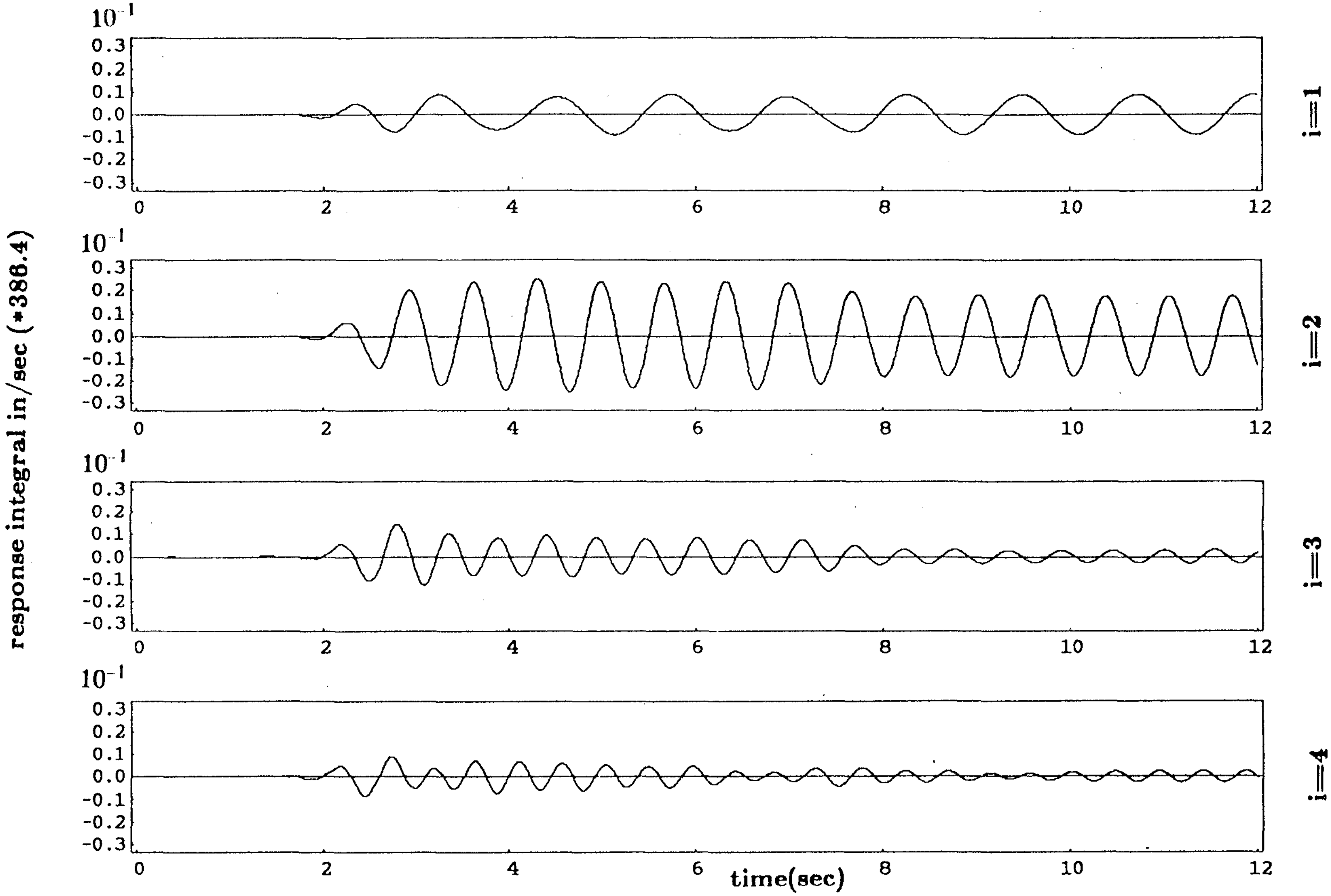

Figure 3.13 Calculated convolution integrals $I_i(t)$ (i=1,2,3,4) from equation (3.24). Forcing function: recorded structure's isolated base acceleration. Table input: $\sqrt{4}$ time scaled San Francisco horizontal span 50, PTA=0.331 g.

Theoretical solution using 2 modes

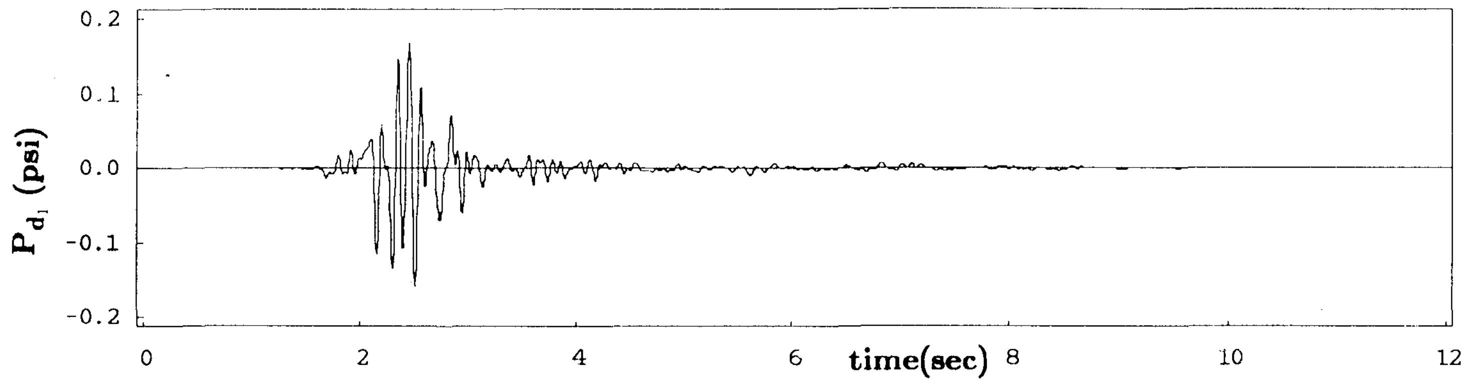

Figure 3.14a Calculated P_{d_1} component from equation (3.25) using two modes. Location: z=-16 in. Forcing function: recorded table acceleration. Table input: $\sqrt{4}$ time scaled San Francisco horizontal span 50, PTA=0.331 g.

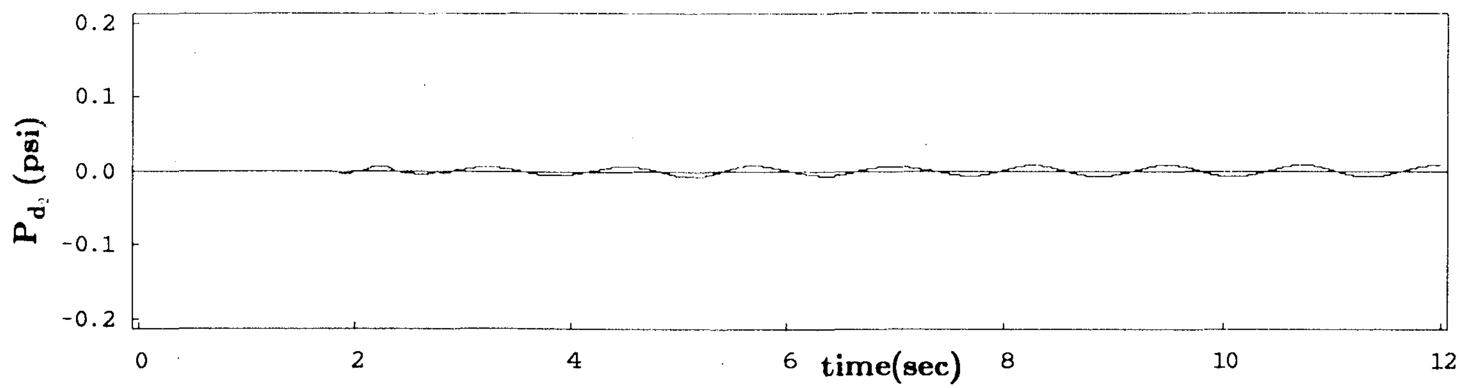

Figure 3.14b Calculated P_{d_2} component from equation (3.26) using two modes. Location: z=-16 in. Forcing function: recorded table acceleration. Table input: $\sqrt{4}$ time scaled San Francisco horizontal span 50, PTA=0.331 g.

Theoretical solution using 2 modes

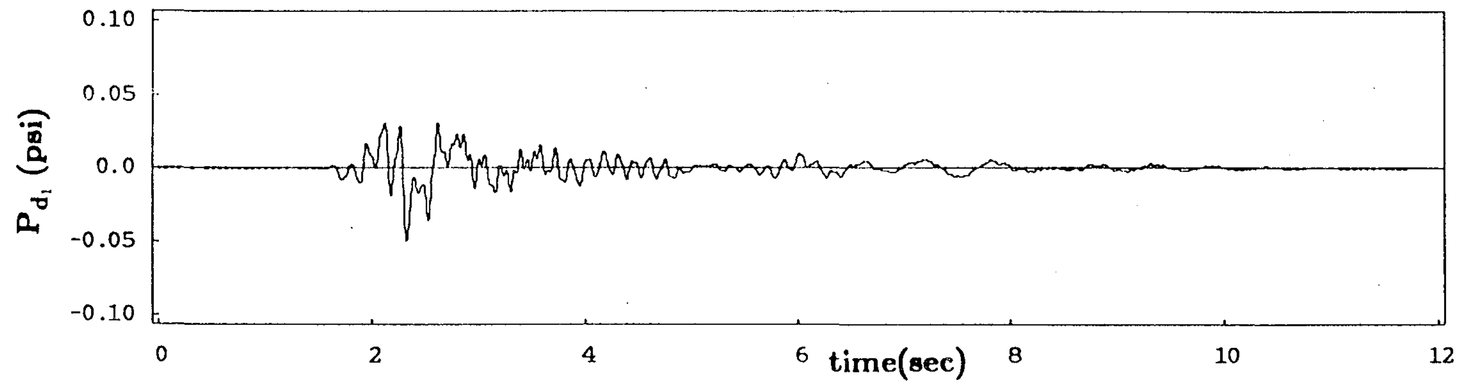

Figure 3.15a Calculated P_{d_1} component from equation (3.25) using two modes. Location: z=-16 in. Forcing function: recorded structure's isolated base acceleration. Table input: $\sqrt{4}$ time scaled San Francisco horizontal span 50, PTA=0.331 g.

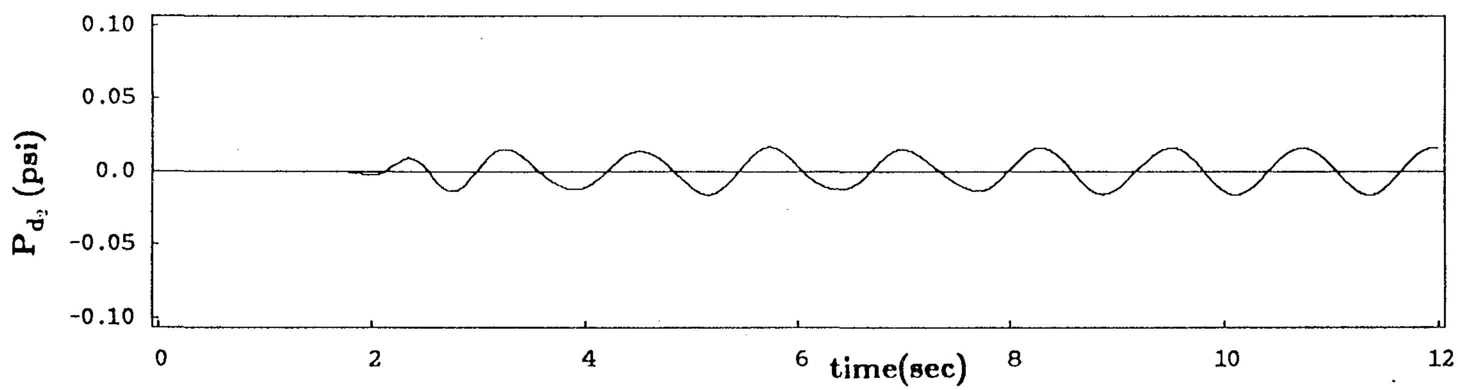

Figure 3.15b Calculated P_{d_2} component from equation (3.26) using two modes. Location: z=-16 in. Forcing function: recorded structure's isolated base acceleration. Table input: $\sqrt{4}$ time scaled San Francisco horizontal span 50, PTA=0.331 g.

Theoretical solution using 2 modes

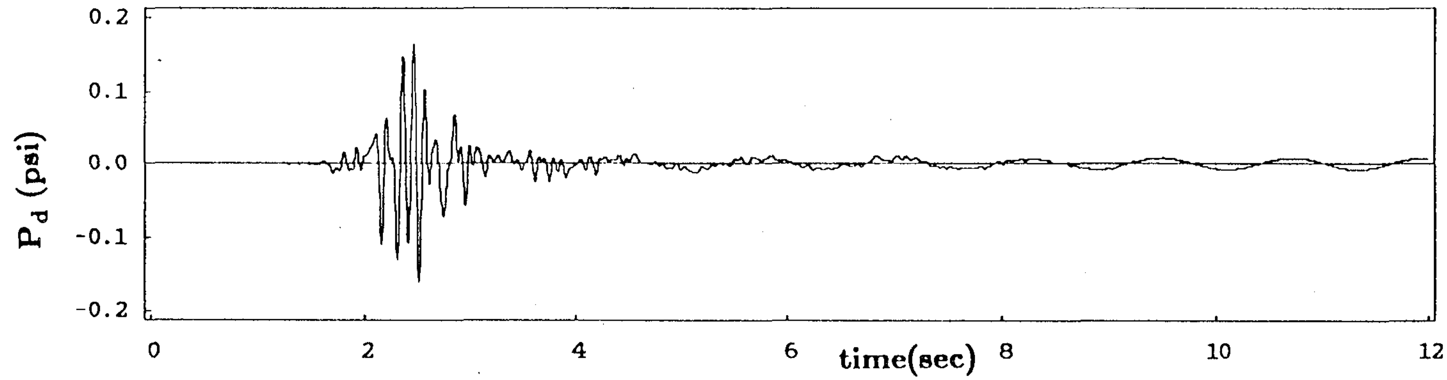

Figure 3.16 Calculated dynamic pressure $P_d = P_{d_1} + P_{d_2}$ component using two modes. Location: z=-16 in. Forcing function: recorded table acceleration. Table input: $\sqrt{4}$ time scaled San Francisco horizontal span 50, PTA=0.331 g.

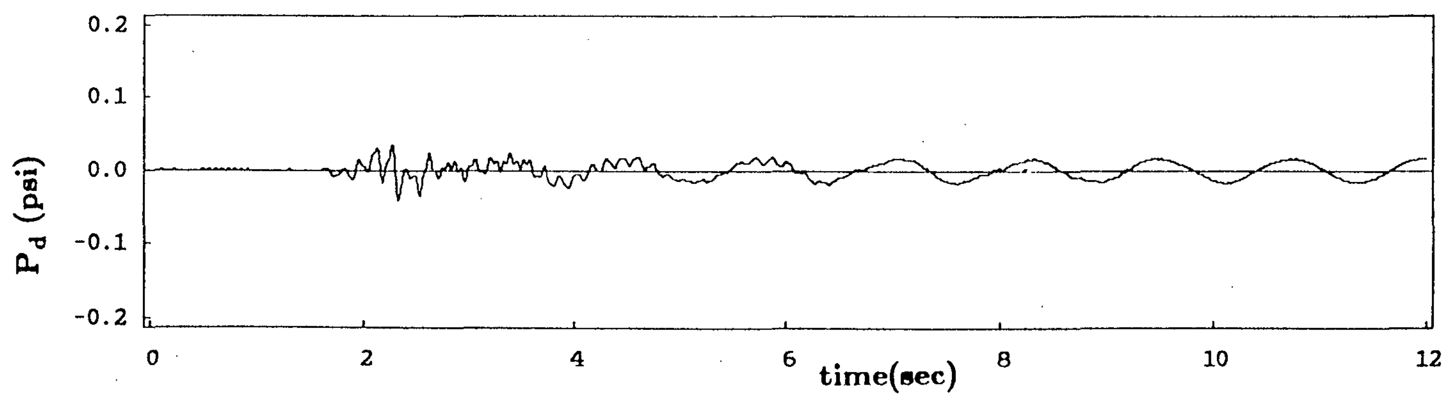

Figure 3.17 Calculated dynamic pressure $P_d = P_{d_1} + P_{d_2}$ using two modes. Location: z=-16 in. Forcing function: recorded structure's isolated base acceleration. Table input: $\sqrt{4}$ time scaled San Francisco horizontal span 50, PTA=0.331 g.

CHAPTER FOUR
TEST RESULTS AND CORRELATION

1. Some Experimental Results.

Seven different ground motion records were applied to the shake table at various spans ranging from 25 to 100. In the following, five records $\sqrt{4}$ time scaled and applied at a horizontal span of 50 will be presented then compared with the theoretical solution in the next section. The main concern is the response of the fluid. Because of the size of the tank models, the shell deformations were not studied in great detail and are not presented here. Shell defermations will be studied on a larger scale model in the next earthquake simulator water tank test.

For each table input, the displacement and acceleration at the tank support along with the north and south water surface deformation measured by the water level gages are shown. For the tank on the table, the table displacement and table acceleration are provided while for the tank on the structure, the structure's base absolute displacement and the structure's base acceleration are shown.

In general, the tanks on the model showed more sloshing and less pressure. The input acceleration was more reflected in the response of tank #1 than it was in the response of tank #2. This is due to the filtering provided by the isolation system.

The calculated frequencies of the fluid surface free vibrations, $\lambda_i = (gn_i \tanh n_i h)^{1/2}$, were compared with the experimental ones by using the FFT of the measured water elevation time histories for both tanks under different ground motions. This is illustrated in Figure 4.1 for the FFTs of tank #1 and tank #2 north water gage time histories.

El Centro

For the El Centro record at 50 horizontal span, the Peak Table Acceleration (PTA) was 0.114 g. The reduction in the accelerations transmitted to the structure's base was of the order of 2. This is shown in Figure 4.2 where the Peak Base Acceleration (PBA) is around 0.05 g. The Peak Table Displacement (PTD) was 0.25 in. while the Peak Base Absolute Displacement was 0.37 in. The sloshing was slightly higher in the tank on the structure; the ratio of the positive peak values in the water surface deformation is about 1.2.

Figure 4.3 shows the dynamic pressure time histories measured at the north bottom transducer for both tanks. The behavior of this transducer is descriptive of all the others with some slight differences. Note the reduction in the pressure for the tank on the structure, and its lower frequency. The ratio of the peak pressure at the bottom of tank #2 to that of tank #1 is 0.76.

San Francisco

For the San Francisco record at 50 horizontal span, the PTA was 0.331 g. This record is of relatively high frequency and high acceleration. For this reason it did not excite the sloshing for the tank on the table while it yielded higher sloshing for the tank in the structure since the whole system was responding at low frequency. The ratio of the peak sloshing values is 1.47 for tank #2 to tank #1. The base acceleration was drastically reduced in this case, and the reduction factor is 3.4 (Figure 4.4).

Figure 4.5 shows a drastic reduction in the dynamic pressure for the tank in the structure. The ratio of the peak values for tank #1 to tank #2 is 4.3. That was expected since equation (3.22) predicts a high dependence of the pressure on the tank support acceleration.

Pacoima Dam

For Pacoima Dam, the reduction in the acceleration at the structure base was not noticeable because this signal at a span of 50 caused a very low PTA of 0.076 g, and the isolation system was not quite activated. The lowering of the input frequency caused slightly higher sloshing while the reduction in the pressure was still present, and the ratio of peak pressure in tank #1 to peak pressure in tank #2 is 1.75 (Figures 4.6 and 4.7).

Parkfield

For the Parkfield record at 50 horizontal span, conclusions similar to the ones for Pacoima Dam can be made. The only difference is that the table displacement here consists of a large sway in one direction followed by small cycles and this sway corresponds to a spike in the acceleration. This behavior was changed by base isolation, the displacement and the acceleration were transformed into more distributed, equally spaced cycles at lower frequency. This is reflected in the pressure time history but to a lesser extent; the few spikes in the dynamic pressure for tank #1 are reduced and distributed for tank #2.

The ratio of Peak Water Elevation in tank #1 to tank #2 is 0.78 while the ratio of peak pressure at z=-16 in. in tank #1 to tank #2 was 1.2 (Figures 4.8 and 4.9).

Taft

For Taft there were no major differences in the response, except the slight reduction in the dynamic pressure for the tank on the structure, the reduction factor was around 1.4 (Figures 4.10 and 4.11).

The peak values of tank support motions and the fluid response are summarized in Table 4.1.

2. Comparison with Theoretical Solution.

The measured pressure time histories were compared with the ones given by equation (3.22) using the first two modes (i=1,2), for the five table motions and for both tanks, and good agreement was found. These are shown in Figures 4.12a to 4.21b. On the average, there is a difference of about 15% between calculated and measured peak pressures. This level of discrepancy is unavoidable because of the difficulty in achieving perfect measurements on one hand, and because of the assumptions made in the theoretical solution on the other hand.

Correlation coefficients between measured and calculated pressure time histories were obtained for most of the table motions and they were 97% for tank #1 and 94% for tank #2 with the El Centro record, 97% for tank #2 with the San Francisco record, 98% for both tanks with the Pacoima Dam record, and 98% for tank #2 with the Parkfield and Taft records.

The water elevation at the tank wall was calculated for El Centro using the first three modes (i=1,2,3) for both tanks. The comparison is shown in Figure 4.22 for the tank on the table and Figure 4.23 for the tank on the structure. Good correlation (97%) was found for both. Obviously, the higher frequencies in the water surface deformation are absent in the calculated time history but the behavior is still well represented and equation (3.28) using three modes can predict spilling or overtopping accurately.

The preceding comparisons show that the expressions for the dynamic pressure and the water surface deformation can be directly used for a prototype to predict the response of the contained fluid under a given ground motion. Furthermore, this formulation gave insight into the advantages of using the approach to isolate a large tank. The pressure and the acceleration are reduced, and the sloshing is slightly increased. If the isolation system is chosen such that it is not in resonance with the first two sloshing modes, the effects on the water elevation will be small. The present experimental results do not represent the behavior of such a tank because the structural model had a fundamental period very close to the first sloshing mode of the 4 ft. diameter tank. Also, the scaling would be very different if the tanks were to be tested without the structural model. In other words, the accelerograms were time scaled by a factor of two because the geometric scale was dictated by the structure: if the 4 ft. diameter tank is used to represent a prototype of, for example, 80 ft. in diameter, the accelerograms should be time scaled by $\sqrt{20}$. This would lead to a ground motion of much higher frequency and thus yield a much better behavior for the isolated tank.

The simplicity of the solution presented renders the transformation of the problem into a mechanical analog unnecessary for tanks under the effect of ground motion. A mechanical analog is needed for tanks that are part of a more complex system, like airplane fuel containers [7], where the tanks need to be incorporated in an overall response analysis of the system.

The equations governing the oscillations of a fluid are similar in nature to those for a spherical pendulum. It has been shown, however, that the motion of a spherical pendulum under an excitation in a vertical plane can become unstable near resonance and deviate from a planar trajectory because of nonlinear coupling [8]. When nonlinear wave theories are used to study forced waves in a fluid container they reveal coupling between the longitudinal modes of oscillation and the transverse modes that linear wave theory ignores. For certain forcing frequencies and certain damping levels in the system, the motion becomes chaotic [9]. These problems are of interest for applications where the tank is subjected to excitations of very long duration, and where there is interaction with the supporting structure, such as for tanks in moving vehicles or in aircrafts. However, for small tanks in structures or large ground supported tanks subjected to earthquake excitation this problem is of less significance and the present research shows that linear wave theory yields accurate results.

Table 4.1 **Peak values of dynamic pressure and water elevation.**

		El Centro span 50	San Francisco span 50	Pacoima Dam span 50	Parkfield span 50	Taft span 50
tank #1 (on table)	Peak Table Acceleration (g)	0.114	0.331	0.076	0.070	0.088
	Peak Table Displacement (in)	0.25	0.25	0.26	0.25	0.26
	Peak Water Elevation at tank wall (in) north gage	1.77	0.70	0.64	0.89	0.93
	Peak Dynamic Pressure (psi) at z=-16 in.	0.071	0.188	0.049	0.035	0.053
tank #2 (on structure)	Peak Base Acceleration (g)	0.052	0.098	0.055	0.038	0.061
	Peak Base Absolute Displacement (in)	0.37	0.48	0.37	0.25	0.31
	Peak Water Elevation at tank wall (in) north gage	2.15	1.03	0.87	1.14	0.96
	Peak Dynamic Pressure (psi) at z=-16 in.	0.054	0.044	0.028	0.029	0.037

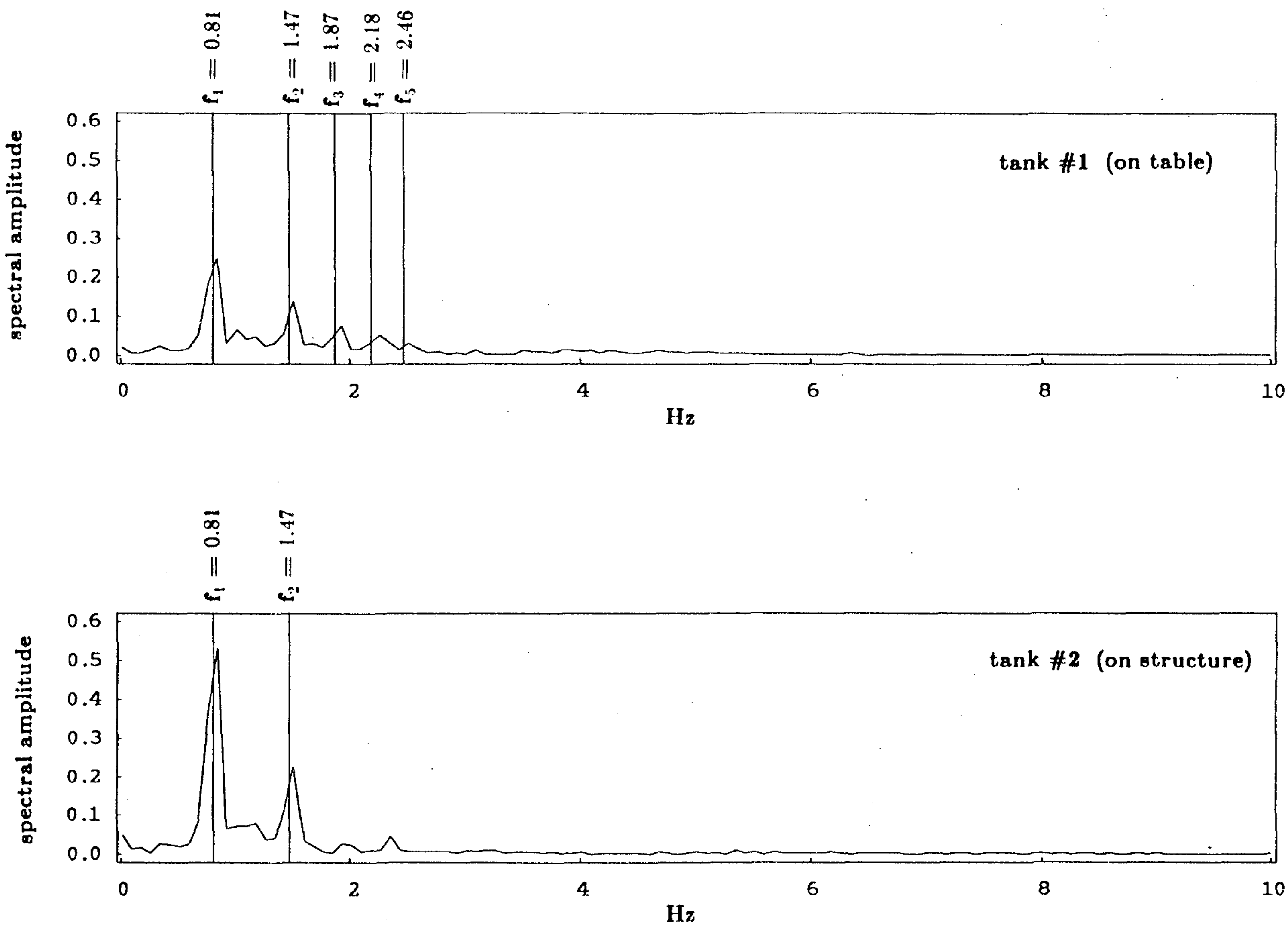

Figure 4.1 **FFT of measured water elevation at tank wall (north gage) for tank #1 and tank #2 under San Francisco span 50, compared to the calculated frequencies of free vibration $F_i = \lambda_i/2\pi = (gn_i \tanh n_i h)^{1/2}/2\pi$.**

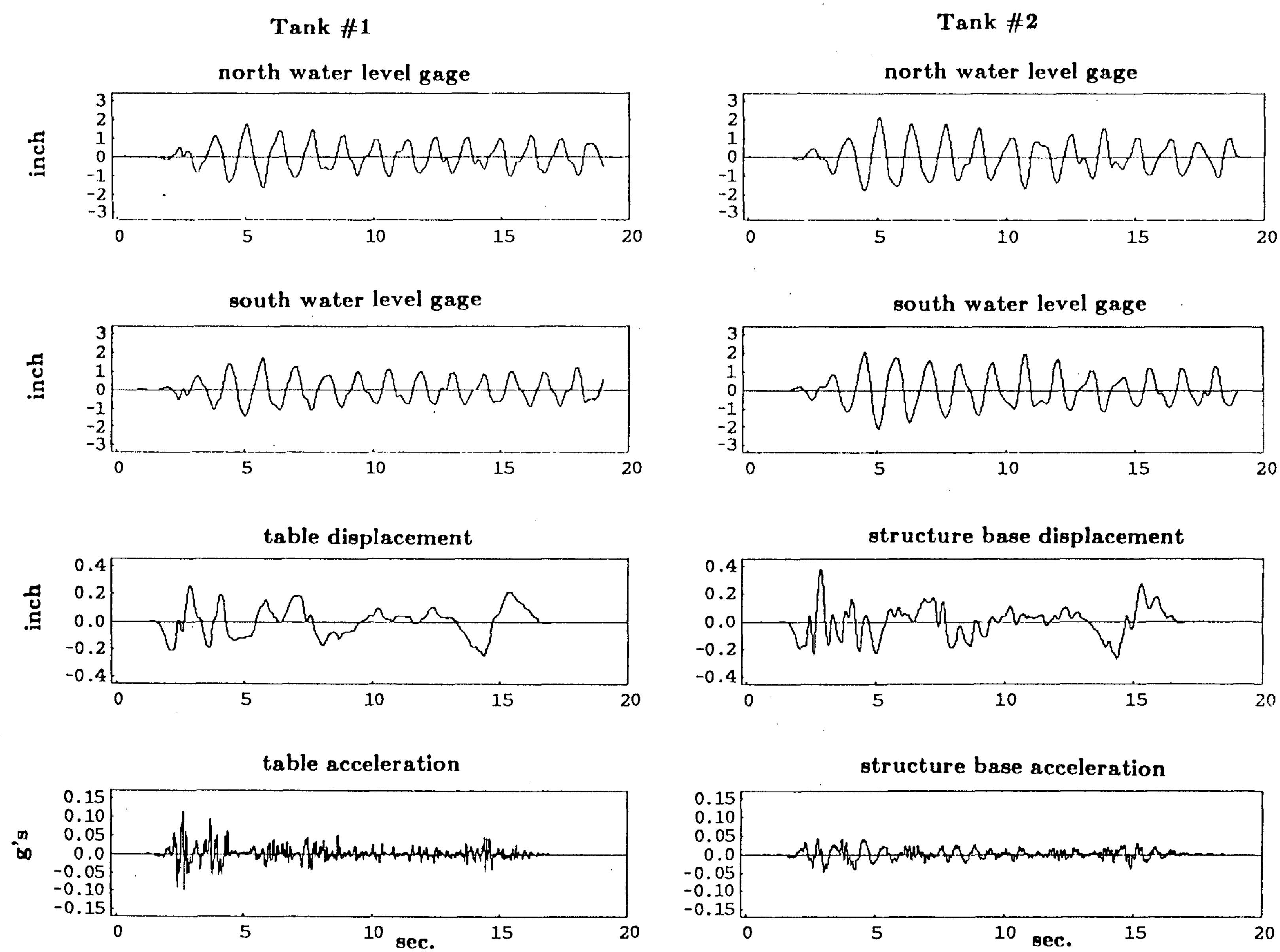

Figure 4.2 Water elevation at tank wall. Tank #1 and tank #2. Table input: $\sqrt{4}$ time scaled El Centro horizontal span 50, PTA=0.114 g.

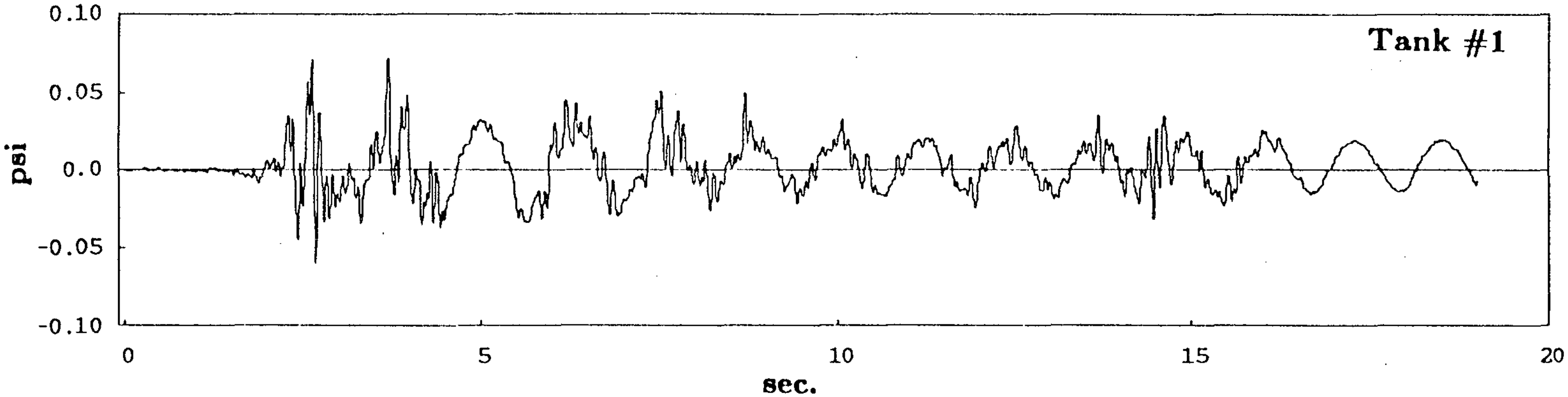

Figure 4.3a Measured pressure, north bottom transducer in tank #1. Table input: $\sqrt{4}$ time scaled El Centro horizontal span 50, PTA=0.114 g.

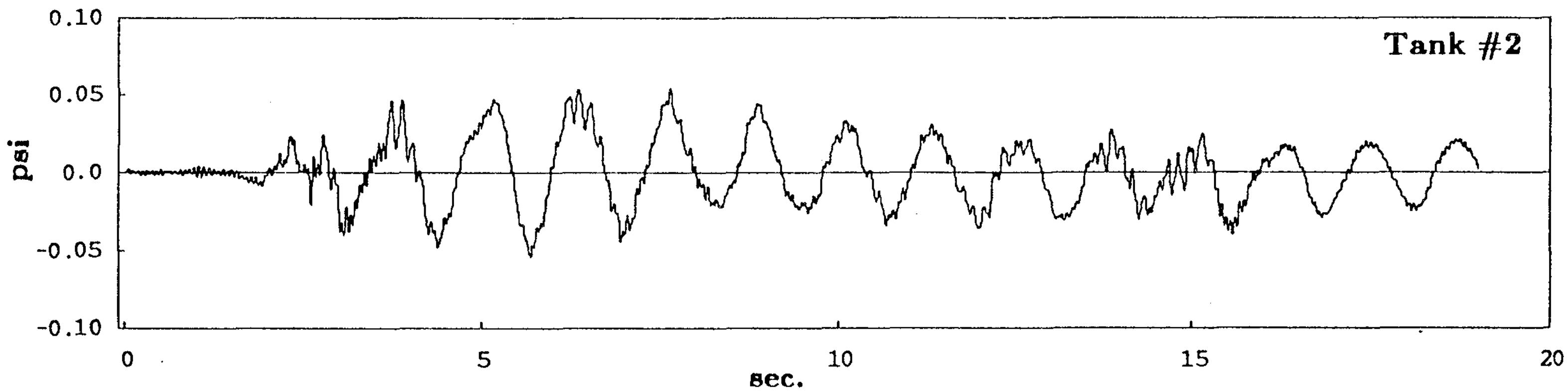

Figure 4.3b Measured pressure, north bottom transducer in tank #2. Table input: $\sqrt{4}$ time scaled El Centro horizontal span 50, PTA=0.114 g.

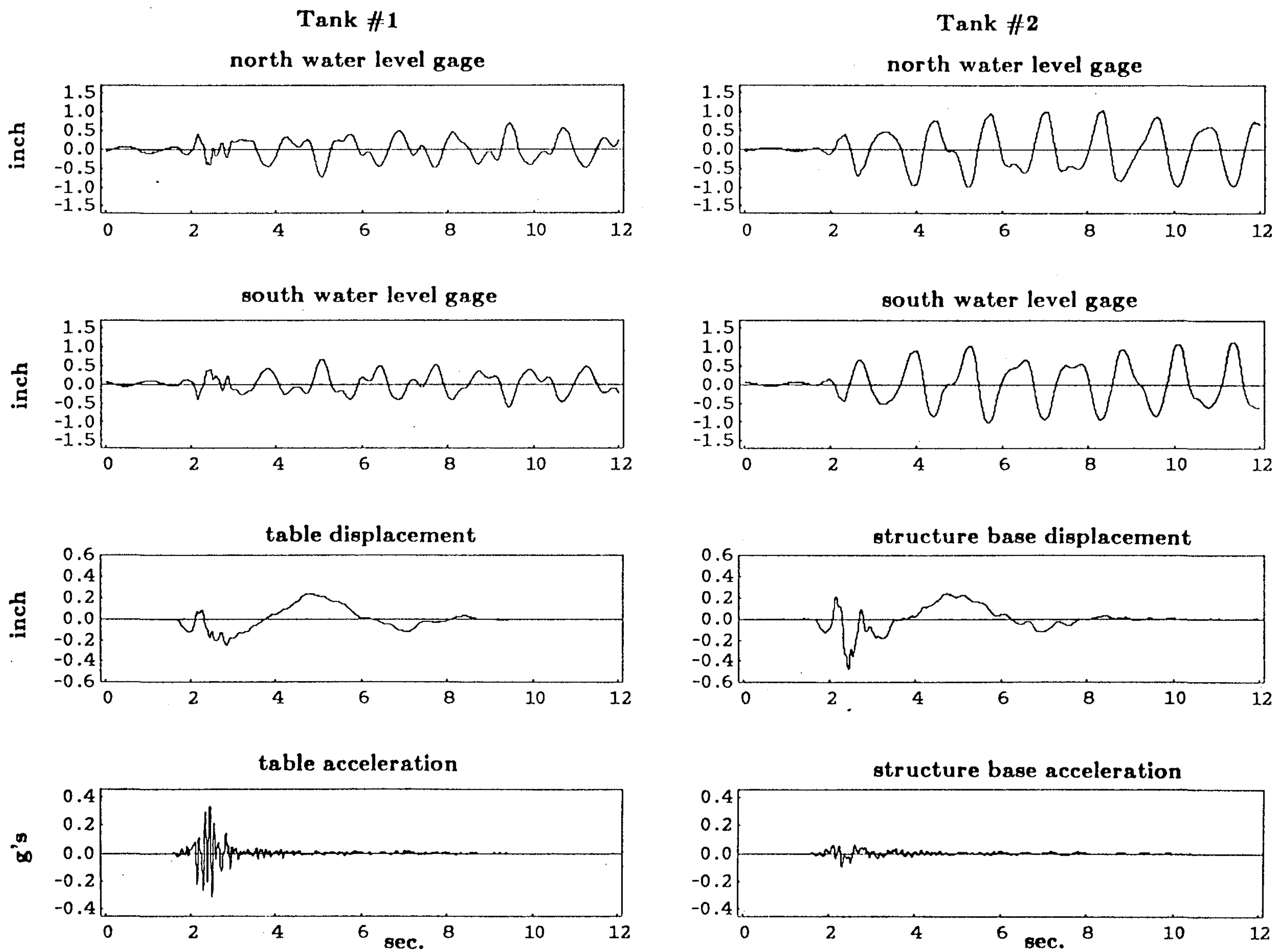

Figure 4.4 Water elevation at tank wall. Tank #1 and tank #2. Table input: $\sqrt{4}$ time scaled San Francisco horizontal span 50, PTA=0.331 g.

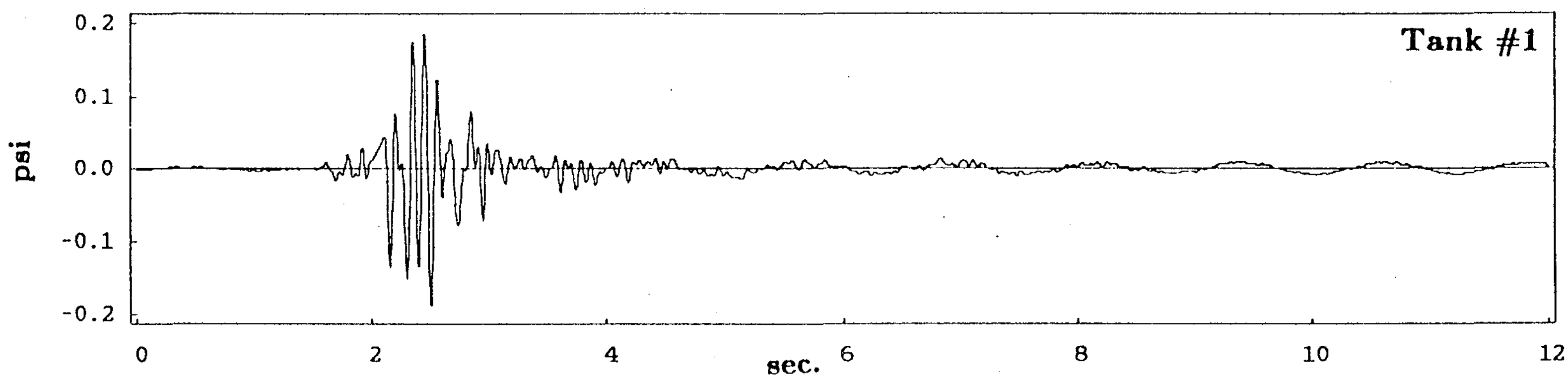

Figure 4.5a Measured pressure, north bottom transducer in tank #1. Table input: $\sqrt{4}$ time scaled San Francisco horizontal span 50, PTA=0.331 g.

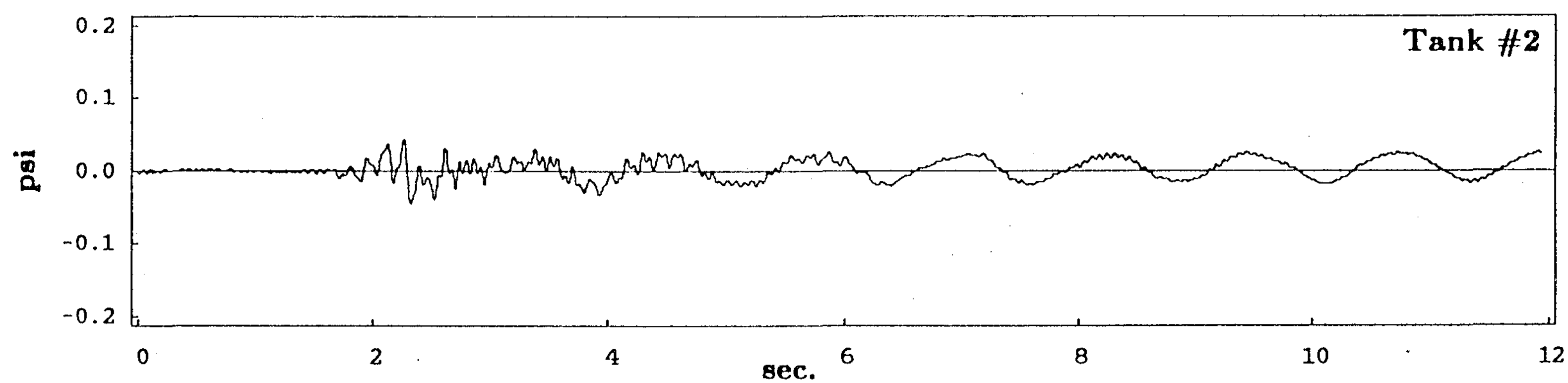

Figure 4.5b Measured pressure, north bottom transducer in tank #2. Table input: $\sqrt{4}$ time scaled San Francisco horizontal span 50, PTA=0.331 g.

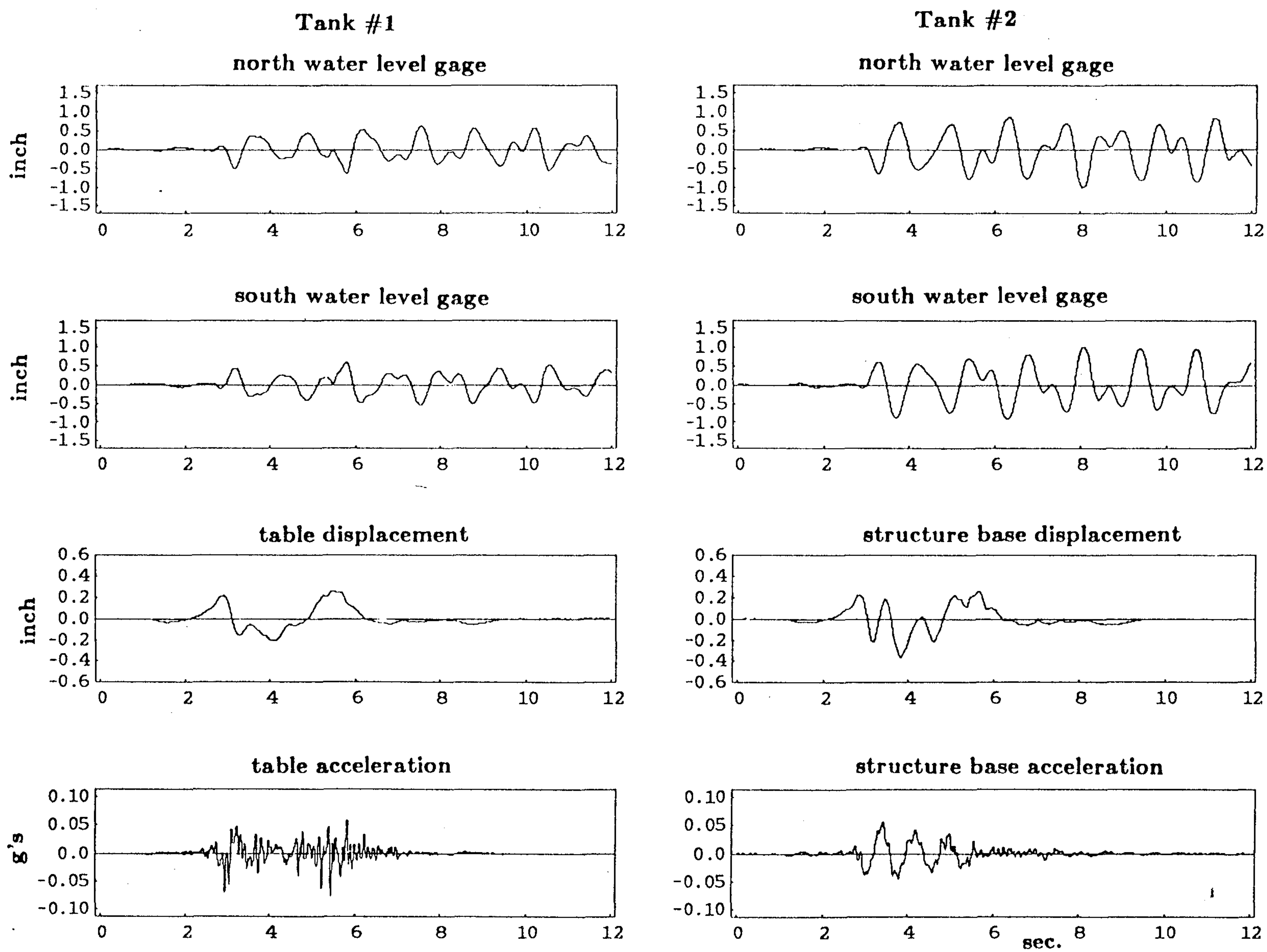

Figure 4.6 Water elevation at tank wall. Tank #1 and tank #2. Table input: $\sqrt{4}$ time scaled Pacoima Dam horizontal span 50, PTA=0.076 g.

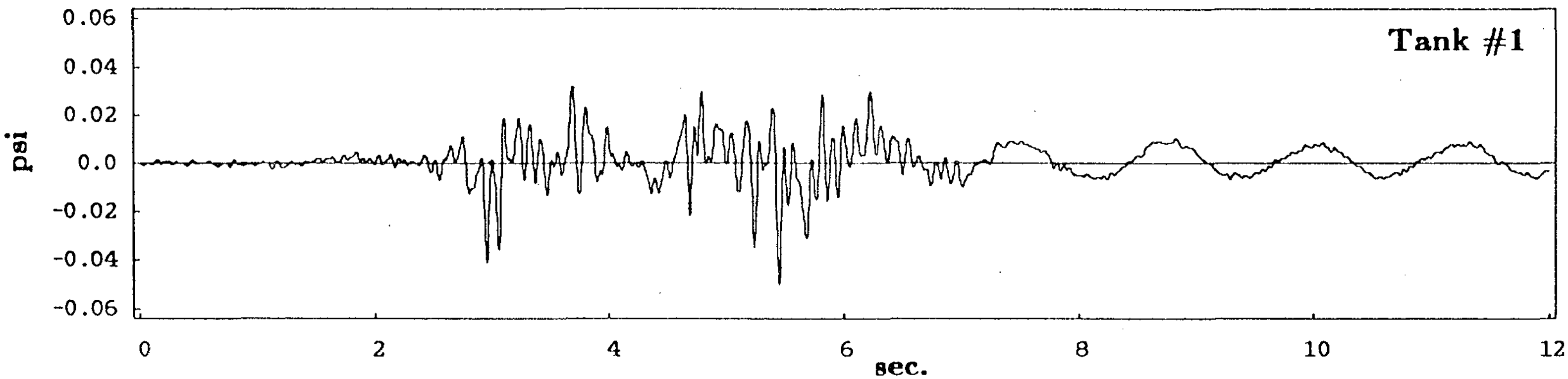

Figure 4.7a Measured pressure, north bottom transducer in tank #1. Table input: √4 time scaled Pacoima Dam horizontal span 50, PTA=0.076 g.

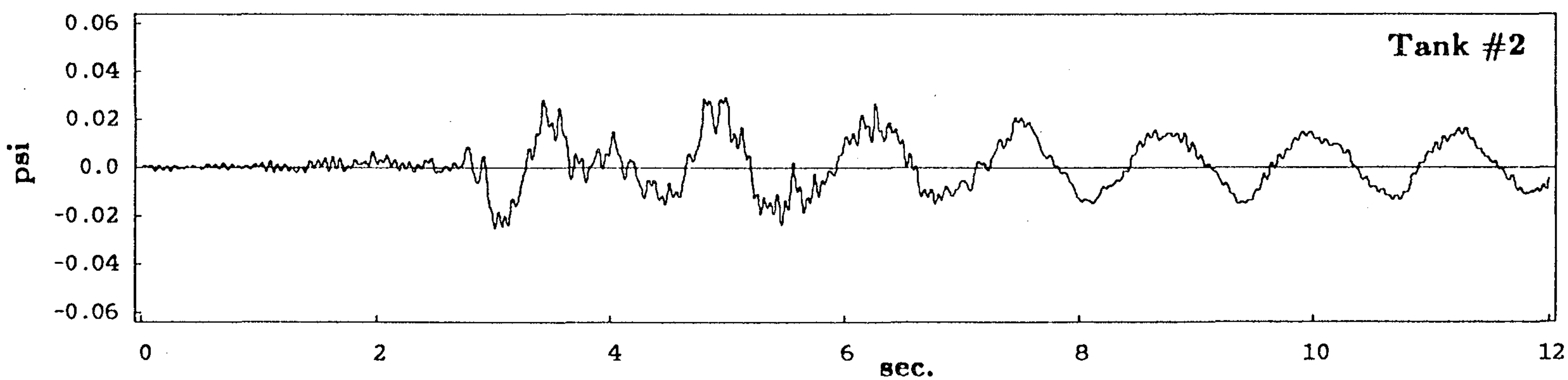

Figure 4.7b Measured pressure, north bottom transducer in tank #2. Table input: √4 time scaled Pacoima Dam horizontal span 50, PTA=0.076 g.

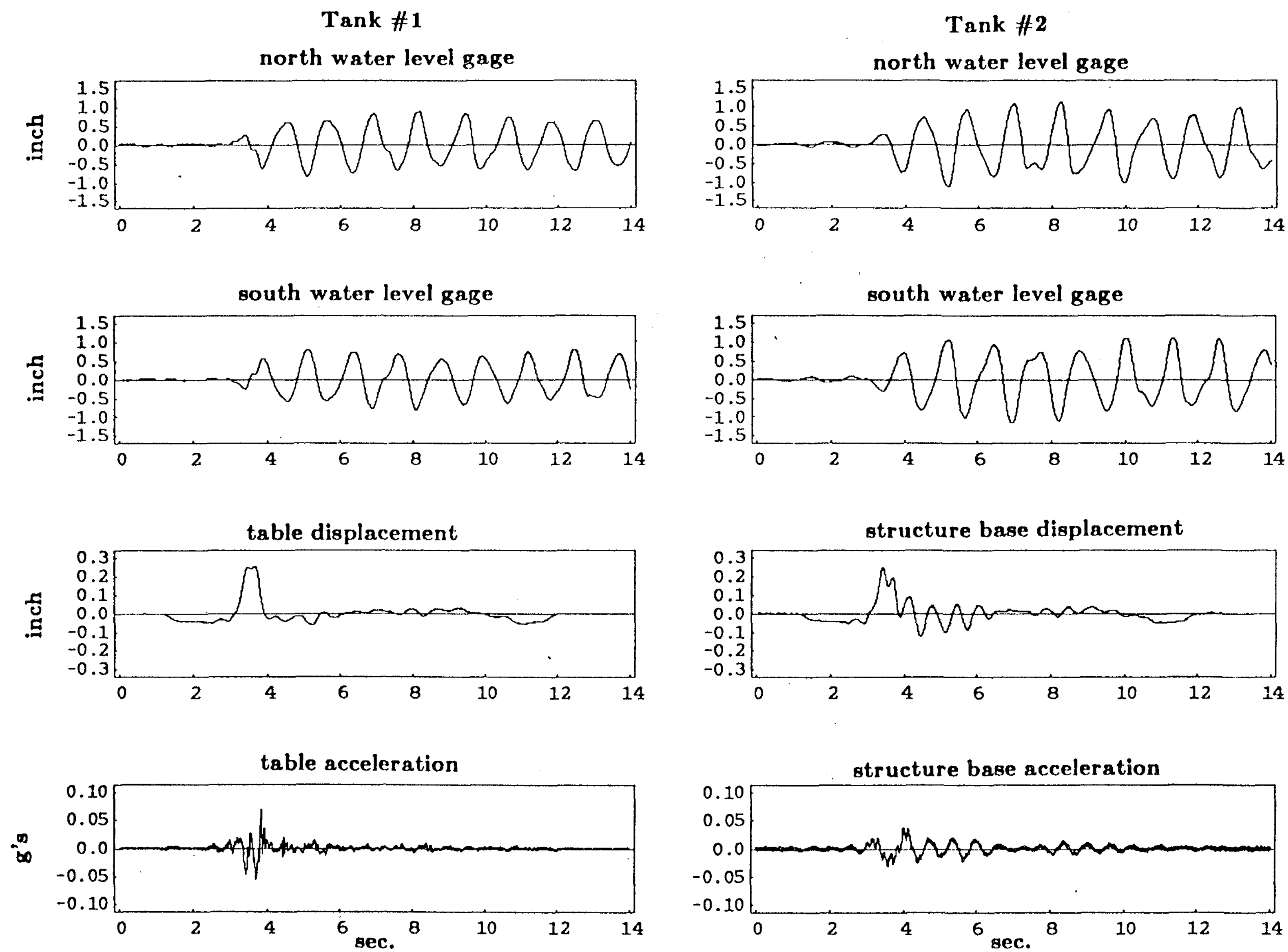

Figure 4.8 Water elevation at tank wall. Tank #1 and tank #2. Table input: $\sqrt{4}$ time scaled Parkfield horizontal span 50, PTA=0.070 g.

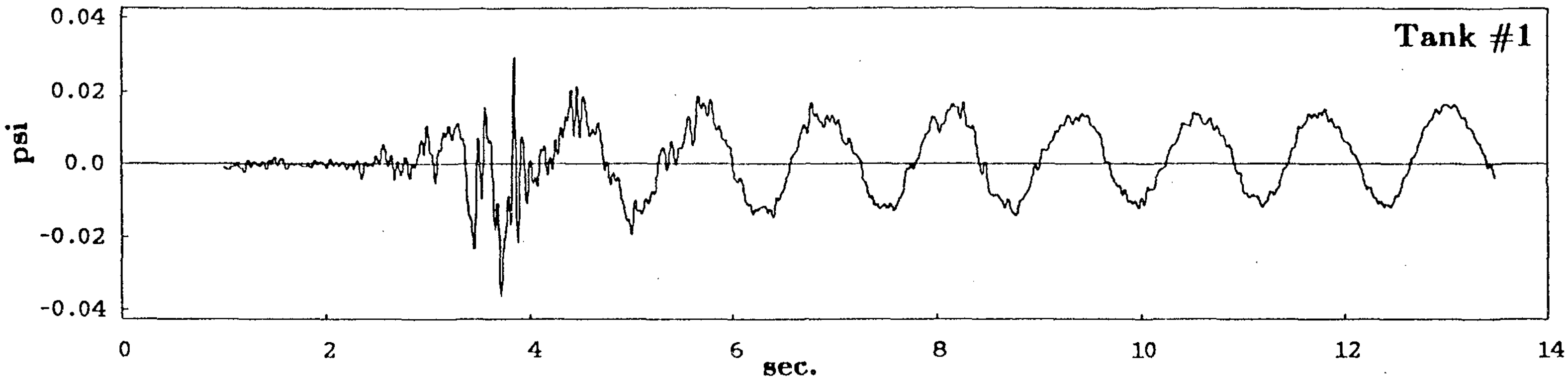

Figure 4.9a Measured pressure, north bottom transducer in tank #1. Table input: $\sqrt{4}$ time scaled Parkfield horizontal span 50, PTA=0.070 g.

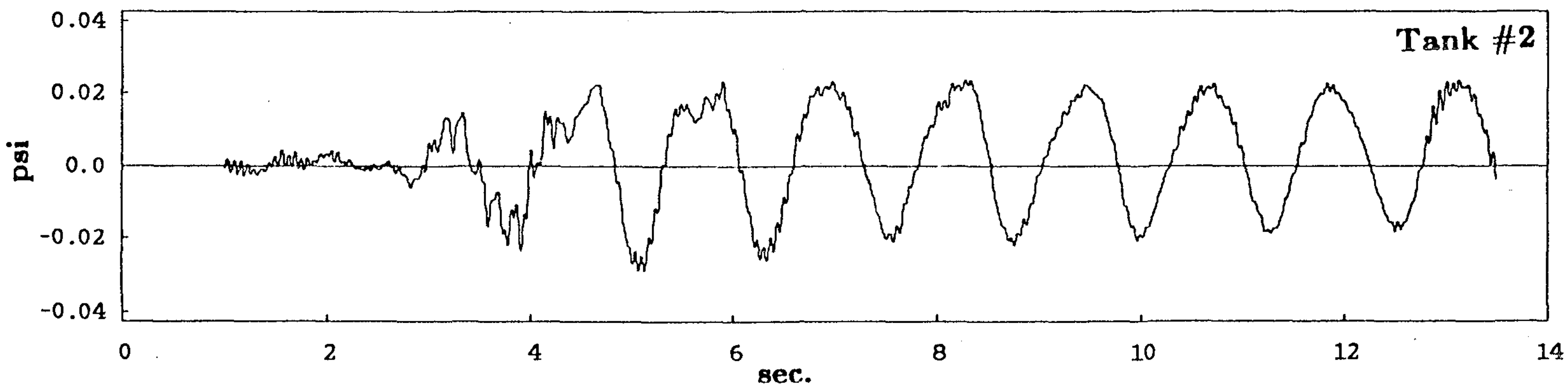

Figure 4.9b Measured pressure, north bottom transducer in tank #2. Table input: $\sqrt{4}$ time scaled Parkfield horizontal span 50, PTA=0.070 g.

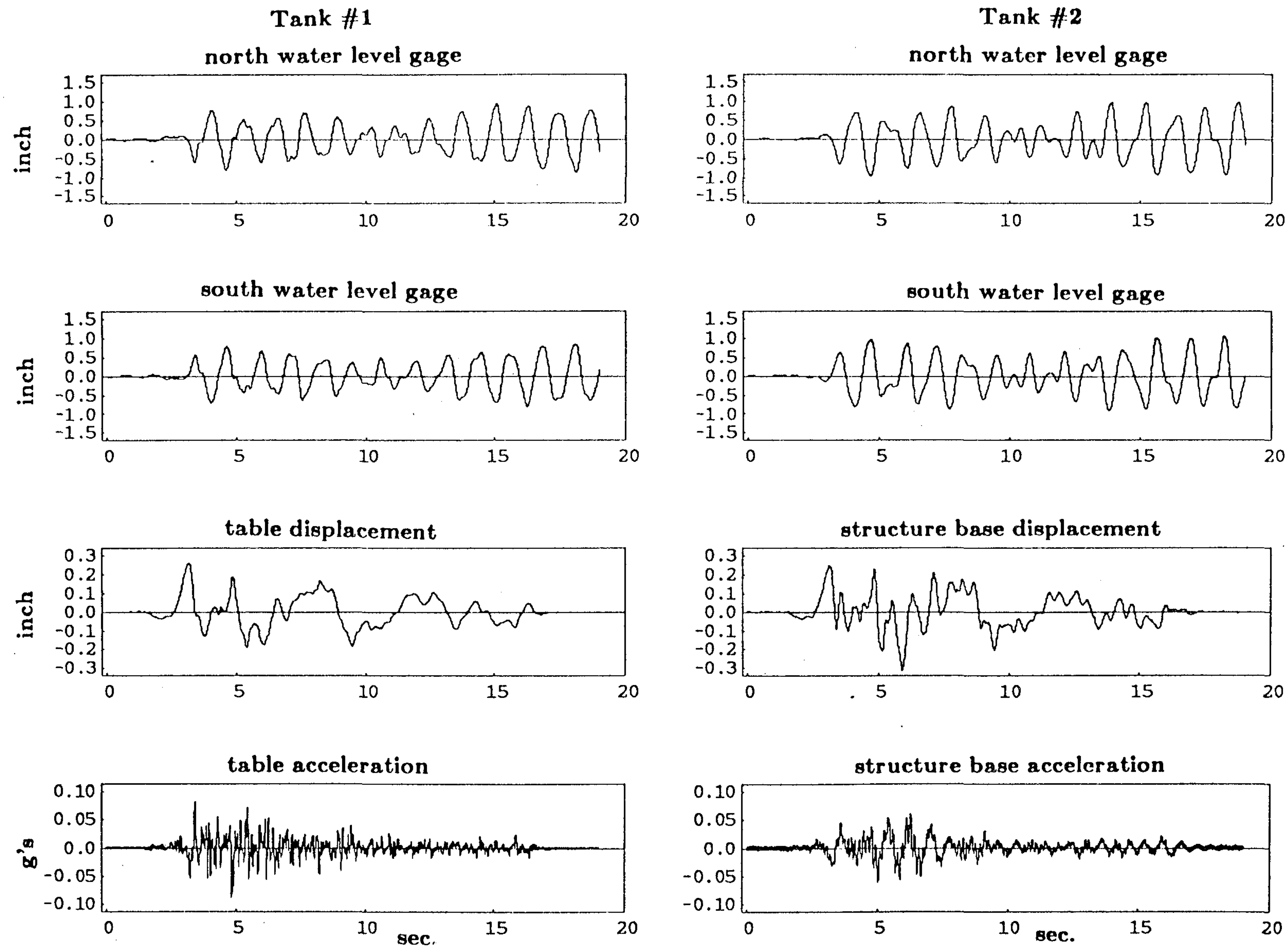

Figure 4.10 Water elevation at tank wall. Tank #1 and tank #2. Table input: $\sqrt{4}$ time scaled Taft horizontal span 50, PTA=0.088 g.

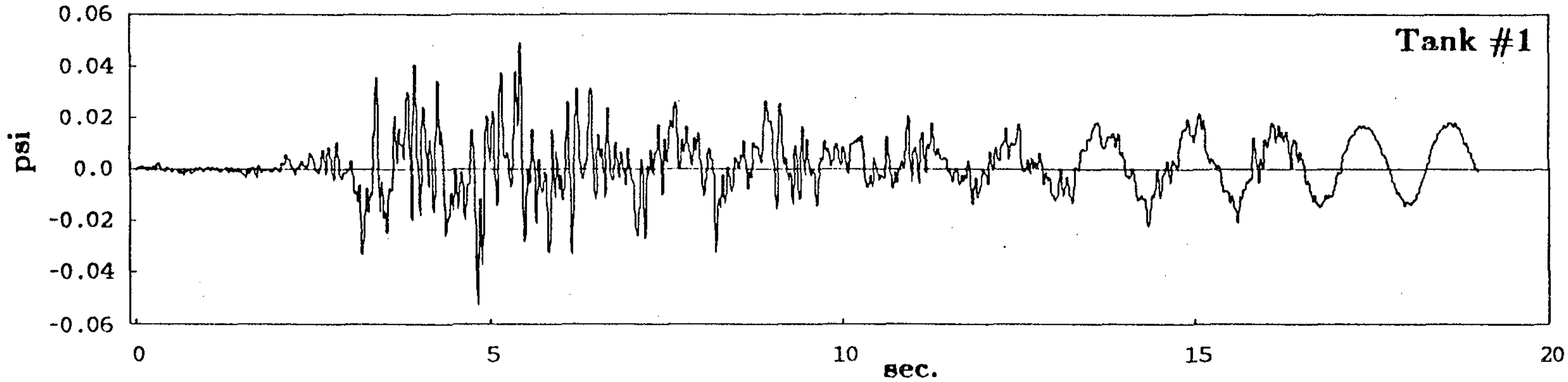

Figure 4.11a Measured pressure, north bottom transducer in tank #1. Table input: $\sqrt{4}$ time scaled Taft horizontal span 50, PTA=0.088 g.

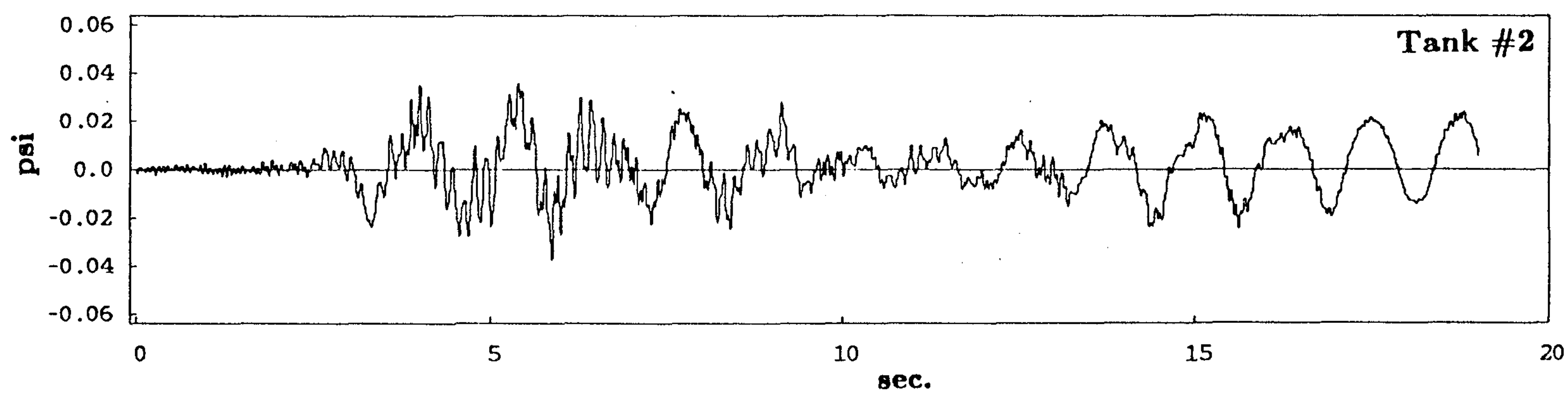

Figure 4.11b Measured pressure, north bottom transducer in tank #2. Table input: $\sqrt{4}$ time scaled Taft horizontal span 50, PTA=0.088 g.

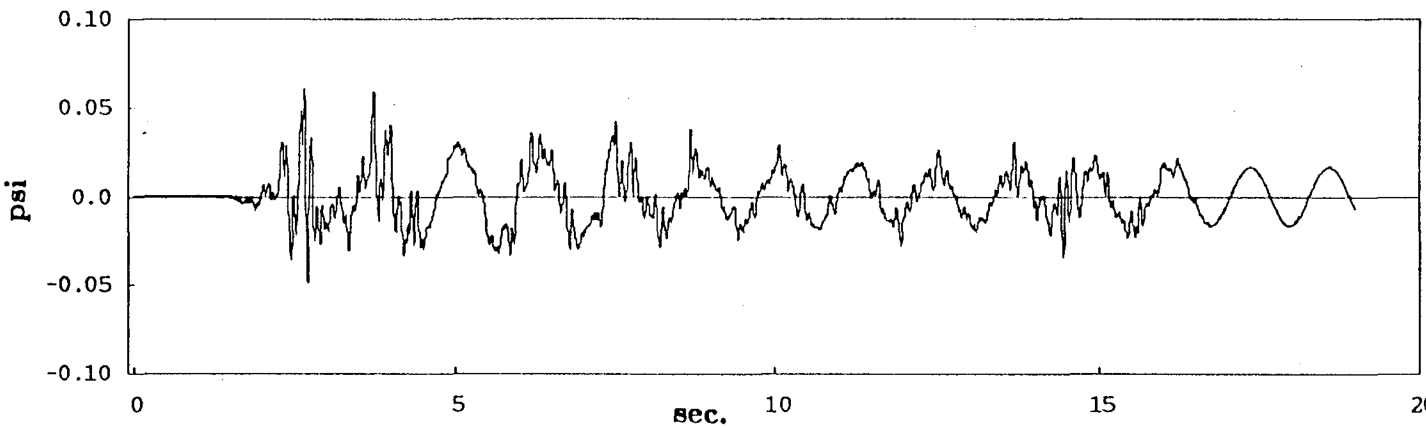

Figure 4.12a Calculated dynamic pressure P_d using two modes. Location: z=-16 in. Forcing function: recorded table acceleration. Table input: $\sqrt{4}$ time scaled El Centro horizontal span 50, PTA=0.114 g.

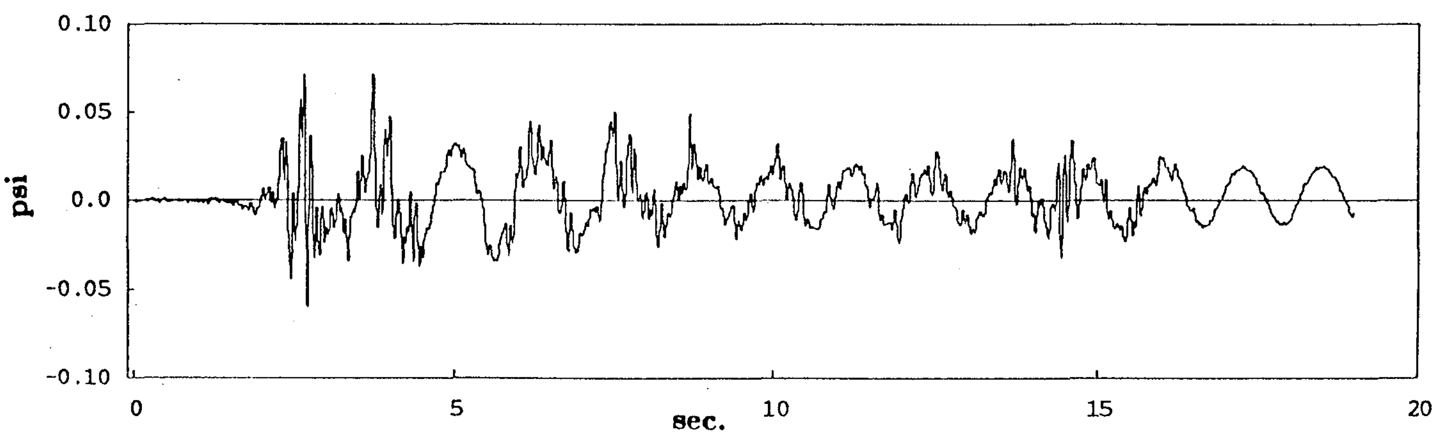

Figure 4.12b Measured dynamic pressure at north bottom transducer in tank #1. Location: z=-16 in. Table input: $\sqrt{4}$ time scaled El Centro horizontal span 50, PTA=0.114 g.

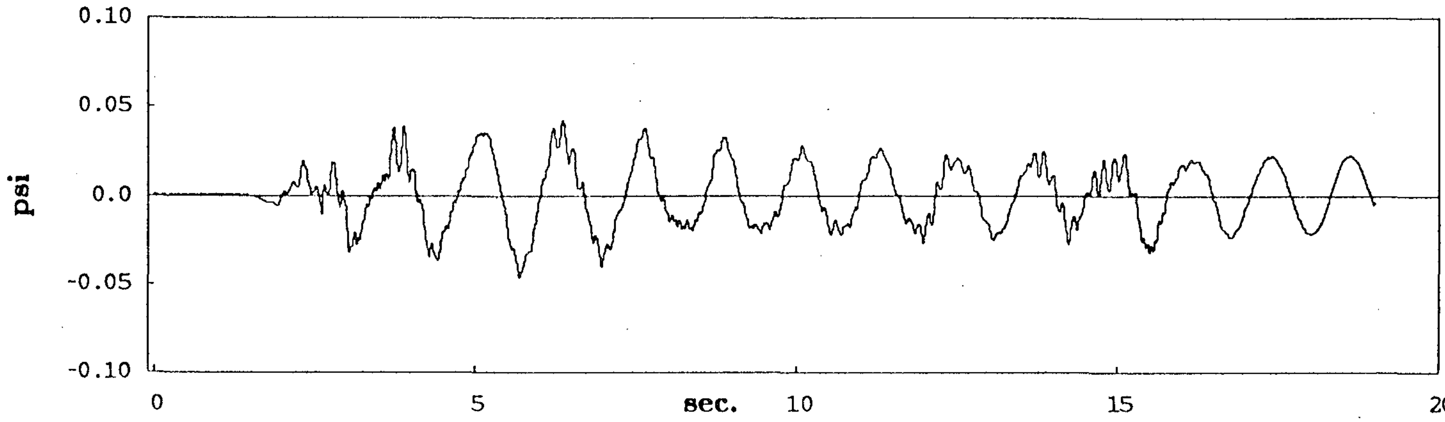

Figure 4.13a Calculated dynamic pressure P_d using two modes. Location: z=-16 in. Forcing function: recorded structure's isolated base acceleration. Table input: $\sqrt{4}$ time scaled El Centro horizontal span 50, PTA=0.114 g.

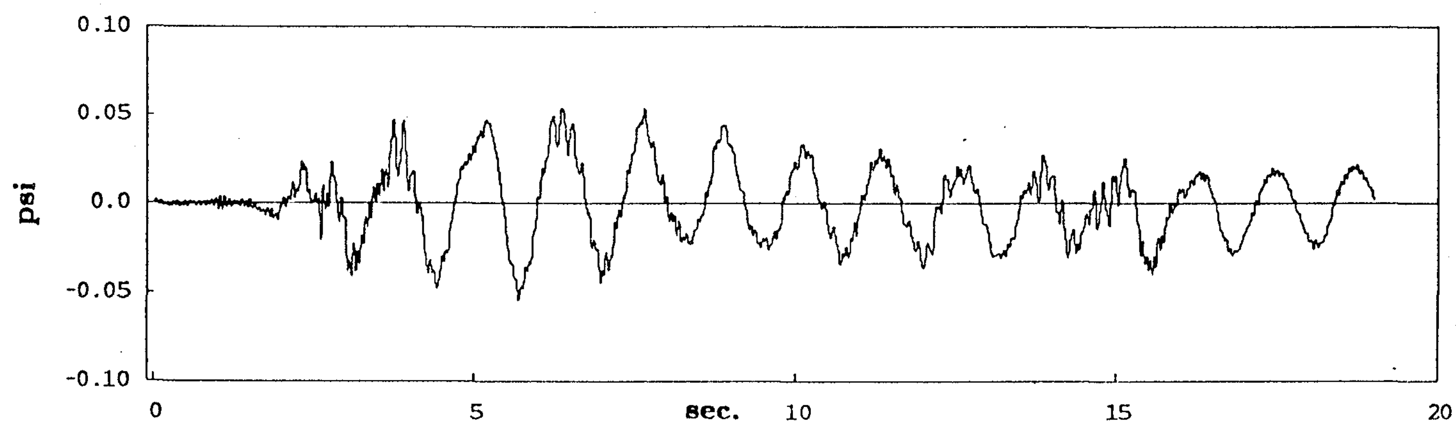

Figure 4.13b Measured dynamic pressure at north bottom transducer in tank #2. Location: z=-16 in. Table input: $\sqrt{4}$ time scaled El Centro horizontal span 50, PTA=0.114 g.

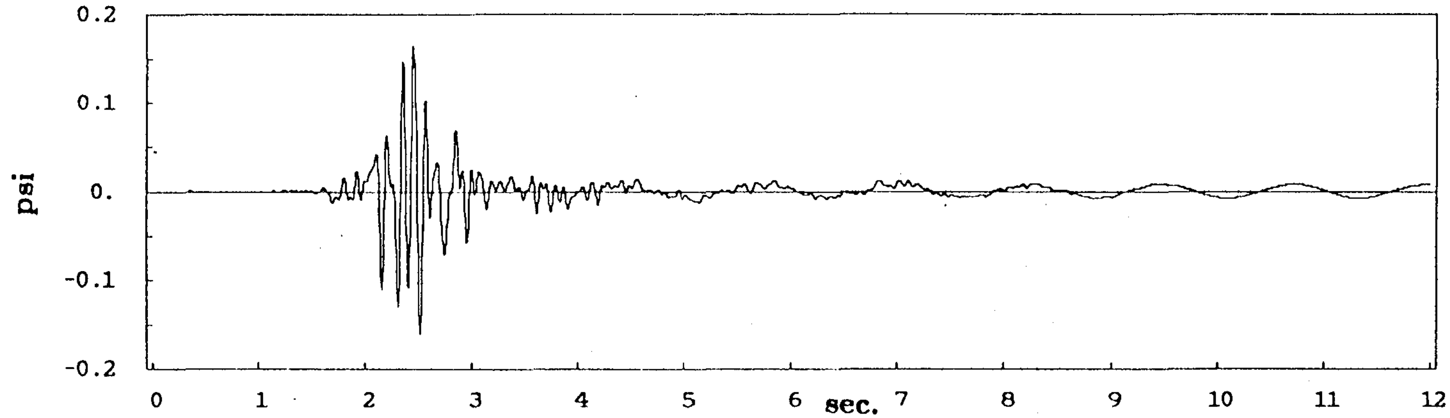

Figure 4.14a Calculated dynamic pressure P_d using two modes. Location: z=-16 in. Forcing function: recorded table acceleration. Table input: $\sqrt{4}$ time scaled San Francisco horizontal span 50, PTA=0.331 g.

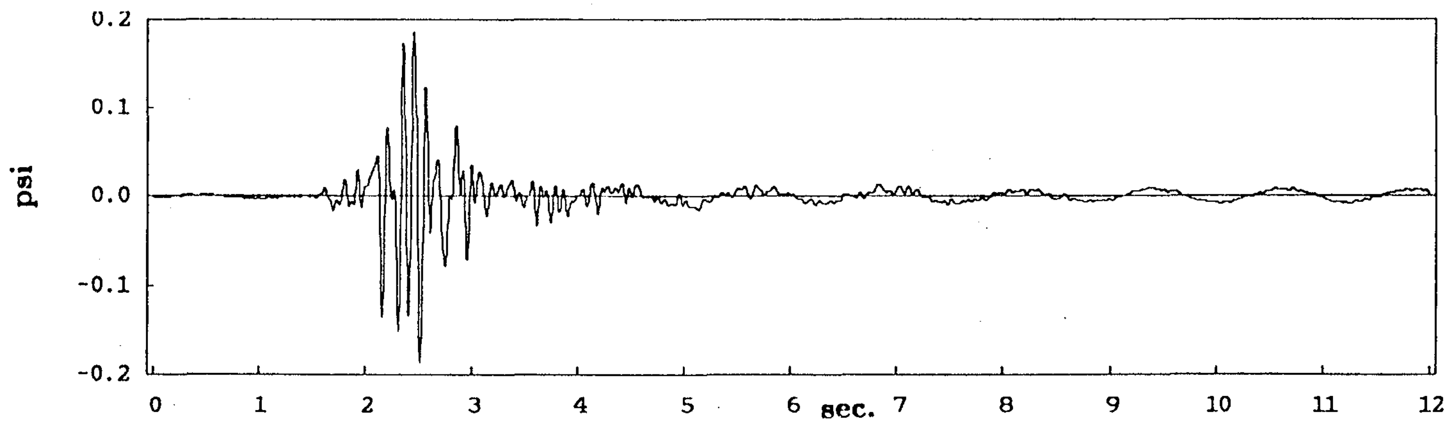

Figure 4.14b Measured dynamic pressure at north bottom transducer in tank #1. Location: z=-16 in. Table input: $\sqrt{4}$ time scaled San Francisco horizontal span 50, PTA=0.331 g.

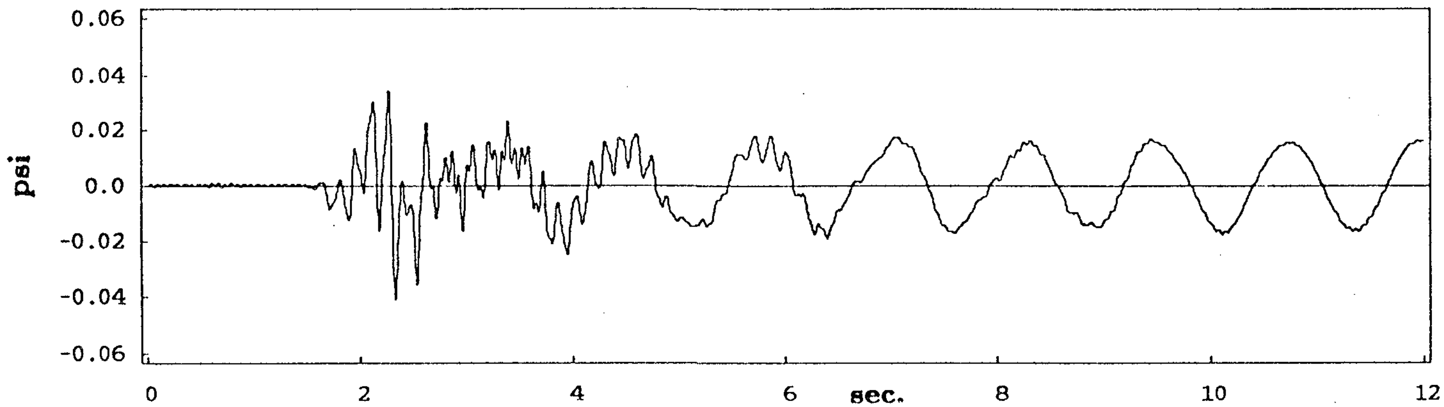

Figure 4.15a Calculated dynamic pressure P_d using two modes. Location: z=-16 in. Forcing function: recorded structure's isolated base acceleration. Table input: $\sqrt{4}$ time scaled San Francisco horizontal span 50, PTA=0.331 g.

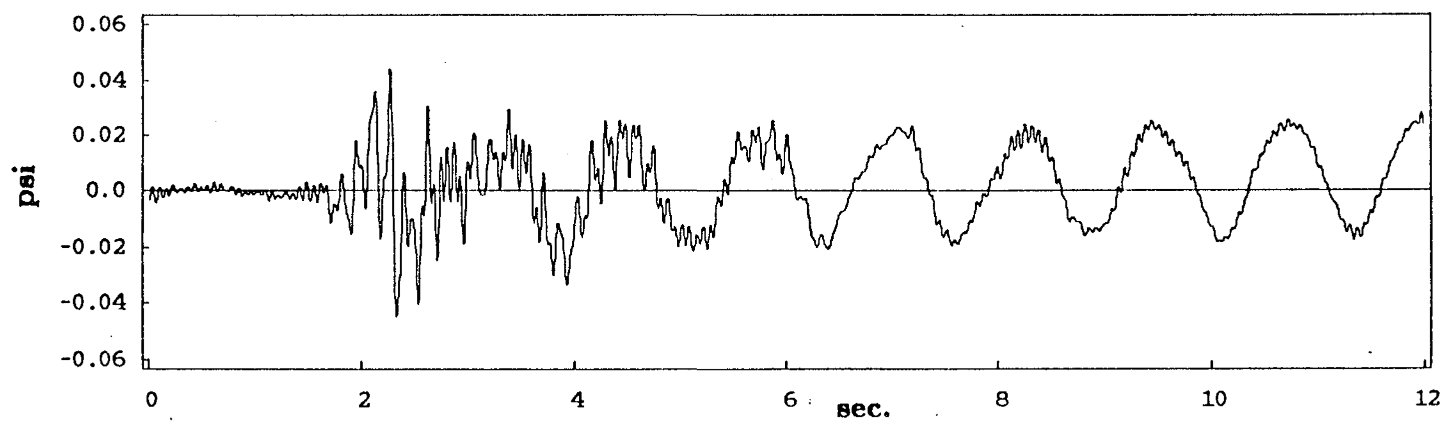

Figure 4.15b Measured dynamic pressure at north bottom transducer in tank #2. Location: z=-16 in. Table input: $\sqrt{4}$ time scaled San Francisco horizontal span 50, PTA=0.331 g.

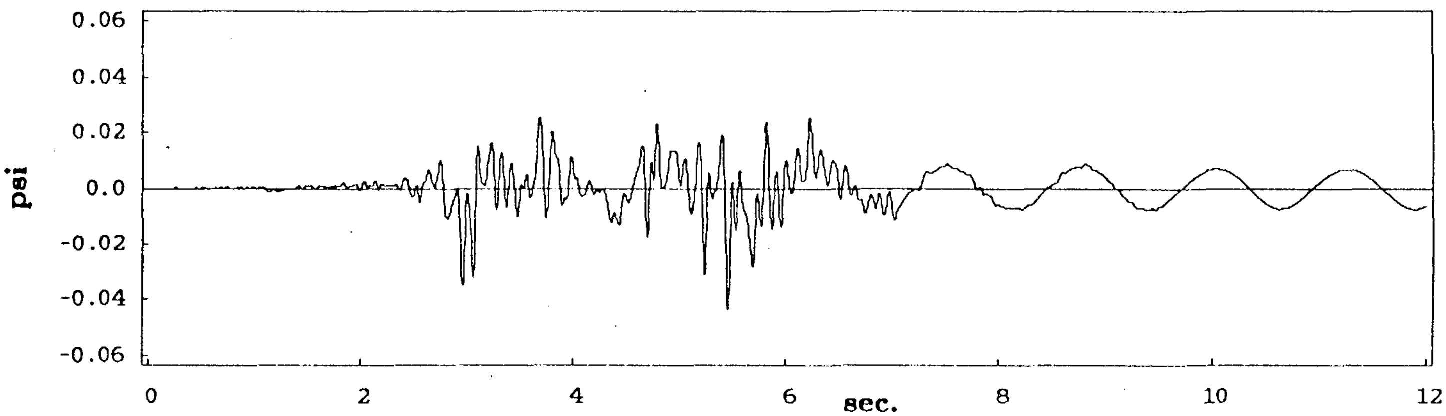

Figure 4.16a Calculated dynamic pressure P_d using two modes. Location: z=-16 in. Forcing function: recorded table acceleration. Table input: $\sqrt{4}$ time scaled Pacoima Dam horizontal span 50, PTA=0.076 g.

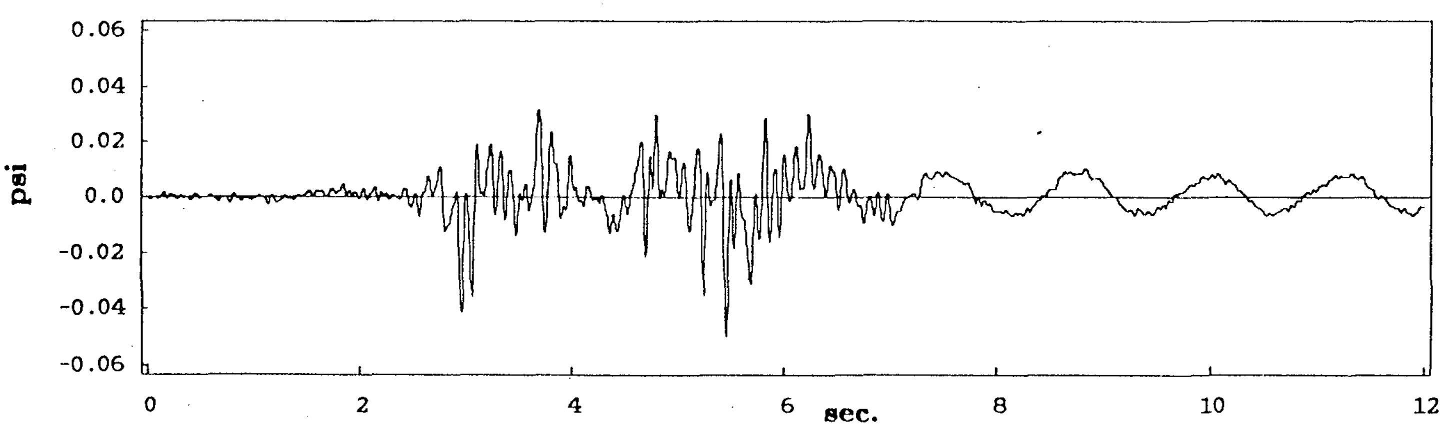

Figure 4.16b Measured dynamic pressure at north bottom transducer in tank #1. Location: z=-16 in. Table input: $\sqrt{4}$ time scaled Pacoima Dam horizontal span 50, PTA=0.076 g.

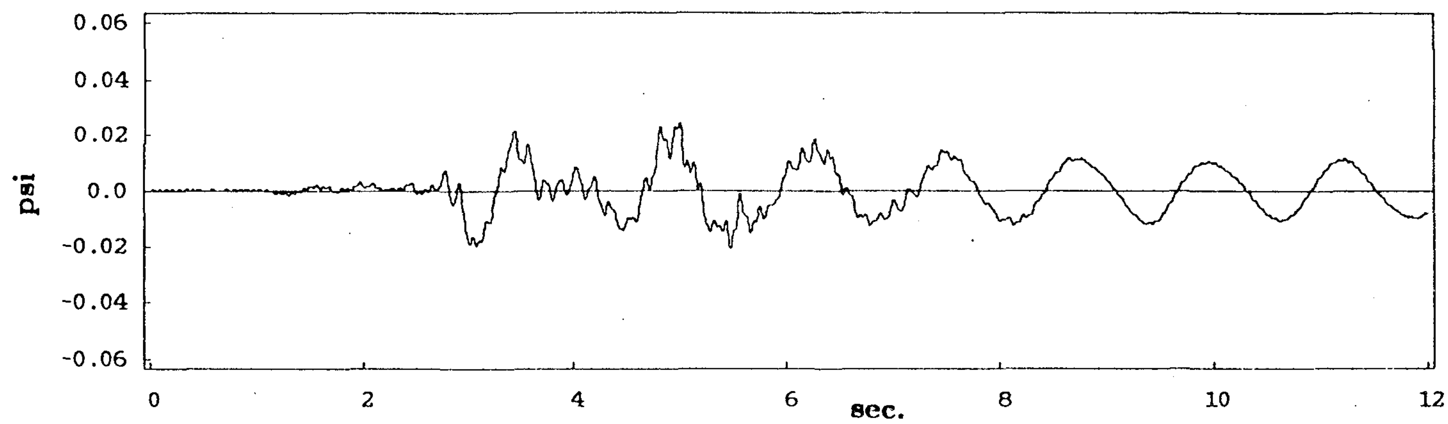

Figure 4.17a Calculated dynamic pressure P_d using two modes. Location: z=-16 in. Forcing function: recorded structure's isolated base acceleration. Table input: $\sqrt{4}$ time scaled Pacoima Dam horizontal span 50, PTA=0.076 g.

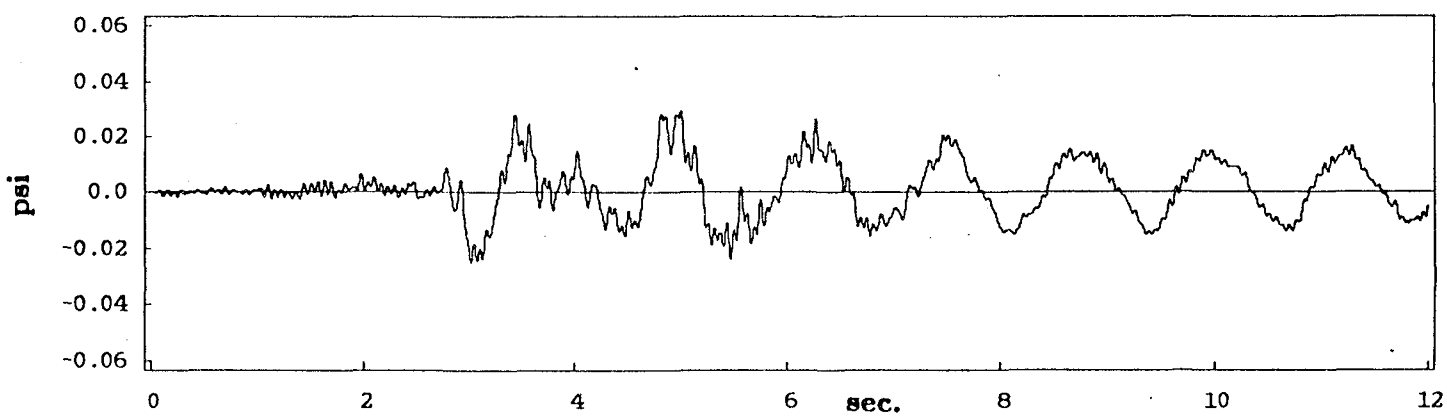

Figure 4.17b Measured dynamic pressure at north bottom transducer in tank #2. Location: z=-16 in. Table input: $\sqrt{4}$ time scaled Pacoima Dam horizontal span 50, PTA=0.076 g.

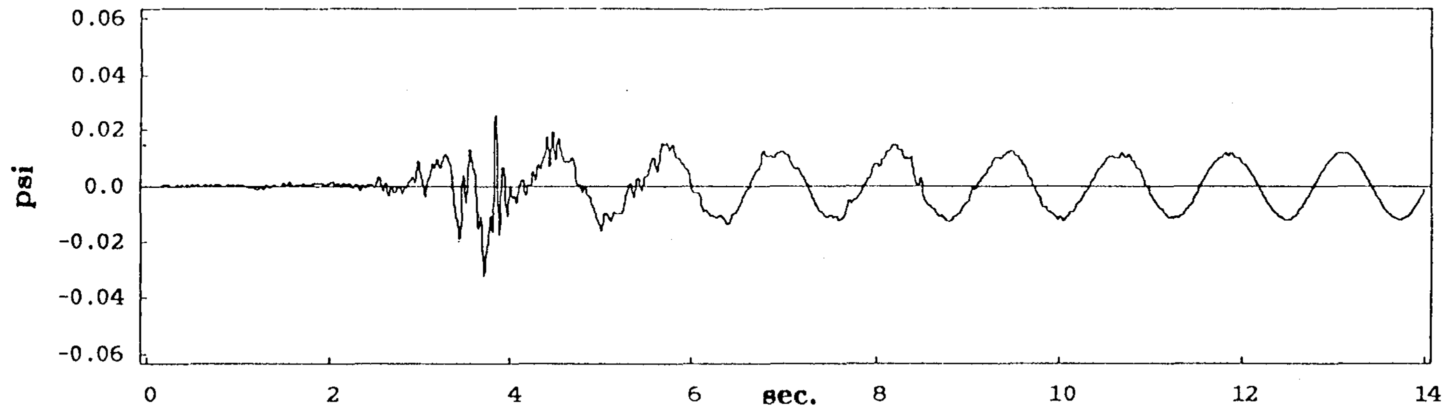

Figure 4.18a Calculated dynamic pressure P_d using two modes. Location: z=-16 in. Forcing function: recorded table acceleration. Table input: $\sqrt{4}$ time scaled Parkfield horizontal span 50, PTA=0.070 g.

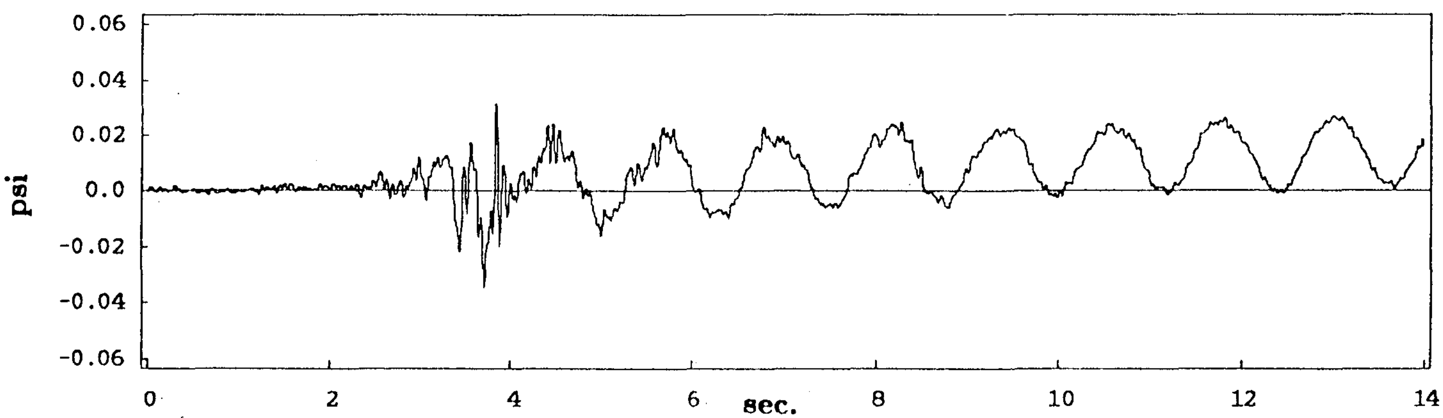

Figure 4.18b Measured dynamic pressure at north bottom transducer in tank #1. Location: z=-16 in. Table input: $\sqrt{4}$ time scaled Parkfield horizontal span 50, PTA=0.070 g.

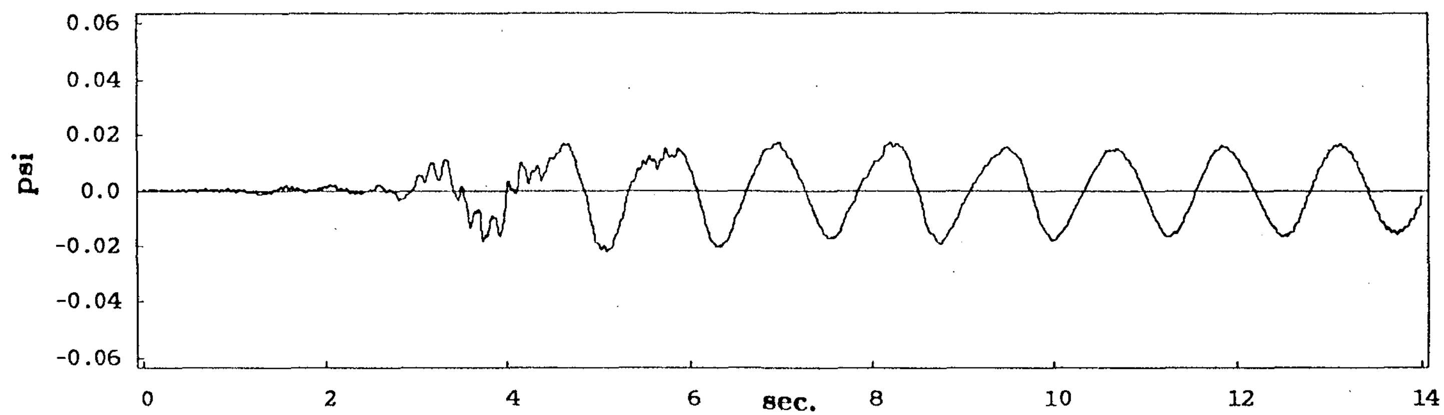

Figure 4.19a Calculated dynamic pressure P_d using two modes. Location: z=-16 in. Forcing function: recorded structure's isolated base acceleration. Table input: $\sqrt{4}$ time scaled Parkfield horizontal span 50, PTA=0.070 g.

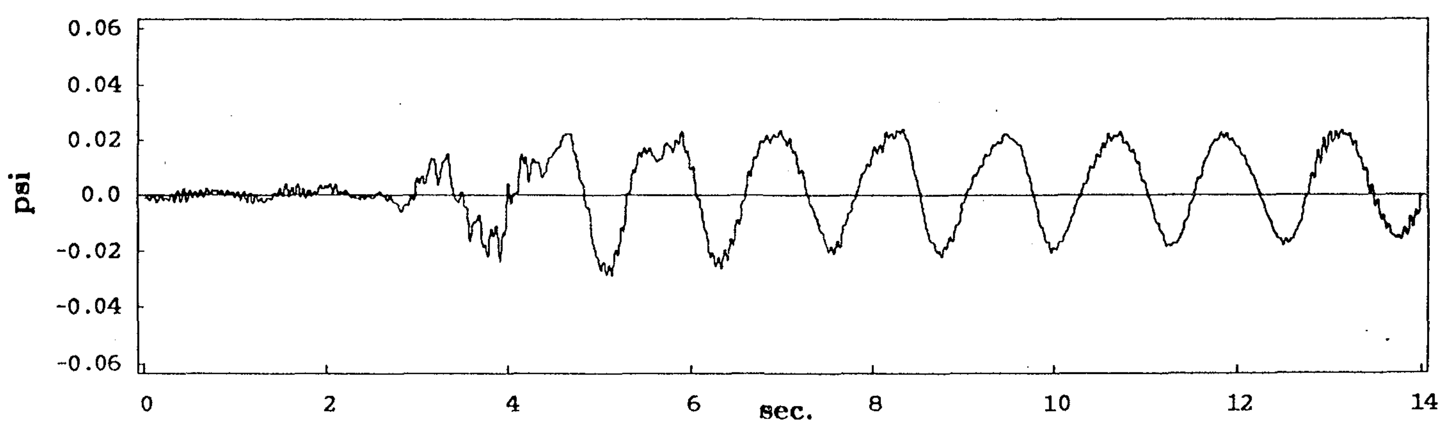

Figure 4.19b Measured dynamic pressure at north bottom transducer in tank #2. Location: z=-16 in. Table input: $\sqrt{4}$ time scaled Parkfield horizontal span 50, PTA=0.070 g.

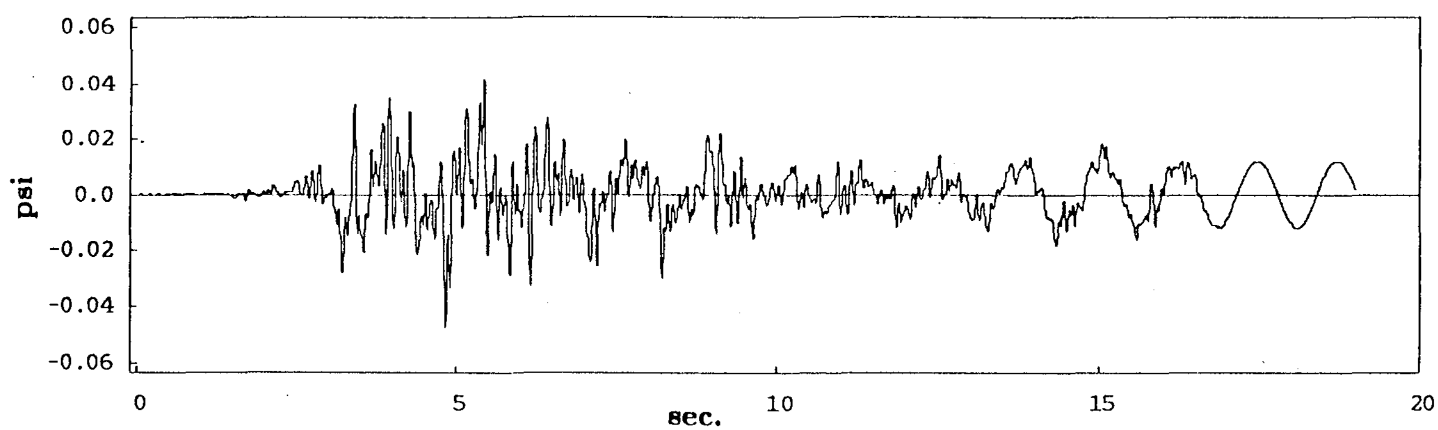

Figure 4.20a **Calculated dynamic pressure P_d using two modes. Location: z=-16 in. Forcing function: recorded table acceleration. Table input: $\sqrt{4}$ time scaled Taft horizontal span 50, PTA=0.088 g.**

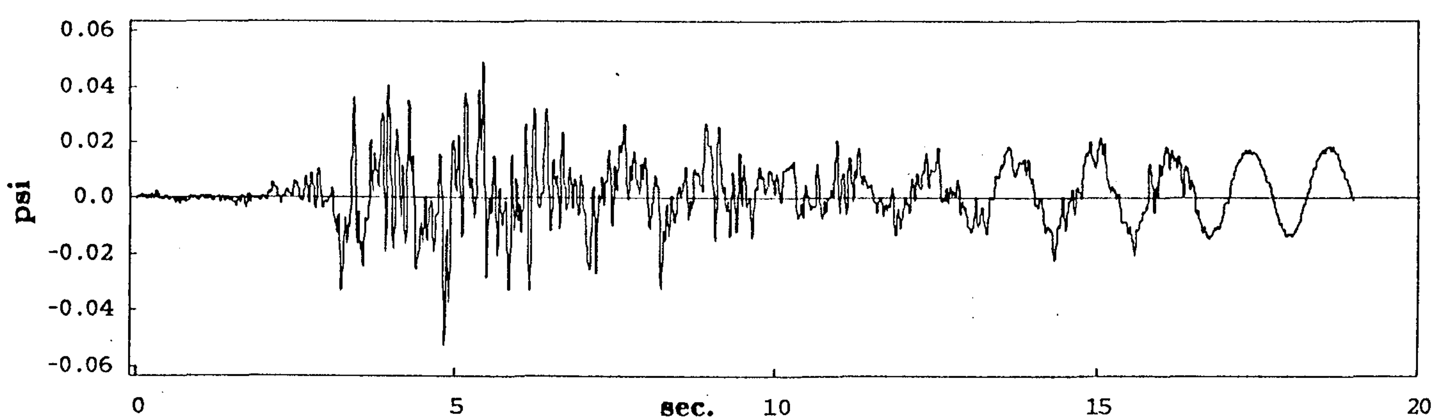

Figure 4.20b **Measured dynamic pressure at north bottom transducer in tank #1. Location: z=-16 in. Table input: $\sqrt{4}$ time scaled Taft horizontal span 50, PTA=0.088 g.**

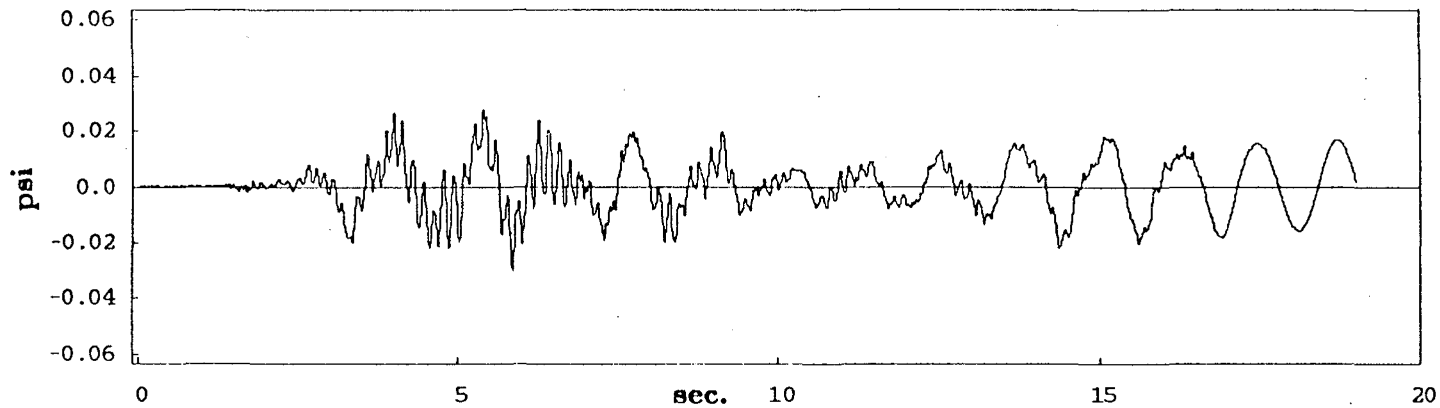

Figure 4.21a Calculated dynamic pressure P_d using two modes. Location: z=-16 in. Forcing function: recorded structure's isolated base acceleration. Table input: $\sqrt{4}$ time scaled Parkfield horizontal span 50, PTA=0.088 g.

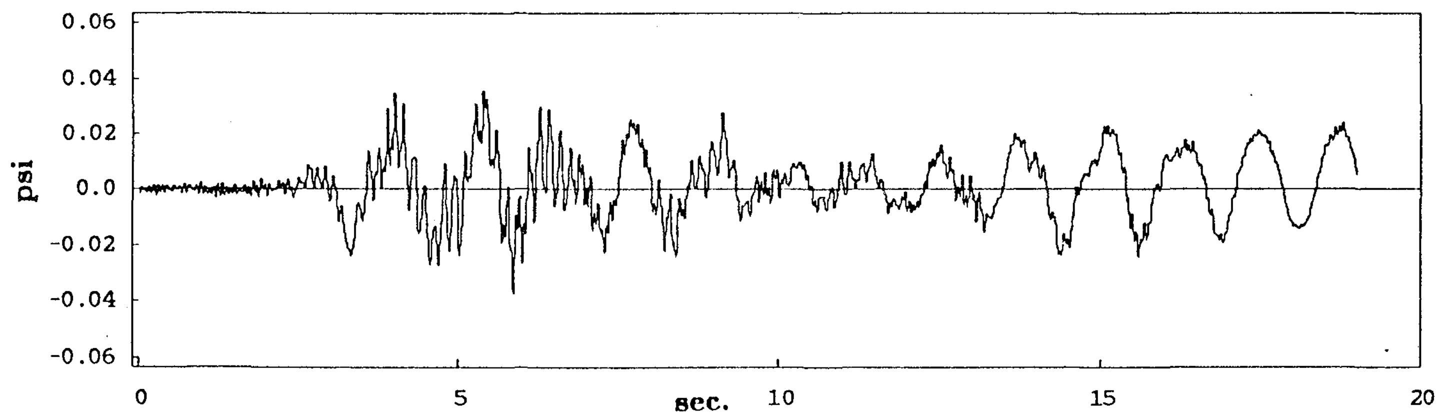

Figure 4.21b Measured dynamic pressure at north bottom transducer in tank #2. Location: z=-16 in. Table input: $\sqrt{4}$ time scaled Taft horizontal span 50, PTA=0.088 g.

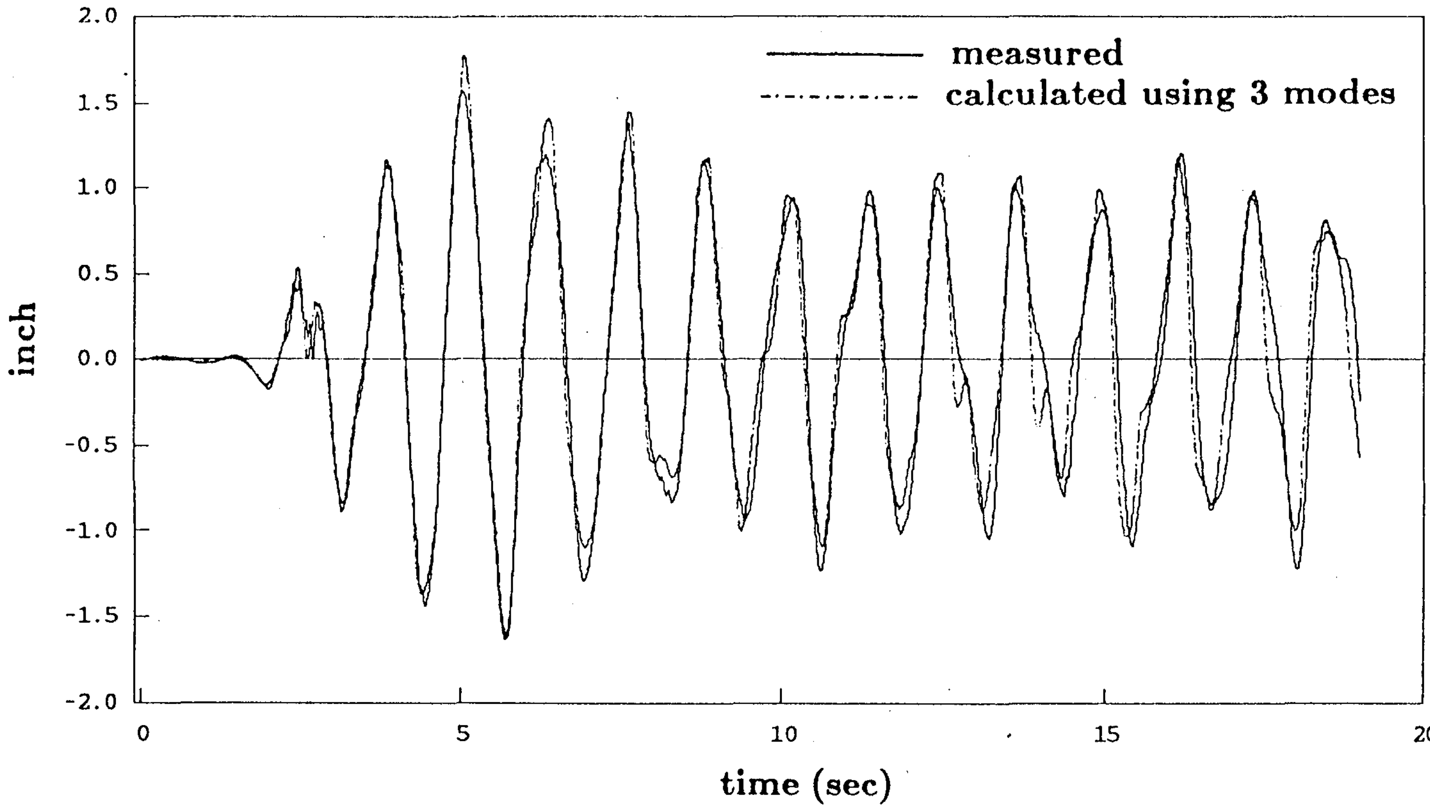

Figure 4.22 Comparison of measured water elevation time history to the calculated one, at tank wall for tank #1 (on table). Table input: $\sqrt{4}$ time scaled El Centro horizontal span 50, PTA=0.114 g.

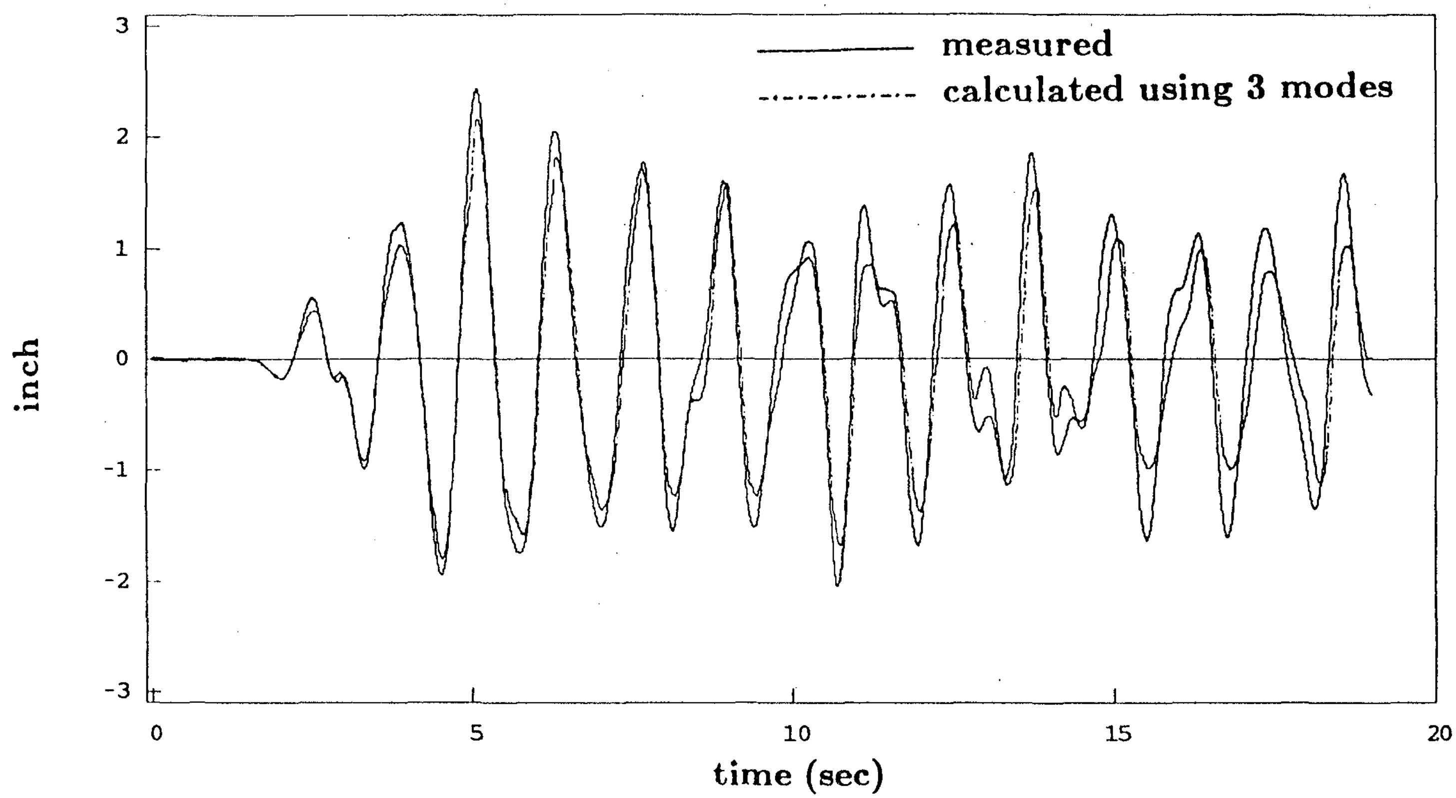

Figure 4.23 Comparison of measured water elevation time history to the calculated one, at tank wall for tank #2 (on structure). Table input: $\sqrt{4}$ time scaled El Centro horizontal span 50, PTA=0.114 g.

CHAPTER FIVE
CONCLUSIONS

Damage to tanks in recent earthquakes has shown the need for new design techniques. In this report, a specific application was pursued. Tanks were treated as internal equipment in a structure mounted on a base isolation system. The findings, however, can be easily applied to tanks supported independently on the ground, or tanks sharing a common rigid slab.

Base isolated structures are characterized by their low frequency motion. There is concern about the effect of this motion on fluid containers housed in such structures. in this study water tanks were mounted on the earthquake simulator and on the structure when a solely rubber isolation system was used. The effect of base isolation on the tanks treated as internal equipment is summarized by a slight increase in sloshing and a reduction in the dynamic pressure exerted by the fluid on the tank wall. A linear wave theory was used in the theoretical solution. The final expressions for the dynamic pressure and the water elevation consist of a term that directly depends on the ground acceleration and a series of convolution integrals each corresponding to an oscillation mode of the fluid. These expressions were compared with the measured pressure and water elevation time histories and very good agreement was found by using only the first few modes. These expressions can be now directly applied to a prototype subjected to an arbitrary support excitation.

Mechanical analogies for this problem have been proposed [6]. The simplicity of the solution presented in this report renders the transformation of the system into a mechanical analog unnecessary. Also, unlike the mechanical models that provide only the overall behavior, the present solution provides the desired quantities at any location in the fluid by using only a few modes. Moreover, the mechanical model proposed in [6], which consists of a number of horizontal single degree-of-freedom oscillators, ignores the effects of vertical support excitation while the proposed formulas accommodate vertical support excitations by replacing the gravitational field acceleration by the resultant vertical acceleration time history.

From the expressions for the pressure and the water elevation time histories, expressions for upper bounds of these quantities are derived and peak response prediction can be easily achieved whenever the design ground motion is provided in terms of its peak acceleration and its response spectra.

A major limitation of the experimental set-up was the scaling problem. It becomes more important to include the deformational characteristics of a tank when its dimensions are larger. The interaction of the shell vibrations with the fluid oscillations can affect the response. In this case, however, the difference between the measured and calculated pressure time histories was the presence of very high frequencies in the measured one. The amplitudes of these superposed high frequencies were very small and did not really affect the response. The earthquakes were time-scaled by a factor of two because of the geometric scaling of the structural model. If the tanks were tested independently, the time-scale factor could be increased to as high as 10 in order to extrapolate the results to realistic, commonly-used tank dimensions.

An important topic of future research is the study of a tank directly mounted on a flexible foundation, and its response determined for different isolation systems of various stiffnesses and damping capacities. Moreover, the use of different water depths in the tank would lead to the formation of waves of different lengths and traveling at different frequencies.

REFERENCES

[1] Sackman J. L., and Kelly J. M., "Rational Design Methods for Light Equipment in Structures Subjected to Ground Motion", *Report No. UCB/EERC-78/19*, Earthquake Engineering Research Center, University of California, Berkeley, California, 1978.

[2] Kelly J. M., and Tsai H. C., "Seismic Response of Light Internal Equipment in Base Isolated Structures", *Report No. UCB/SESM 84-17*, University of California, Berkeley, September 1984.

[3] Chalhoub M.S., "Theoretical and Experimental Studies on Earthquake Isolation and Fluid Containers", *Ph.D. Dissertation*, University of California, Berkeley, 1987.

[4] Lamb Sir H., "Hydrodynamics", 6th edition, Dover Publications, Inc., New York, 1945.

[5] Wiegel R. L., "Oceanographical Engineering", Prentice Hall, Inc., 1964.

[6] Housner G. W., "Dynamic Pressures on Accelerated Fluid Containers", *Bulletin of the Seismological Society of America*, Vol. 47, No. 1, pp. 15-36, January 1957.

[7] Graham E. W., and Rodriguez A. M., "The Characteristics of Fuel Motion which Affect Airplane Dynamics", *Journal of Applied Mechanics*, ASME Conference, Los Angeles, California, June 26-28, 1952.

[8] Miles J. W., "Resonant Motion of a Spherical Pendulum", *Physica 11D*, pp. 309-323, North-Holland, Amsterdam, 1984.

[9] Miles J. W., "Resonantly Forced Surface Waves in a Circular Cylinder", *Journal of Fluid Mechanics*, Vol. 149, pp. 15-31, 1984.

EARTHQUAKE ENGINEERING RESEARCH CENTER REPORT SERIES

EERC reports are available from the National Information Service for Earthquake Engineering(NISEE) and from the National Technical Information Service(NTIS). Numbers in parentheses are Accession Numbers assigned by the National Technical Information Service; these are followed by a price code. Contact NTIS, 5285 Port Royal Road, Springfield Virginia, 22161 for more information. Reports without Accession Numbers were not available from NTIS at the time of printing. For a current complete list of EERC reports (from EERC 67-1) and availablity information, please contact University of California, EERC, NISEE, 1301 South 46th Street, Richmond, California 94804.

UCB/EERC-80/01 "Earthquake Response of Concrete Gravity Dams Including Hydrodynamic and Foundation Interaction Effects," by Chopra, A.K., Chakrabarti, P. and Gupta, S., January 1980, (AD-A087297)A10.

UCB/EERC-80/02 "Rocking Response of Rigid Blocks to Earthquakes," by Yim, C.S., Chopra, A.K. and Penzien, J., January 1980, (PB80 166 002)A04.

UCB/EERC-80/03 "Optimum Inelastic Design of Seismic-Resistant Reinforced Concrete Frame Structures," by Zagajeski, S.W. and Bertero, V.V., January 1980, (PB80 164 635)A06.

UCB/EERC-80/04 "Effects of Amount and Arrangement of Wall-Panel Reinforcement on Hysteretic Behavior of Reinforced Concrete Walls," by Iliya, R. and Bertero, V.V., February 1980, (PB81 122 525)A09.

UCB/EERC-80/05 "Shaking Table Research on Concrete Dam Models," by Niwa, A. and Clough, R.W., September 1980, (PB81 122 368)A06.

UCB/EERC-80/06 "The Design of Steel Energy-Absorbing Restrainers and their Incorporation into Nuclear Power Plants for Enhanced Safety (Vol 1a): Piping with Energy Absorbing Restrainers: Parameter Study on Small Systems," by Powell, G.H., Oughourlian, C. and Simons, J., June 1980.

UCB/EERC-80/07 "Inelastic Torsional Response of Structures Subjected to Earthquake Ground Motions," by Yamazaki, Y., April 1980, (PB81 122 327)A08.

UCB/EERC-80/08 "Study of X-Braced Steel Frame Structures under Earthquake Simulation," by Ghanaat, Y., April 1980, (PB81 122 335)A11.

UCB/EERC-80/09 "Hybrid Modelling of Soil-Structure Interaction," by Gupta, S., Lin, T.W. and Penzien, J., May 1980, (PB81 122 319)A07.

UCB/EERC-80/10 "General Applicability of a Nonlinear Model of a One Story Steel Frame," by Sveinsson, B.I. and McNiven, H.D., May 1980, (PB81 124 877)A06.

UCB/EERC-80/11 "A Green-Function Method for Wave Interaction with a Submerged Body," by Kioka, W., April 1980, (PB81 122 269)A07.

UCB/EERC-80/12 "Hydrodynamic Pressure and Added Mass for Axisymmetric Bodies.," by Nilrat, F., May 1980, (PB81 122 343)A08.

UCB/EERC-80/13 "Treatment of Non-Linear Drag Forces Acting on Offshore Platforms," by Dao, B.V. and Penzien, J., May 1980, (PB81 153 413)A07.

UCB/EERC-80/14 "2D Plane/Axisymmetric Solid Element (Type 3-Elastic or Elastic-Perfectly Plastic)for the ANSR-II Program," by Mondkar, D.P. and Powell, G.H., July 1980, (PB81 122 350)A03.

UCB/EERC-80/15 "A Response Spectrum Method for Random Vibrations," by Der Kiureghian, A., June 1981, (PB81 122 301)A03.

UCB/EERC-80/16 "Cyclic Inelastic Buckling of Tubular Steel Braces," by Zayas, V.A., Popov, E.P. and Mahin, S.A., June 1981, (PB81 124 885)A10.

UCB/EERC-80/17 "Dynamic Response of Simple Arch Dams Including Hydrodynamic Interaction," by Porter, C.S. and Chopra, A.K., July 1981, (PB81 124 000)A13.

UCB/EERC-80/18 "Experimental Testing of a Friction Damped Aseismic Base Isolation System with Fail-Safe Characteristics," by Kelly, J.M., Beucke, K.E. and Skinner, M.S., July 1980, (PB81 148 595)A04.

UCB/EERC-80/19 "The Design of Steel Energy-Absorbing Restrainers and their Incorporation into Nuclear Power Plants for Enhanced Safety (Vol.1B): Stochastic Seismic Analyses of Nuclear Power Plant Structures and Piping Systems Subjected to Multiple Supported Excitations," by Lee, M.C. and Penzien, J., June 1980, (PB82 201 872)A08.

UCB/EERC-80/20 "The Design of Steel Energy-Absorbing Restrainers and their Incorporation into Nuclear Power Plants for Enhanced Safety (Vol 1C): Numerical Method for Dynamic Substructure Analysis," by Dickens, J.M. and Wilson, E.L., June 1980.

UCB/EERC-80/21 "The Design of Steel Energy-Absorbing Restrainers and their Incorporation into Nuclear Power Plants for Enhanced Safety (Vol 2): Development and Testing of Restraints for Nuclear Piping Systems," by Kelly, J.M. and Skinner, M.S., June 1980.

UCB/EERC-80/22 "3D Solid Element (Type 4-Elastic or Elastic-Perfectly-Plastic) for the ANSR-II Program," by Mondkar, D.P. and Powell, G.H., July 1980, (PB81 123 242)A03.

UCB/EERC-80/23 "Gap-Friction Element (Type 5) for the Ansr-II Program," by Mondkar, D.P. and Powell, G.H., July 1980, (PB81 122 285)A03.

UCB/EERC-80/24 "U-Bar Restraint Element (Type 11) for the ANSR-II Program," by Oughourlian, C. and Powell, G.H., July 1980, (PB81 122 293)A03.

UCB/EERC-80/25 "Testing of a Natural Rubber Base Isolation System by an Explosively Simulated Earthquake," by Kelly, J.M., August 1980, (PB81 201 360)A04.

UCB/EERC-80/26 "Input Identification from Structural Vibrational Response," by Hu, Y., August 1980, (PB81 152 308)A05.

UCB/EERC-80/27 "Cyclic Inelastic Behavior of Steel Offshore Structures," by Zayas, V.A., Mahin, S.A. and Popov, E.P., August 1980, (PB81 196 180)A15.

UCB/EERC-80/28 "Shaking Table Testing of a Reinforced Concrete Frame with Biaxial Response," by Oliva, M.G., October 1980, (PB81 154 304)A10.

UCB/EERC-80/29 "Dynamic Properties of a Twelve-Story Prefabricated Panel Building," by Bouwkamp, J.G., Kollegger, J.P. and Stephen, R.M., October 1980, (PB82 138 777)A07.

UCB/EERC-80/30 "Dynamic Properties of an Eight-Story Prefabricated Panel Building," by Bouwkamp, J.G., Kollegger, J.P. and Stephen, R.M., October 1980, (PB81 200 313)A05.

UCB/EERC-80/31 "Predictive Dynamic Response of Panel Type Structures under Earthquakes," by Kollegger, J.P. and Bouwkamp, J.G., October 1980, (PB81 152 316)A04.

UCB/EERC-80/32 "The Design of Steel Energy-Absorbing Restrainers and their Incorporation into Nuclear Power Plants for Enhanced Safety (Vol 3): Testing of Commercial Steels in Low-Cycle Torsional Fatigue," by Spanner, P., Parker, E.R., Jongewaard, E. and Dory, M., 1980.

UCB/EERC-80/33 "The Design of Steel Energy-Absorbing Restrainers and their Incorporation into Nuclear Power Plants for Enhanced Safety (Vol 4): Shaking Table Tests of Piping Systems with Energy-Absorbing Restrainers," by Stiemer, S.F. and Godden, W.G., September 1980, (PB82 201 880)A05.

UCB/EERC-80/34 "The Design of Steel Energy-Absorbing Restrainers and their Incorporation into Nuclear Power Plants for Enhanced Safety (Vol 5): Summary Report," by Spencer, P., 1980.

UCB/EERC-80/35 "Experimental Testing of an Energy-Absorbing Base Isolation System," by Kelly, J.M., Skinner, M.S. and Beucke, K.E., October 1980, (PB81 154 072)A04.

UCB/EERC-80/36 "Simulating and Analyzing Artificial Non-Stationary Earth Ground Motions," by Nau, R.F., Oliver, R.M. and Pister, K.S., October 1980, (PB81 153 397)A04.

UCB/EERC-80/37 "Earthquake Engineering at Berkeley - 1980," by , September 1980, (PB81 205 674)A09.

UCB/EERC-80/38 "Inelastic Seismic Analysis of Large Panel Buildings," by Schricker, V. and Powell, G.H., September 1980, (PB81 154 338)A13.

UCB/EERC-80/39 "Dynamic Response of Embankment, Concrete-Gavity and Arch Dams Including Hydrodynamic Interation," by Hall, J.F. and Chopra, A.K., October 1980, (PB81 152 324)A11.

UCB/EERC-80/40 "Inelastic Buckling of Steel Struts under Cyclic Load Reversal.," by Black, R.G., Wenger, W.A. and Popov, E.P., October 1980, (PB81 154 312)A08.

UCB/EERC-80/41 "Influence of Site Characteristics on Buildings Damage during the October 3,1974 Lima Earthquake," by Repetto, P., Arango, I. and Seed, H.B., September 1980, (PB81 161 739)A05.

UCB/EERC-80/42 "Evaluation of a Shaking Table Test Program on Response Behavior of a Two Story Reinforced Concrete Frame," by Blondet, J.M., Clough, R.W. and Mahin, S.A., December 1980, (PB82 196 544)A11.

UCB/EERC-80/43 "Modelling of Soil-Structure Interaction by Finite and Infinite Elements," by Medina, F., December 1980, (PB81 229 270)A04.

UCB/EERC-81/01 "Control of Seismic Response of Piping Systems and Other Structures by Base Isolation," by Kelly, J.M., January 1981, (PB81 200 735)A05.

UCB/EERC-81/02 "OPTNSR- An Interactive Software System for Optimal Design of Statically and Dynamically Loaded Structures with Nonlinear Response," by Bhatti, M.A., Ciampi, V. and Pister, K.S., January 1981, (PB81 218 851)A09.

UCB/EERC-81/03 "Analysis of Local Variations in Free Field Seismic Ground Motions," by Chen, J.-C., Lysmer, J. and Seed, H.B., January 1981, (AD-A099508)A13.

UCB/EERC-81/04 "Inelastic Structural Modeling of Braced Offshore Platforms for Seismic Loading," by Zayas, V.A., Shing, P.-S.B., Mahin, S.A. and Popov, E.P., January 1981, (PB82 138 777)A07.

UCB/EERC-81/05 "Dynamic Response of Light Equipment in Structures," by Der Kiureghian, A., Sackman, J.L. and Nour-Omid, B., April 1981, (PB81 218 497)A04.

UCB/EERC-81/06 "Preliminary Experimental Investigation of a Broad Base Liquid Storage Tank," by Bouwkamp, J.G., Kollegger, J.P. and Stephen, R.M., May 1981, (PB82 140 385)A03.

UCB/EERC-81/07 "The Seismic Resistant Design of Reinforced Concrete Coupled Structural Walls," by Aktan, A.E. and Bertero, V.V., June 1981, (PB82 113 358)A11.

UCB/EERC-81/08 "Unassigned," by Unassigned, 1981.

UCB/EERC-81/09 "Experimental Behavior of a Spatial Piping System with Steel Energy Absorbers Subjected to a Simulated Differential Seismic Input," by Stiemer, S.F., Godden, W.G. and Kelly, J.M., July 1981, (PB82 201 898)A04.

UCB/EERC-81/10 "Evaluation of Seismic Design Provisions for Masonry in the United States," by Sveinsson, B.I., Mayes, R.L. and McNiven, H.D., August 1981, (PB82 166 075)A08.

UCB/EERC-81/11 "Two-Dimensional Hybrid Modelling of Soil-Structure Interaction," by Tzong, T.-J., Gupta, S. and Penzien, J., August 1981, (PB82 142 118)A04.

UCB/EERC-81/12 "Studies on Effects of Infills in Seismic Resistant R/C Construction," by Brokken, S. and Bertero, V.V., October 1981, (PB82 166 190)A09.

UCB/EERC-81/13 "Linear Models to Predict the Nonlinear Seismic Behavior of a One-Story Steel Frame," by Valdimarsson, H., Shah, A.H. and McNiven, H.D., September 1981, (PB82 138 793)A07.

UCB/EERC-81/14 "TLUSH: A Computer Program for the Three-Dimensional Dynamic Analysis of Earth Dams," by Kagawa, T., Mejia, L.H., Seed, H.B. and Lysmer, J., September 1981, (PB82 139 940)A06.

UCB/EERC-81/15 "Three Dimensional Dynamic Response Analysis of Earth Dams," by Mejia, L.H. and Seed, H.B., September 1981, (PB82 137 274)A12.

UCB/EERC-81/16 "Experimental Study of Lead and Elastomeric Dampers for Base Isolation Systems," by Kelly, J.M. and Hodder, S.B., October 1981, (PB82 166 182)A05.

UCB/EERC-81/17 "The Influence of Base Isolation on the Seismic Response of Light Secondary Equipment," by Kelly, J.M., April 1981, (PB82 255 266)A04.

UCB/EERC-81/18 "Studies on Evaluation of Shaking Table Response Analysis Procedures," by Blondet, J. M., November 1981, (PB82 197 278)A10.

UCB/EERC-81/19 "DELIGHT.STRUCT: A Computer-Aided Design Environment for Structural Engineering," by Balling, R.J., Pister, K.S. and Polak, E., December 1981, (PB82 218 496)A07.

UCB/EERC-81/20 "Optimal Design of Seismic-Resistant Planar Steel Frames," by Balling, R.J., Ciampi, V. and Pister, K.S., December 1981, (PB82 220 179)A07.

UCB/EERC-82/01 "Dynamic Behavior of Ground for Seismic Analysis of Lifeline Systems," by Sato, T. and Der Kiureghian, A., January 1982, (PB82 218 926)A05.

UCB/EERC-82/02 "Shaking Table Tests of a Tubular Steel Frame Model," by Ghanaat, Y. and Clough, R.W., January 1982, (PB82 220 161)A07.

UCB/EERC-82/03 "Behavior of a Piping System under Seismic Excitation: Experimental Investigations of a Spatial Piping System supported by Mechanical Shock Arrestors," by Schneider, S., Lee, H.-M. and Godden, W. G., May 1982, (PB83 172 544)A09.

UCB/EERC-82/04 "New Approaches for the Dynamic Analysis of Large Structural Systems," by Wilson, E.L., June 1982, (PB83 148 080)A05.

UCB/EERC-82/05 "Model Study of Effects of Damage on the Vibration Properties of Steel Offshore Platforms," by Shahrivar, F. and Bouwkamp, J.G., June 1982, (PB83 148 742)A10.

UCB/EERC-82/06 "States of the Art and Pratice in the Optimum Seismic Design and Analytical Response Prediction of R/C Frame Wall Structures," by Aktan, A.E. and Bertero, V.V., July 1982, (PB83 147 736)A05.

UCB/EERC-82/07 "Further Study of the Earthquake Response of a Broad Cylindrical Liquid-Storage Tank Model," by Manos, G.C. and Clough, R.W., July 1982, (PB83 147 744)A11.

UCB/EERC-82/08 "An Evaluation of the Design and Analytical Seismic Response of a Seven Story Reinforced Concrete Frame," by Charney, F.A. and Bertero, V.V., July 1982, (PB83 157 628)A09.

UCB/EERC-82/09 "Fluid-Structure Interactions: Added Mass Computations for Incompressible Fluid," by Kuo, J.S.-H., August 1982, (PB83 156 281)A07.

UCB/EERC-82/10 "Joint-Opening Nonlinear Mechanism: Interface Smeared Crack Model," by Kuo, J.S.-H., August 1982, (PB83 149 195)A05.

UCB/EERC-82/11 "Dynamic Response Analysis of Techi Dam," by Clough, R.W., Stephen, R.M. and Kuo, J.S.-H., August 1982, (PB83 147 496)A06.

UCB/EERC-82/12 "Prediction of the Seismic Response of R/C Frame-Coupled Wall Structures," by Aktan, A.E., Bertero, V.V. and Piazzo, M., August 1982, (PB83 149 203)A09.

UCB/EERC-82/13 "Preliminary Report on the Smart 1 Strong Motion Array in Taiwan," by Bolt, B.A., Loh, C.H., Penzien, J. and Tsai, Y.B., August 1982, (PB83 159 400)A10.

UCB/EERC-82/14 "Shaking-Table Studies of an Eccentrically X-Braced Steel Structure," by Yang, M.S., September 1982, (PB83 260 778)A12.

UCB/EERC-82/15 "The Performance of Stairways in Earthquakes," by Roha, C., Axley, J.W. and Bertero, V.V., September 1982, (PB83 157 693)A07.

UCB/EERC-82/16 "The Behavior of Submerged Multiple Bodies in Earthquakes," by Liao, W.-G., September 1982, (PB83 158 709)A07.

UCB/EERC-82/17 "Effects of Concrete Types and Loading Conditions on Local Bond-Slip Relationships," by Cowell, A.D., Popov, E.P. and Bertero, V.V., September 1982, (PB83 153 577)A04.

UCB/EERC-82/18 "Mechanical Behavior of Shear Wall Vertical Boundary Members: An Experimental Investigation," by Wagner, M.T. and Bertero, V.V., October 1982, (PB83 159 764)A05.

UCB/EERC-82/19 "Experimental Studies of Multi-support Seismic Loading on Piping Systems," by Kelly, J.M. and Cowell, A.D., November 1982.

UCB/EERC-82/20 "Generalized Plastic Hinge Concepts for 3D Beam-Column Elements," by Chen, P. F.-S. and Powell, G.H., November 1982, (PB83 247 981)A13.

UCB/EERC-82/21 "ANSR-II: General Computer Program for Nonlinear Structural Analysis," by Oughourlian, C.V. and Powell, G.H., November 1982, (PB83 251 330)A12.

UCB/EERC-82/22 "Solution Strategies for Statically Loaded Nonlinear Structures," by Simons, J.W. and Powell, G.H., November 1982, (PB83 197 970)A06.

UCB/EERC-82/23 "Analytical Model of Deformed Bar Anchorages under Generalized Excitations," by Ciampi, V., Eligehausen, R., Bertero, V.V. and Popov, E.P., November 1982, (PB83 169 532)A06.

UCB/EERC-82/24 "A Mathematical Model for the Response of Masonry Walls to Dynamic Excitations," by Sucuoglu, H., Mengi, Y. and McNiven, H.D., November 1982, (PB83 169 011)A07.

UCB/EERC-82/25 "Earthquake Response Considerations of Broad Liquid Storage Tanks," by Cambra, F.J., November 1982, (PB83 251 215)A09.

UCB/EERC-82/26 "Computational Models for Cyclic Plasticity, Rate Dependence and Creep," by Mosaddad, B. and Powell, G.H., November 1982, (PB83 245 829)A08.

UCB/EERC-82/27 "Inelastic Analysis of Piping and Tubular Structures," by Mahasuverachai, M. and Powell, G.H., November 1982, (PB83 249 987)A07.

UCB/EERC-83/01 "The Economic Feasibility of Seismic Rehabilitation of Buildings by Base Isolation," by Kelly, J.M., January 1983, (PB83 197 988)A05.

UCB/EERC-83/02 "Seismic Moment Connections for Moment-Resisting Steel Frames.," by Popov, E.P., January 1983, (PB83 195 412)A04.

UCB/EERC-83/03 "Design of Links and Beam-to-Column Connections for Eccentrically Braced Steel Frames," by Popov, E.P. and Malley, J.O., January 1983, (PB83 194 811)A04.

UCB/EERC-83/04 "Numerical Techniques for the Evaluation of Soil-Structure Interaction Effects in the Time Domain," by Bayo, E. and Wilson, E.L., February 1983, (PB83 245 605)A09.

UCB/EERC-83/05 "A Transducer for Measuring the Internal Forces in the Columns of a Frame-Wall Reinforced Concrete Structure," by Sause, R. and Bertero, V.V., May 1983, (PB84 119 494)A06.

UCB/EERC-83/06 "Dynamic Interactions Between Floating Ice and Offshore Structures," by Croteau, P., May 1983, (PB84 119 486)A16.

UCB/EERC-83/07 "Dynamic Analysis of Multiply Tuned and Arbitrarily Supported Secondary Systems," by Igusa, T. and Der Kiureghian, A., July 1983, (PB84 118 272)A11.

UCB/EERC-83/08 "A Laboratory Study of Submerged Multi-body Systems in Earthquakes," by Ansari, G.R., June 1983, (PB83 261 842)A17.

UCB/EERC-83/09 "Effects of Transient Foundation Uplift on Earthquake Response of Structures," by Yim, C.-S. and Chopra, A.K., June 1983, (PB83 261 396)A07.

UCB/EERC-83/10 "Optimal Design of Friction-Braced Frames under Seismic Loading," by Austin, M.A. and Pister, K.S., June 1983, (PB84 119 288)A06.

UCB/EERC-83/11 "Shaking Table Study of Single-Story Masonry Houses: Dynamic Performance under Three Component Seismic Input and Recommendations," by Manos, G.C., Clough, R.W. and Mayes, R.L., July 1983, (UCB/EERC-83/11)A08.

UCB/EERC-83/12 "Experimental Error Propagation in Pseudodynamic Testing," by Shiing, P.B. and Mahin, S.A., June 1983, (PB84 119 270)A09.

UCB/EERC-83/13 "Experimental and Analytical Predictions of the Mechanical Characteristics of a 1/5-scale Model of a 7-story R/C Frame-Wall Building Structure," by Aktan, A.E., Bertero, V.V., Chowdhury, A.A. and Nagashima, T., June 1983, (PB84 119 213)A07.

UCB/EERC-83/14 "Shaking Table Tests of Large-Panel Precast Concrete Building System Assemblages," by Oliva, M.G. and Clough, R.W., June 1983, (PB86 110 210/AS)A11.

UCB/EERC-83/15 "Seismic Behavior of Active Beam Links in Eccentrically Braced Frames," by Hjelmstad, K.D. and Popov, E.P., July 1983, (PB84 119 676)A09.

UCB/EERC-83/16 "System Identification of Structures with Joint Rotation," by Dimsdale, J.S., July 1983, (PB84 192 210)A06.

UCB/EERC-83/17 "Construction of Inelastic Response Spectra for Single-Degree-of-Freedom Systems," by Mahin, S. and Lin, J., June 1983, (PB84 208 834)A05.

UCB/EERC-83/18 "Interactive Computer Analysis Methods for Predicting the Inelastic Cyclic Behaviour of Structural Sections," by Kaba, S. and Mahin, S., July 1983, (PB84 192 012)A06.

UCB/EERC-83/19 "Effects of Bond Deterioration on Hysteretic Behavior of Reinforced Concrete Joints," by Filippou, F.C., Popov, E.P. and Bertero, V.V., August 1983, (PB84 192 020)A10.

UCB/EERC-83/20 "Correlation of Analytical and Experimental Responses of Large-Panel Precast Building Systems," by Oliva, M.G., Clough, R.W., Velkov, M. and Gavrilovic, P., May 1988.

UCB/EERC-83/21 "Mechanical Characteristics of Materials Used in a 1/5 Scale Model of a 7-Story Reinforced Concrete Test Structure," by Bertero, V.V., Aktan, A.E., Harris, H.G. and Chowdhury, A.A., October 1983, (PB84 193 697)A05.

UCB/EERC-83/22 "Hybrid Modelling of Soil-Structure Interaction in Layered Media," by Tzong, T.-J. and Penzien, J., October 1983, (PB84 192 178)A08.

UCB/EERC-83/23 "Local Bond Stress-Slip Relationships of Deformed Bars under Generalized Excitations," by Eligehausen, R., Popov, E.P. and Bertero, V.V., October 1983, (PB84 192 848)A09.

UCB/EERC-83/24 "Design Considerations for Shear Links in Eccentrically Braced Frames," by Malley, J.O. and Popov, E.P., November 1983, (PB84 192 186)A07.

UCB/EERC-84/01 "Pseudodynamic Test Method for Seismic Performance Evaluation: Theory and Implementation," by Shing, P.-S.B. and Mahin, S.A., January 1984, (PB84 190 644)A08.

UCB/EERC-84/02 "Dynamic Response Behavior of Kiang Hong Dian Dam," by Clough, R.W., Chang, K.-T., Chen, H.-Q. and Stephen, R.M., April 1984, (PB84 209 402)A08.

UCB/EERC-84/03 "Refined Modelling of Reinforced Concrete Columns for Seismic Analysis," by Kaba, S.A. and Mahin, S.A., April 1984, (PB84 234 384)A06.

UCB/EERC-84/04 "A New Floor Response Spectrum Method for Seismic Analysis of Multiply Supported Secondary Systems," by Asfura, A. and Der Kiureghian, A., June 1984, (PB84 239 417)A06.

UCB/EERC-84/05 "Earthquake Simulation Tests and Associated Studies of a 1/5th-scale Model of a 7-Story R/C Frame-Wall Test Structure," by Bertero, V.V., Aktan, A.E., Charney, F.A. and Sause, R., June 1984, (PB84 239 409)A09.

UCB/EERC-84/06 "R/C Structural Walls: Seismic Design for Shear," by Aktan, A.E. and Bertero, V.V., 1984.

UCB/EERC-84/07 "Behavior of Interior and Exterior Flat-Plate Connections subjected to Inelastic Load Reversals," by Zee, H.L. and Moehle, J.P., August 1984, (PB86 117 629/AS)A07.

UCB/EERC-84/08 "Experimental Study of the Seismic Behavior of a Two-Story Flat-Plate Structure," by Moehle, J.P. and Diebold, J.W., August 1984, (PB86 122 553/AS)A12.

UCB/EERC-84/09 "Phenomenological Modeling of Steel Braces under Cyclic Loading," by Ikeda, K., Mahin, S.A. and Dermitzakis, S.N., May 1984, (PB86 132 198/AS)A08.

UCB/EERC-84/10 "Earthquake Analysis and Response of Concrete Gravity Dams," by Fenves, G. and Chopra, A.K., August 1984, (PB85 193 902/AS)A11.

UCB/EERC-84/11 "EAGD-84: A Computer Program for Earthquake Analysis of Concrete Gravity Dams," by Fenves, G. and Chopra, A.K., August 1984, (PB85 193 613/AS)A05.

UCB/EERC-84/12 "A Refined Physical Theory Model for Predicting the Seismic Behavior of Braced Steel Frames," by Ikeda, K. and Mahin, S.A., July 1984, (PB85 191 450/AS)A09.

UCB/EERC-84/13 "Earthquake Engineering Research at Berkeley - 1984," by , August 1984, (PB85 197 341/AS)A10.

UCB/EERC-84/14 "Moduli and Damping Factors for Dynamic Analyses of Cohesionless Soils," by Seed, H.B., Wong, R.T., Idriss, I.M. and Tokimatsu, K., September 1984, (PB85 191 468/AS)A04.

UCB/EERC-84/15 "The Influence of SPT Procedures in Soil Liquefaction Resistance Evaluations," by Seed, H.B., Tokimatsu, K., Harder, L.F. and Chung, R.M., October 1984, (PB85 191 732/AS)A04.

UCB/EERC-84/16 "Simplified Procedures for the Evaluation of Settlements in Sands Due to Earthquake Shaking," by Tokimatsu, K. and Seed, H.B., October 1984, (PB85 197 887/AS)A03.

UCB/EERC-84/17 "Evaluation of Energy Absorption Characteristics of Highway Bridges Under Seismic Conditions - Volume I and Volume II (Appendices)," by Imbsen, R.A. and Penzien, J., September 1986.

UCB/EERC-84/18 "Structure-Foundation Interactions under Dynamic Loads," by Liu, W.D. and Penzien, J., November 1984, (PB87 124 889/AS)A11.

UCB/EERC-84/19 "Seismic Modelling of Deep Foundations," by Chen, C.-H. and Penzien, J., November 1984, (PB87 124 798/AS)A07.

UCB/EERC-84/20 "Dynamic Response Behavior of Quan Shui Dam," by Clough, R.W., Chang, K.-T., Chen, H.-Q., Stephen, R.M., Ghanaat, Y. and Qi, J.-H., November 1984, (PB86 115177/AS)A07.

UCB/EERC-85/01 "Simplified Methods of Analysis for Earthquake Resistant Design of Buildings," by Cruz, E.F. and Chopra, A.K., February 1985, (PB86 112299/AS)A12.

UCB/EERC-85/02 "Estimation of Seismic Wave Coherency and Rupture Velocity using the SMART 1 Strong-Motion Array Recordings," by Abrahamson, N.A., March 1985, (PB86 214 343)A07.

UCB/EERC-85/03 "Dynamic Properties of a Thirty Story Condominium Tower Building," by Stephen, R.M., Wilson, E.L. and Stander, N., April 1985, (PB86 118965/AS)A06.

UCB/EERC-85/04 "Development of Substructuring Techniques for On-Line Computer Controlled Seismic Performance Testing," by Dermitzakis, S. and Mahin, S., February 1985, (PB86 132941/AS)A08.

UCB/EERC-85/05 "A Simple Model for Reinforcing Bar Anchorages under Cyclic Excitations," by Filippou, F.C., March 1985, (PB86 112 919/AS)A05.

UCB/EERC-85/06 "Racking Behavior of Wood-framed Gypsum Panels under Dynamic Load," by Oliva, M.G., June 1985.

UCB/EERC-85/07 "Earthquake Analysis and Response of Concrete Arch Dams," by Fok, K.-L. and Chopra, A.K., June 1985, (PB86 139672/AS)A10.

UCB/EERC-85/08 "Effect of Inelastic Behavior on the Analysis and Design of Earthquake Resistant Structures," by Lin, J.P. and Mahin, S.A., June 1985, (PB86 135340/AS)A08.

UCB/EERC-85/09 "Earthquake Simulator Testing of a Base-Isolated Bridge Deck," by Kelly, J.M., Buckle, I.G. and Tsai, H.-C., January 1986, (PB87 124 152/AS)A06.

UCB/EERC-85/10 "Simplified Analysis for Earthquake Resistant Design of Concrete Gravity Dams," by Fenves, G. and Chopra, A.K., June 1986, (PB87 124 160/AS)A08.

UCB/EERC-85/11 "Dynamic Interaction Effects in Arch Dams," by Clough, R.W., Chang, K.-T., Chen, H.-Q. and Ghanaat, Y., October 1985, (PB86 135027/AS)A05.

UCB/EERC-85/12 "Dynamic Response of Long Valley Dam in the Mammoth Lake Earthquake Series of May 25-27, 1980," by Lai, S. and Seed, H.B., November 1985, (PB86 142304/AS)A05.

UCB/EERC-85/13 "A Methodology for Computer-Aided Design of Earthquake-Resistant Steel Structures," by Austin, M.A., Pister, K.S. and Mahin, S.A., December 1985, (PB86 159480/AS)A10 .

UCB/EERC-85/14 "Response of Tension-Leg Platforms to Vertical Seismic Excitations," by Liou, G.-S., Penzien, J. and Yeung, R.W., December 1985, (PB87 124 871/AS)A08.

UCB/EERC-85/15 "Cyclic Loading Tests of Masonry Single Piers: Volume 4 - Additional Tests with Height to Width Ratio of 1," by Sveinsson, B., McNiven, H.D. and Sucuoglu, H., December 1985.

UCB/EERC-85/16 "An Experimental Program for Studying the Dynamic Response of a Steel Frame with a Variety of Infill Partitions," by Yanev, B. and McNiven, H.D., December 1985.

UCB/EERC-86/01 "A Study of Seismically Resistant Eccentrically Braced Steel Frame Systems," by Kasai, K. and Popov, E.P., January 1986, (PB87 124 178/AS)A14.

UCB/EERC-86/02 "Design Problems in Soil Liquefaction," by Seed, H.B., February 1986, (PB87 124 186/AS)A03.

UCB/EERC-86/03 "Implications of Recent Earthquakes and Research on Earthquake-Resistant Design and Construction of Buildings," by Bertero, V.V., March 1986, (PB87 124 194/AS)A05.

UCB/EERC-86/04 "The Use of Load Dependent Vectors for Dynamic and Earthquake Analyses," by Leger, P., Wilson, E.L. and Clough, R.W., March 1986, (PB87 124 202/AS)A12.

UCB/EERC-86/05 "Two Beam-To-Column Web Connections," by Tsai, K.-C. and Popov, E.P., April 1986, (PB87 124 301/AS)A04.

UCB/EERC-86/06 "Determination of Penetration Resistance for Coarse-Grained Soils using the Becker Hammer Drill," by Harder, L.F. and Seed, H.B., May 1986, (PB87 124 210/AS)A07.

UCB/EERC-86/07 "A Mathematical Model for Predicting the Nonlinear Response of Unreinforced Masonry Walls to In-Plane Earthquake Excitations," by Mengi, Y. and McNiven, H.D., May 1986, (PB87 124 780/AS)A06.

UCB/EERC-86/08 "The 19 September 1985 Mexico Earthquake: Building Behavior," by Bertero, V.V., July 1986.

UCB/EERC-86/09 "EACD-3D: A Computer Program for Three-Dimensional Earthquake Analysis of Concrete Dams," by Fok, K.-L., Hall, J.F. and Chopra, A.K., July 1986, (PB87 124 228/AS)A08.

UCB/EERC-86/10 "Earthquake Simulation Tests and Associated Studies of a 0.3-Scale Model of a Six-Story Concentrically Braced Steel Structure," by Uang, C.-M. and Bertero, V.V., December 1986, (PB87 163 564/AS)A17.

UCB/EERC-86/11 "Mechanical Characteristics of Base Isolation Bearings for a Bridge Deck Model Test," by Kelly, J.M., Buckle, I.G. and Koh, C.-G., November 1987.

UCB/EERC-86/12 "Effects of Axial Load on Elastomeric Isolation Bearings," by Koh, C.-G. and Kelly, J.M., November 1987.

UCB/EERC-87/01 "The FPS Earthquake Resisting System: Experimental Report," by Zayas, V.A., Low, S.S. and Mahin, S.A., June 1987.

UCB/EERC-87/02 "Earthquake Simulator Tests and Associated Studies of a 0.3-Scale Model of a Six-Story Eccentrically Braced Steel Structure," by Whittaker, A., Uang, C.-M. and Bertero, V.V., July 1987.

UCB/EERC-87/03 "A Displacement Control and Uplift Restraint Device for Base-Isolated Structures," by Kelly, J.M., Griffith, M.C. and Aiken, I.D., April 1987.

UCB/EERC-87/04 "Earthquake Simulator Testing of a Combined Sliding Bearing and Rubber Bearing Isolation System," by Kelly, J.M. and Chalhoub, M.S., 1987.

UCB/EERC-87/05 "Three-Dimensional Inelastic Analysis of Reinforced Concrete Frame-Wall Structures," by Moazzami, S. and Bertero, V.V., May 1987.

UCB/EERC-87/06 "Experiments on Eccentrically Braced Frames with Composite Floors," by Ricles, J. and Popov, E., June 1987.

UCB/EERC-87/07 "Dynamic Analysis of Seismically Resistant Eccentrically Braced Frames," by Ricles, J. and Popov, E., June 1987.

UCB/EERC-87/08 "Undrained Cyclic Triaxial Testing of Gravels-The Effect of Membrane Compliance," by Evans, M.D. and Seed, H.B., July 1987.

UCB/EERC-87/09 "Hybrid Solution Techniques for Generalized Pseudo-Dynamic Testing," by Thewalt, C. and Mahin, S.A., July 1987.

UCB/EERC-87/10 "Ultimate Behavior of Butt Welded Splices in Heavy Rolled Steel Sections," by Bruneau, M., Mahin, S.A. and Popov, E.P., July 1987.

UCB/EERC-87/11 "Residual Strength of Sand from Dam Failures in the Chilean Earthquake of March 3, 1985," by De Alba, P., Seed, H.B., Retamal, E. and Seed, R.B., September 1987.

UCB/EERC-87/12 "Inelastic Seismic Response of Structures with Mass or Stiffness Eccentricities in Plan," by Bruneau, M. and Mahin, S.A., September 1987, (PB90 262 650)A14.

UCB/EERC-87/13 "CSTRUCT: An Interactive Computer Environment for the Design and Analysis of Earthquake Resistant Steel Structures," by Austin, M.A., Mahin, S.A. and Pister, K.S., September 1987.

UCB/EERC-87/14 "Experimental Study of Reinforced Concrete Columns Subjected to Multi-Axial Loading," by Low, S.S. and Moehle, J.P., September 1987.

UCB/EERC-87/15 "Relationships between Soil Conditions and Earthquake Ground Motions in Mexico City in the Earthquake of Sept. 19, 1985," by Seed, H.B., Romo, M.P., Sun, J., Jaime, A. and Lysmer, J., October 1987.

UCB/EERC-87/16 "Experimental Study of Seismic Response of R. C. Setback Buildings," by Shahrooz, B.M. and Moehle, J.P., October 1987.

UCB/EERC-87/17 "The Effect of Slabs on the Flexural Behavior of Beams," by Pantazopoulou, S.J. and Moehle, J.P., October 1987, (PB90 262 700)A07.

UCB/EERC-87/18 "Design Procedure for R-FBI Bearings," by Mostaghel, N. and Kelly, J.M., November 1987, (PB90 262 718)A04.

UCB/EERC-87/19 "Analytical Models for Predicting the Lateral Response of R C Shear Walls: Evaluation of their Reliability," by Vulcano, A. and Bertero, V.V., November 1987.

UCB/EERC-87/20 "Earthquake Response of Torsionally-Coupled Buildings," by Hejal, R. and Chopra, A.K., December 1987.

UCB/EERC-87/21 "Dynamic Reservoir Interaction with Monticello Dam," by Clough, R.W., Ghanaat, Y. and Qiu, X-F., December 1987.

UCB/EERC-87/22 "Strength Evaluation of Coarse-Grained Soils," by Siddiqi, F.H., Seed, R.B., Chan, C.K., Seed, H.B. and Pyke, R.M., December 1987.

UCB/EERC-88/01 "Seismic Behavior of Concentrically Braced Steel Frames," by Khatib, I., Mahin, S.A. and Pister, K.S., January 1988.

UCB/EERC-88/02 "Experimental Evaluation of Seismic Isolation of Medium-Rise Structures Subject to Uplift," by Griffith, M.C., Kelly, J.M., Coveney, V.A. and Koh, C.G., January 1988.

UCB/EERC-88/03 "Cyclic Behavior of Steel Double Angle Connections," by Astaneh-Asl, A. and Nader, M.N., January 1988.

UCB/EERC-88/04 "Re-evaluation of the Slide in the Lower San Fernando Dam in the Earthquake of Feb. 9, 1971," by Seed, H.B., Seed, R.B., Harder, L.F. and Jong, H.-L., April 1988.

UCB/EERC-88/05 "Experimental Evaluation of Seismic Isolation of a Nine-Story Braced Steel Frame Subject to Uplift," by Griffith, M.C., Kelly, J.M. and Aiken, I.D., May 1988.

UCB/EERC-88/06 "DRAIN-2DX User Guide.," by Allahabadi, R. and Powell, G.H., March 1988.

UCB/EERC-88/07 "Theoretical and Experimental Studies of Cylindrical Water Tanks in Base-Isolated Structures," by Chalhoub, M.S. and Kelly, J.M. , April 1988.